UNIVERSITAT ROVIRA I VIRGILI

SOLUTION PROCESSED INORGANIC SEMICONDUCTOR SOLAR CELLS

José Manuel Marín Beloqui

Dipòsit Legal: T 68-2016

José Manuel Marín Beloqui

Solution Processed Inorganic Semiconductor Solar Cells

Doctoral Thesis

Supervised by Prof. Dr. Emilio Palomares Gil

Institut Català d'Investigació Química

UNIVERSITAT ROVIRA I VIRGILI
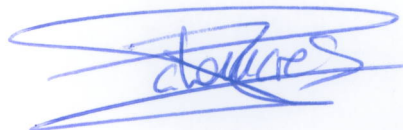
Tarragona
2015

Emilio Palomares Gil, Group Leades at the Institute of Chemical Research of Catalonia (ICIQ), Tarragona and Research Professor at the Catalan Institutions for Research and Advanced Studies (ICREA), Barcelona.

CERTIFIES:

That the present research study, entitled "Solution Processed Inorganic Semiconductor Solar Cells" presented by José Manuel Marín Beloqui for the award of the degree of Doctor, has been carried out under my supervision in ICIQ.

Tarragona September 2015

Prof. Dr. Emilio Palomares Gil

UNIVERSITAT ROVIRA I VIRGILI

ICIQ[R]
Institut
Català
d'Investigació
Química

Acknowledgements

Finished! This stage finally has come to an end. But it would be so selfish to underestimate the people that have helped me to get here. First of all, not only because is characteristic for most of the thesis (I think that maybe compulsory), it is also because he deserves it, to my supervisor Prof. Emilio Palomares. He was the one who took the bad decision to hire me, and then he did not fire me. But putting away the jokes, it has been a pleasure to meet such a good person as Emilio that helped me in the worst moments of these four years, although he has got me in the nerves all along these four years.

Also, as the usual acknowledgements structure of the usual thesis dictates, it is time to thank the ICIQ for provides me a place and the salary, as a fellowship, needed to develop the work that you have in your hands (or you are reading in your screen). Besides, according to the funding of my PhD, I would highly thank to the Ministry. Thank you for adding each year a new requirement to avoid me to be rewarded for a FPU, although I was one of the first by merits in order to receive them.

UNIVERSITAT ROVIRA I VIRGILI
SOLUTION PROCESSED INORGANIC SEMICONDUCTOR SOLAR CELLS
José Manuel Marín Beloqui
Dipòsit Legal: T 68-2016

Acknowledgements   **PhD Thesis**

Now it's turn to thank all my colleagues. First person I met in the group was Josep, he taught me everything I have to known about QDs and other interesting stuff. But, you still owe me a valencian paella!! I don't know how, but not matter how mad I was, he was always able to make me smile. A funny valencian, that was unbelievable.

Now it is turn of the Irish team. First, the Mr "Tranquilo, tranquilo" man, John N. Clifford. In the end, I think I learnt that thing about relaxing, but not quite much… Thank you for teaching how not to make antimonium sulfide solar cells, jajajaja, what was that noisy thing called TAS (TAS, TAS, TAS) and above all, how to survive under a PhD under Emilio's supervision. Ah! And don't forget about those English corrections where EVERYTHING was corrected in red but you always said "It was very good". I hope to meet in Málaga to you to try the campero!

Then, the second Irish guy, my master in all those β and Υ Dr. James (Jaimito) Ryan (you have to read this as an WWE intro), that showed me to love those never ending sessions of measuring the CE under bias in photophysics. Besides, you also helped me to be more methodical and ordered, what was very useful for the QDs.

And going on with the people that have to order their minds, I want to highly thank Aurelien. He was the person to ask for if you need anything in the lab, he always had time for you to help to buy anything, to help you with the nitrogen to or to make any reaction. Moreover, it meant to me a lot that he was the only one left to support me and talk with me after the QDs cells did not work. Also, he showed me that vegetarian pumpkin quiche was totally AWESOME!

I also want to thank Vijay, I think that you are the happiest person alive, and it is contagious!!! I hope we meet again and we can go Bollywood dancing!! But not like Rome, that u had little amount of days and you had to visit it. Don't forget about the lamb curry!!

I can't forget to mention Iván, the first person in the group that told me to go out one night. Until that day, I only went from work to home and viceversa. I won't forget that huge beer tube in La Nau, and then, we went to see a football match and to drink Guiness (the football was the excuse).

Moreover, I want to thank all my colleagues that favoured the good environment in the lab and showed me many things off the lab: Georgiana, Laia, Nùria, Lydia, Toni, Werther and Dani.

To the next Palomares generation (Cristina, Ilario and Sofía) I can only tell them to have patience, because this is a long way to go and you will need it. It was a pleasure to meet you all.

I think that the next people are surely of the most underrated people, not only in our group. They are our secretaries, Eva and Bea (sorry, but once Palomares forever Palomares). They not only make their job, which has not to be easy to arrange things to the bosses, they also are able to help with everything you need, accommodation, taxes, a travel, a fellowship when they don't have to.

Next I want to remember my kids (they were not kids even when they started with me!), Luis and David, for helping me for a summer and for two respectively. Thank you very much, and in the end I will have to ask you for a job.

But not only my colleagues have helped to get to this point, it has been a very long way to be here.

I would like to thank to al those teachers that inspired me during school, high school and college. I think that they should deserve more respect than they do. But, I have to be critic and focused only in the teachers that really want to transmit something, not only to go there everyday to show us how to pass the test.

Also, this thesis could not be possible with all my friends that were there to listen to me while I was complaining about TPVs that didn't make sense without them knowing anything of that. Specially I have to name Dani and Martin, they have been with me along this entire road. We will always have those doorframes, South Park episodes and those games that Dani don't like because they are "to random" (he loses). Besides, I want to thank to the "Muñizos" for the conversation and for that Saturdays when I was in ICIQ alone.

Next, I have to be more sentimental because is the turn of my parents. It is difficult to resume in few lines so many things. I know that you have been the ones that most suffered these four years, even when it is still far from the end. Thank you for your hard work that let me focus on my work and for your indescribable support.

Besides, I want to thank Esther for the support she provides to my parents while I am not there.

Also, there is has to be a special section to my Zerg-bro. This could have been even more painful without our Proleague discussions (Protoss OP), and those misfits and the community episodes. With the LotV release, I hope to try the archon-mode together it will be funny for sure.

Even though these last years have not been the best years in our relationship, I have to also thank my cousin Jose (Petardo), because he has strongly influenced in my life. Sorry, for not being a physiotherapist, but you know that it was not my thing.

And finally, as it common to say, last but not least, the person that I sometimes don't know how can stand me after all these years, Alba. She has shared with me all these years, and suffered with me as she was also with me doing the PhD, and in the same group. She has been the one that has support me the most, and the one that has hear my complaints the most. Now, we have to arrange the things to our next stage!!

To Mom, dad, Javito, Alba and Carmela
"What are we going to do? What we are doing"

Index

Chapter 1

General Introduction

UNIVERSITAT ROVIRA I VIRGILI
SOLUTION PROCESSED INORGANIC SEMICONDUCTOR SOLAR CELLS
José Manuel Marín Beloqui
Dipòsit Legal: T 68-2016

PhD Thesis   **Chapter 1**

Solar energy has the potential to substitute fossil fuels as energy source, but its price has shown to be a large barrier for this technology to be economically profitable. Organic Solar Cells (OSCs), also called third generation solar cells, seem to be a good option to overcome this problem due to their potential low cost of fabrication and manufacturing. The solution-processed methods, used to make these solar cells, highly decrease the fabrication costs of a photovoltaic device due to the roll-to-roll technique.

A proper characterization of these devices is vital in order to understand how the solar cells work. With this knowledge is possible to increase both, efficiency and stability of the devices. In this thesis, optical and optoelectronic techniques have been used to understand the kinetics of the charge transfer reactions that occur in the different interfaces inside the solar cell.

J-V Curve

The first measurement performed to a solar cell is the *J-V* curve. In this measurement the cell is illuminated with a calibrated lamp that imitates the solar spectrum, being in total agreement with the AM 1.5 Global solar spectrum. The solar simulator is calibrated with a silicon diode in order to obtain a concordance between different labs worldwide.

While the solar cell is illuminated, a source meter is applying voltage while, at the same time, is measuring the current that the solar cell provides. In order to set a standard, as the current is proportional to the area of the device, the current is divided by the active area to obtain the current density, *J*. The *J-V* data obtained in this measurement is used to represent the *J-V* curve, as seen in **Figure 1**.
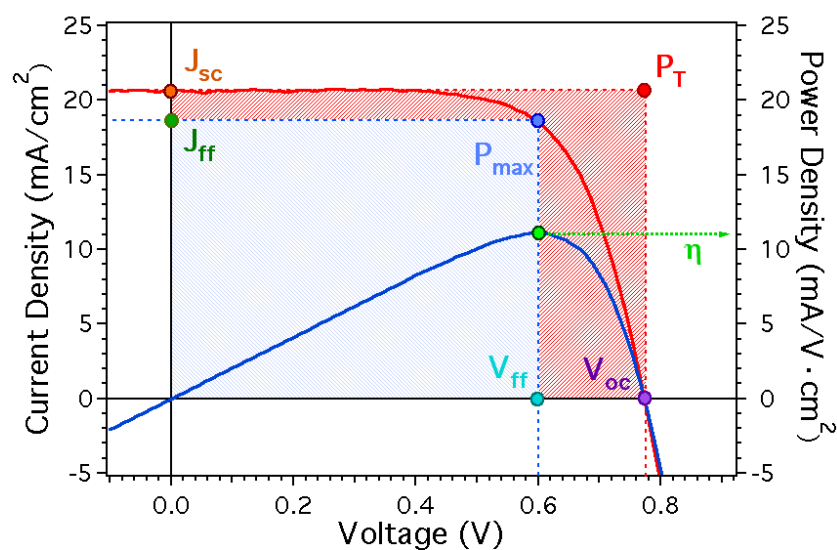
Figure 1. Example of a *J-V* and Power Density-Voltage from a Perovskite/OMeTAD Solar Cell.

There are 4 key parameters that can be obtained from the *J-V* curve, that are described next:

- **J_{sc} (mA/cm²) Short-Circuit Current**. It is the current that the cell gives when no voltage is applied. It is the point where the *J-V* curve crosses the y-axis.

- **V_{oc} (V) Open-Circuit Voltage**. It is the Voltage where the current is 0, because the potential is the same at both electrodes of the solar cell. It is the point where the curve intercepts the x-axis

- **FF (%) Fill Factor**. It gives information about the shape ("squareness") of the *J-V* curve. It is the ratio between the maximum possible output power (P_{max}) and the maximum theoretical power (P_T), obtained by the multiplication of the J_{sc} and the V_{oc} (**Equation 1**).

$$FF\ (\%) = \frac{I_{ff}\ V_{ff}}{I_{sc}\ V_{oc}} \quad \textbf{Equation 1}$$

- **η (%) Power Conversion Efficiency (PCE)** is the overall efficiency of the solar cell, i.e. how much incident light it can convert into current. It is the solar cell power divided by the the incidence light power. Although the formula for the efficiency is the one shown in **Equation 2**, the usual way to calculate it is changing the product $I_{ff}·V_{ff}$ by *FF·Isc·Voc*, because they are the most used parameters (**Equation 3**).

$$\eta\ (\%) = 100\ \frac{I_{ff}\ V_{ff}}{P_{in}} \quad \textbf{Equation 2}$$

$$\eta\ (\%) = 100\ \frac{I_{sc}\ V_{oc}\ FF}{P_{in}} \quad \textbf{Equation 3}$$

Also, some calibrated filters can be used to decrease the light intensity in order to obtain the *J-V* curve at different irradiation power (**Figure 2**).
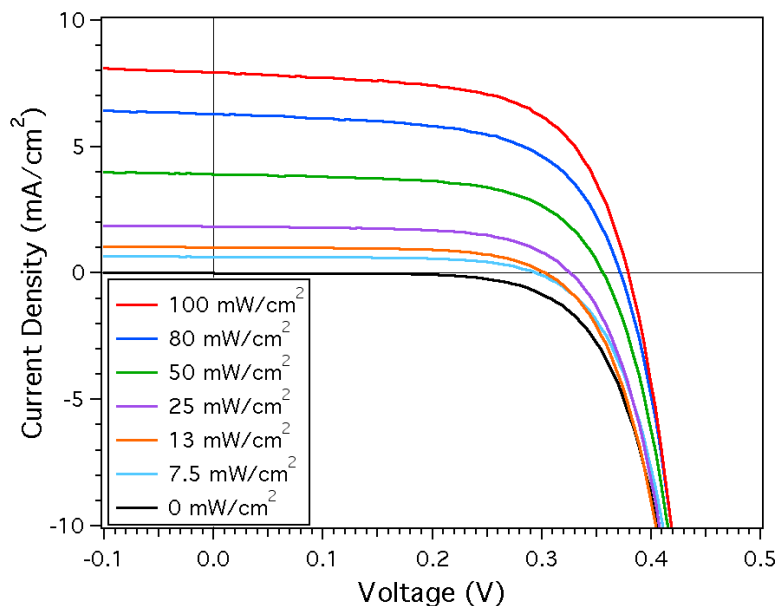
Figure 2. J-V curve of a ITO/PbS-QD/C60/Al solar cell at different light intensities.

The Short-Circuit Current Density relationship with the Light Intensity (LI) follows the **Equation 4**. When α=1 (meaning linear dependence), means that there are no negligible losses at short circuit, this is a condition to perform further measurements[1,2].

$$J_{sc} \propto Ligh\ Intensity^{\alpha}\ \textbf{Equation 4}$$

On the other hand, Open-Circuit Voltage depends of Light Intensity in an ideal diode as shown in **Equation 5**, where k_B is the Boltzmann constant, e the elementary charge and T the temperature. The ideality factor, n_{id}, terms how different is the variation of Voc with LI from the ideal equation diode. Also, the value of n_{id} gives us some information about the process that determines the recombination dynamics. If the value of the ideality factor is 1, the device is ruled by bimolecular recombination. Otherwise, if $n_{id}=2$ there will be Shockley-Read-Hall recombination[2,3].

$$dV_{oc} = n_{id}\frac{k_B T}{e}dln(LI)\ \textbf{Equation 5}$$
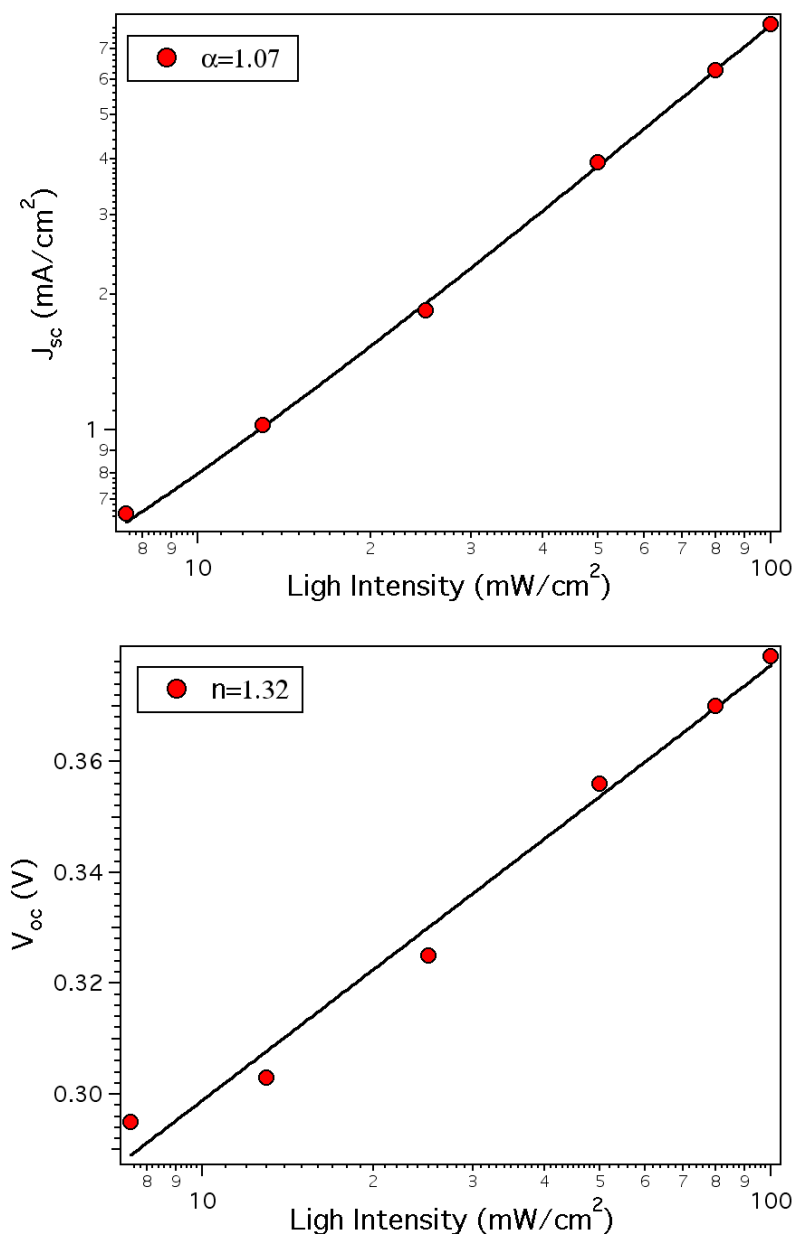
Figure 3. a) Plot of J_{sc} .at different light intensities from the PbS-QD/C60 device shown in Figure 2. The fitting (black line) was added to help the eye. **b)** Plot of V_{oc} .at different light intensities from the PbS-QD/C60 device shown in Figure 2. The fitting (black line) was added to help the eye.

Is also possible to obtain from the J-V curve the shunt resistance and the series resistance of the device.

The series resistance, R_s, in a photovoltaic device is the opposition that a charge finds to get to the electrode and to follow the whole circuit. As higher the R_s

lower will be the efficiency of our device as it decreases the Fill Factor and even the V_{oc}. A higher series resistance decrease the slope of the J-V at V_{oc}.

The proper way to calculate (**Figure 4**) it is to measure the J-V curve in dark conditions at high voltages, until the J-V curve becomes linear. Once the J-V relationship becomes linear the Ohm's law can be use and the series resistance can be calculated as the inverse of the slope.
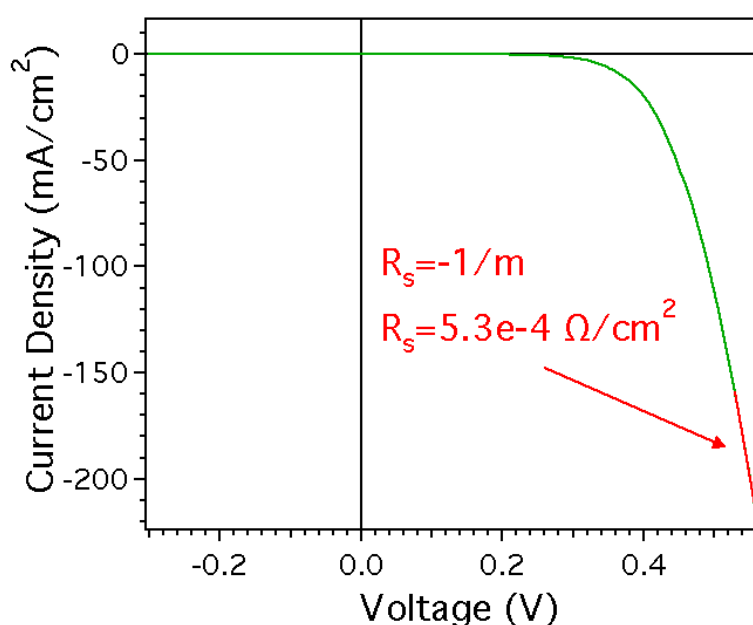
Figure 4. J-V curve measured in dark conditions (green line) of a PbS/C60 solar cell. The R_s was calculated from the fitting when the J-V dependence is lineal (red line).

In contrast, the shunt resistance is beneficial to our solar device, as higher the shunt resistance, R_{sh}, higher will be the FF. This resistance is the force that avoids the charges to go by an outer circuit in order to get to the opposite contact. As shown in **Figure 5**, this resistance will be the inverse of the slope of the J-V curve at 1 sun under short-circuit conditions.
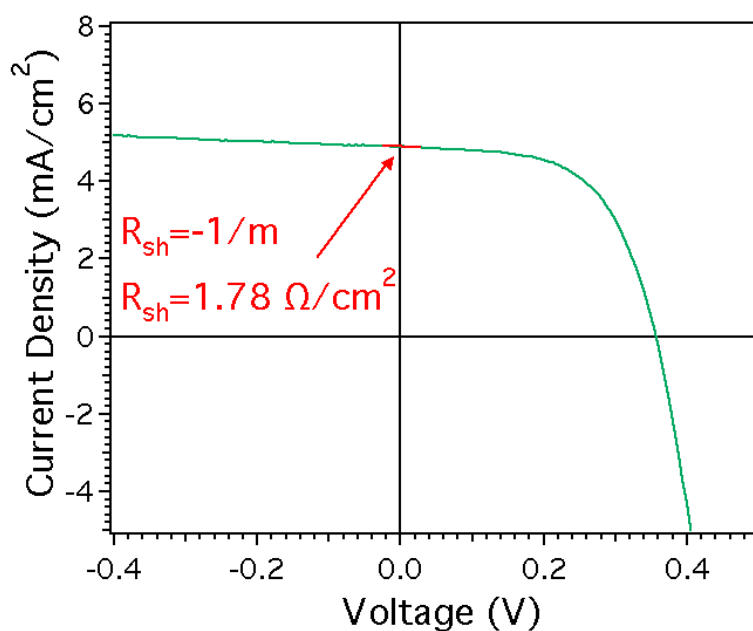
Figure 5. J-V curve measured at 1 sun conditions (green line) of a PbS/C60 solar cell. The R_{sh} of the device is calculated from the fitting (red) at V=0.

In **Figure 6** is possible to see two different J-V curves to show the effect of Rs and Rsh in a J-V curve and their effect on Fill Factor.
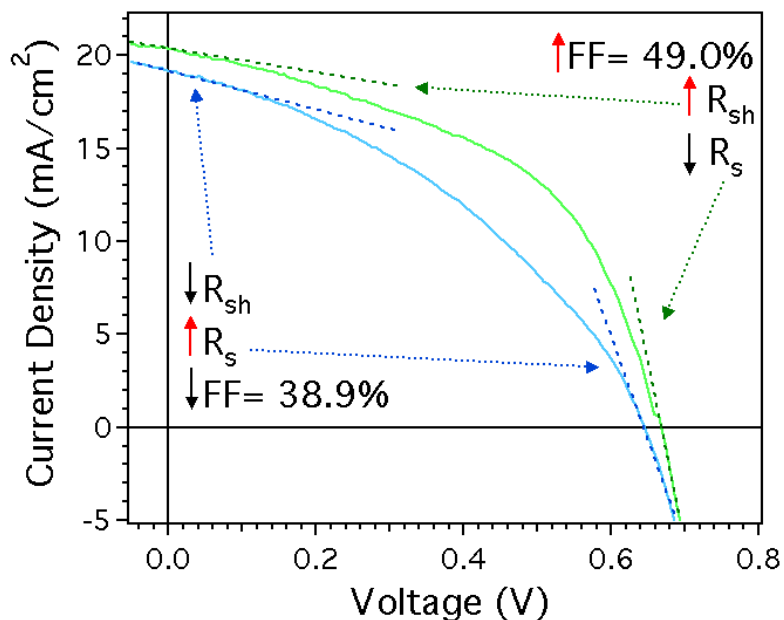
Figure 6. J-V curve plot of two different mpTiO2/Perovskite/PTB7 devices. One of them with lower FF (blue line) and the other one with higher FF (green line). Also, the linear fittings to calculate both resistances were added as dashed lines.

Incident Photon-to-Current Conversion Efficiency

Incident Photon-to-Current Efficiency (IPCE), also called External Quantum Efficiency (EQE) is a technique used to measure the ratio of the incident photons that the device is capable to transform into electrons at a given wavelength.
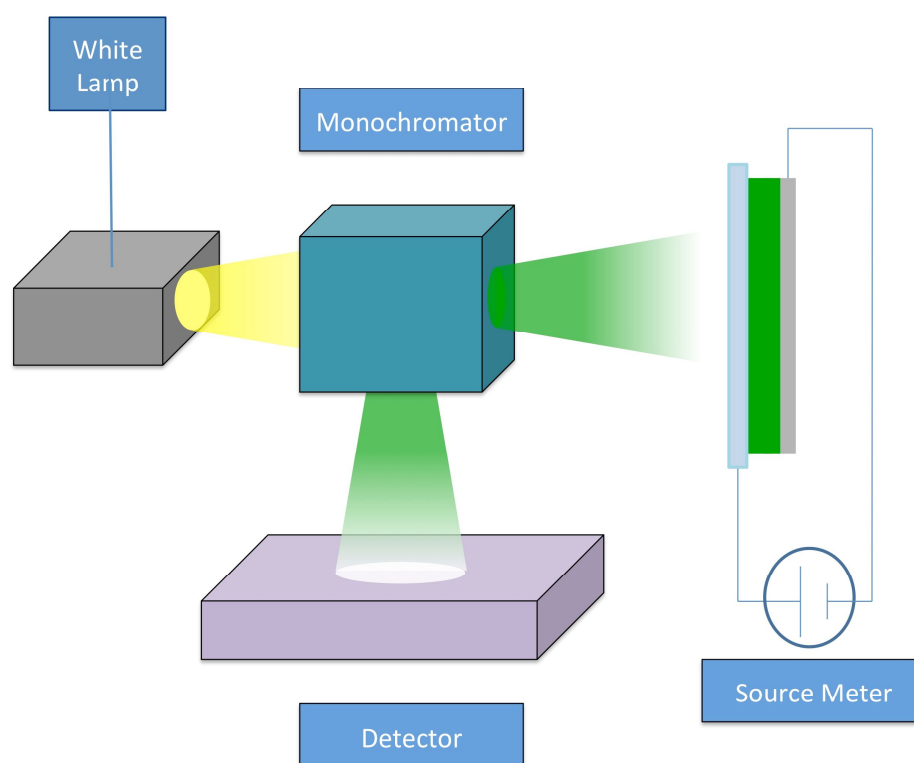
Figure 7. Scheme of a typical IPCE system.

A typical setup of a IPCE is shown in **Figure 7**. A polychromatic lamp source white light goes through a monochromator, obtaining a monochromatic light. This light is divided in two, one of the beams is directed to the solar cell, while the other one is going to a detector to know the power of the light at this wavelength. Also, the current produced with this light by the cells is measured by a source meter. The value of the IPCE at each wavelength is obtained following the **Equation 6**:

$$PCE\ (\%) = n_{id}\frac{1240 \cdot J_{sc}}{\lambda \cdot P_{lamp}} \quad \textbf{Equation 6}$$

UNIVERSITAT ROVIRA I VIRGILI
SOLUTION PROCESSED INORGANIC SEMICONDUCTOR SOLAR CELLS
José Manuel Marín Beloqui
Dipòsit Legal: T 68-2016

PhD Thesis   **Chapter 1**

This measurement is done at a wide range of wavelengths to obtain a IPCE spectrum, as seen in **Figure 8**.
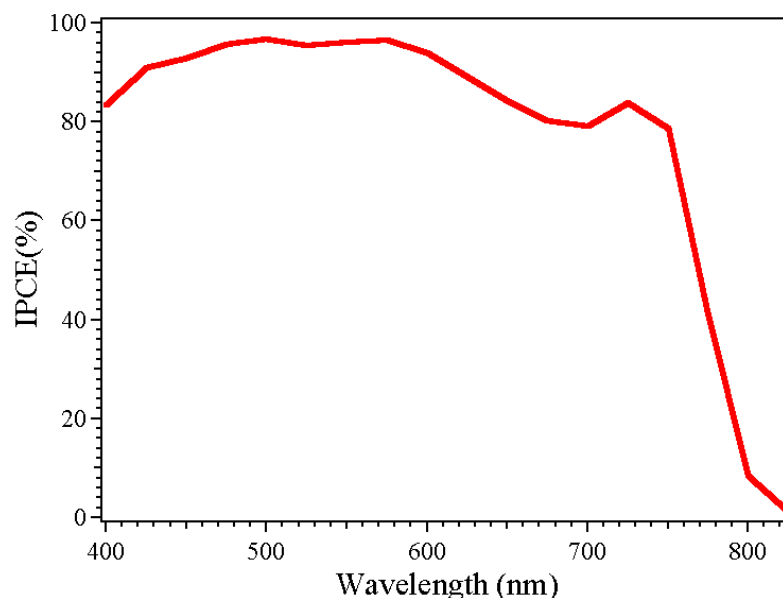
Figure 8. Example of a IPCE spectrum of a Perovskite/Polymer solar cell.

With the data obtained by this technique and the spectral absorbance is possible to also calculate the Absorbed Photon Conversion Efficiency (APCE) or Internal Quantum Efficiency (IQE), **Equation 7.** APCE is the ratio of the photons that are transformed into electrons to the number of photons that are absorbed by the device. Ligh Harvesting Efficiency (LHE) is the fraction of the incident photons of light that are absorbed by the material, and it is calculated as shown in **Equation 8**.

$$APCE\ (\%) = \frac{IPCE\ (\%)}{LHE\ (\%)} \quad \textbf{Equation 7}$$

$$LHE\ (\%) = 1 - 10^{-Absorbance} \quad \textbf{Equation 8}$$

Photo-Induced Charge Extraction (PICE)

With this technique the charge inside the active layer of a device under working conditions is measured. A diagram with the typical PICE home-made setup is showed in **Figure 9**, similar to the one described by Maurano et al[4]. This measurement can be performed in different ways. In Photo-Induced Charge Extraction under light bias, the device is held at open-circuit conditions while a bias is applied with white light from a series of LEDs. This voltage can be adjusted varying the intensity of the applied light, reaching from more than 1 sun to dark conditions. The LEDs are illuminating the device a certain amount of time, allowing the device to reach steady state conditions without thermal degradation problems. Then, at the same time as the LEDs are switched off (in 300 ns, which denotes the resolution of the technique) the device is short-circuited, and charges pass through a 50 Ω resistor. The voltage decay after the circuit is short-circuited is measured with a digital oscilloscope. This voltage decay is transformed by the Ohm's law (dividing by the 50 Ω resistance from the resistor) and then is integrated to obtain the total charges extracted from the active layer of the device at each voltage point. At the end, varying the light intensity of the LEDs, a plot of the variation of the charge of the device with the applied voltage can be obtained (**Figure 10**).

In some cases the bias is applied by an external source, as for example a Keithley digital source meter. In these cases LEDs are stood at a fixed light intensity while the voltage to reach the steady state is applied with the external source meter (Keithley). While the experiment is going on, a current is produced by the device and measured by the source meter. This current is used to correct the voltage applied to the device with the **Equation 9**. This correction makes the assumption that the device follows the Ohm's law.

$$V_{cell} = V_{app} - I \cdot R_{s\ dark} \quad \textbf{Equation 9}$$

Being V_{cell} the real voltage that is applied in the device, the one that will be plotted, V_{app} the one applied with the Keithley, I is the current measured with the Keithley and $R_{s\ dark}$ the series resistance calculated from dark J-V curve.
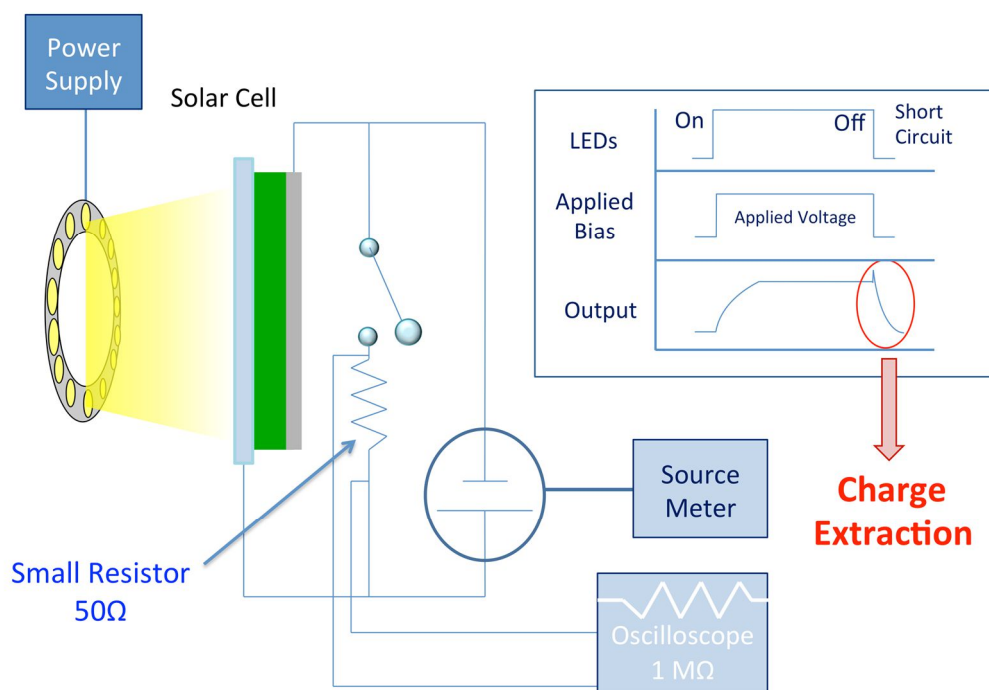
Figure 9. Scheme of a Photo-Induced Charge Extraction system.

For external applied bias PICE is also recommended to apply a correction to the resistance when the voltage is integrated to obtain the charge (**Equation 10**).

$$R_{total} = 50\Omega + R_{s\,dark}$$ **Equation 10**

In general, charge extraction is done from voltages slightly higher than V_{oc} to 0 Volts, or negative bias in some cases. From PICE as explained before and in dark conditions applying negative bias with the source meter it is possible to obtain the geometrical capacitance, i.e. the charge that is accumulated in the electrodes when the device is acting as a capacitor and the charges are not generated in the bulk.

Figure 10 shows an example of the plots of PICEs performed at different conditions.
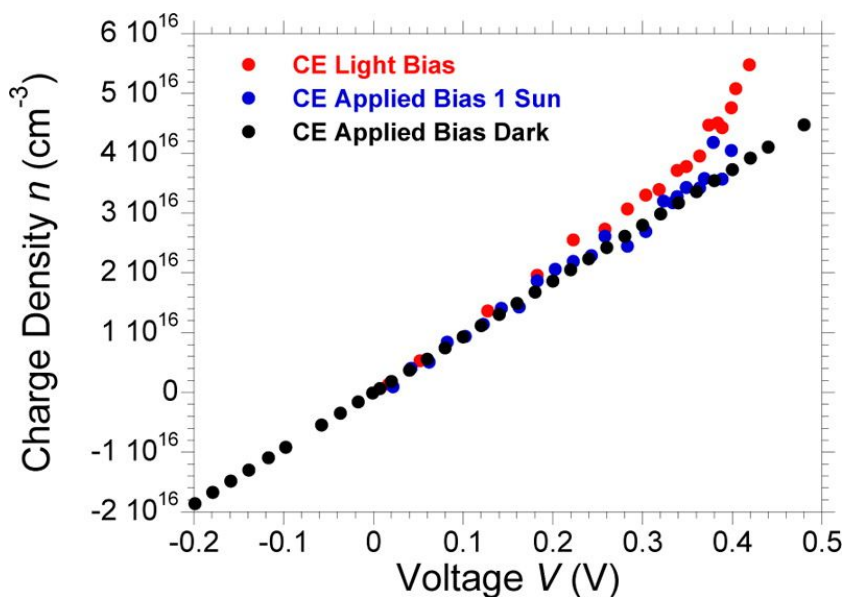
Figure 10. Plot of Photo-Induced Charge Extraction at Open circuit (red dots),
1sun (blue dots) and dark (black dots) conditions of a PbS-QD/C60 device.

The shape of the charge density distribution against the voltage will tell us where the charge are stored while is illuminated.

If the distribution is linear, **Equation 11, it** will be similar to the distribution of the charges stored in a capacitor, **Equation 12**. If this is the case, as in a capacitor, charges will be stored in the electrodes, because the electrodes are not selective and the charges get trapped there. The slope of a charge distribution in this case is called "geometric capacitance" as it is similar to the capacitor capacitance.

$$n(V) = m \cdot V \quad \textbf{Equation 11}$$

$$Q(V) = C \cdot V \quad \textbf{Equation 12}$$

On the other hand, if the distribution is exponential, **Equation 13**, the distribution will be more similar to the Nerst equation (**Equation 14**). In this case, the charges are located in the bulk of the device, and the capacitance of this distribution is called "chemical capacitance". Being γ the preexponential factor, F the Faraday constant and E-Eº the difference of chemical potencial.

$$n(V) = n_0 \cdot e^{\gamma \cdot V} \quad \textbf{Equation 13}$$

$$Q = e^{\frac{nF}{RT}(E-E^\circ)} \quad \textbf{Equation 14}$$

Photo-Induced Transient PhotoVoltage (PIT-PV)

Photo-Induced Transient PhotoVoltage (PIT-PV) is a technique used to obtain the lifetime of the charge carriers generated in the device. The diagram of the PIT-PV setup is shown in **Figure 11** as described in the bibliography[4]. The device is connected to a high resistance to maintain open circuit conditions while a voltage is applied by illumination with a ring of LEDs. Once the steady state is reached, a small perturbation is made with a low intensity laser pulse, generating a little amount of extra charge carriers, creating a little voltage increase. As the device is under open circuit conditions the excess charges can only recombine to go back to the steady state, and this recombination is recorded as a voltage decay with a digital oscilloscope. The wavelength used by the laser to create the small voltage perturbation in the device has to be near the maximum of the absorption peak of the absorber material to achieve a uniform generation along its thickness and simultaneously obtain an adequate signal. The perturbation has only to be of few mV, very small compared with the V_{oc} of hundreds of mV of the usual devices. The reason for this is to guarantee the pseudo first order regime of the voltage decay and obtain a proper monoexponential fitting. The lifetime of this monoexponential decay (**Equation 15**) is the value of the recombination time of the charges generated in the device. A graded neutral density filter is used to control the intensity of the light obtained from the laser to maintain the perturbation between 5 and 20 mV.

$$V(t) = V_0 + \Delta V_0 \cdot e^{-\tau \cdot t} \quad \textbf{Equation 15}$$

With the data obtained from near V_{oc} values to low applied bias, and by varying the light intensity of the ring of LEDs is possible to obtain a relationship between the charge carrier lifetime and the applied voltage (**Equation 16**).

$$\tau(V) = \tau_0 \cdot e^{-\beta \cdot V} \quad \textbf{Equation 16}$$

However, if lifetimes of two different kinds of cells have to be compared, it is not completely right to compare their lifetime variation with voltage but their number of charges. This is because not all devices at the same value of voltage has the same number of charges and as higher the number of charges the faster will be the recombination, because there are more available places to recombine. From the slope

(β/γ) in a log vs log plot, the reaction order of the recombination order can be obtained ($\beta/\gamma+1$). Both factors, β and γ, come from the PIT-PV and PICE respectively, as is shown in **Equation 17**,**18**,**19 and 20**. In **Equation 17** the voltage comes from **Equation 13. Equation 18** comes from **Equation 16** applying in both sides of the equation napierian logarithm. Then, **Equation 17** is included in **Equation 18**, obtaining **Equation 19**. **Equation 20** is a simplification of **Equation 19** being A a constant.

$$V = {}^1\!/_\gamma \cdot [\ln(n) - \ln(n_0)] \quad \textbf{Equation 17}$$

$$\ln\big(\tau(V)\big) = \ln(\tau_0) - \beta \cdot V \quad \textbf{Equation 18}$$

$$\ln\big(\tau(V)\big) = \ln(\tau_0) - {}^\beta\!/_\gamma \cdot [[\ln(n) - \ln(n_0)]] \quad \textbf{Equation 19}$$

$$\ln\big(\tau(V)\big) = A - {}^\beta\!/_\gamma \cdot \ln(n) \quad \textbf{Equation 20}$$
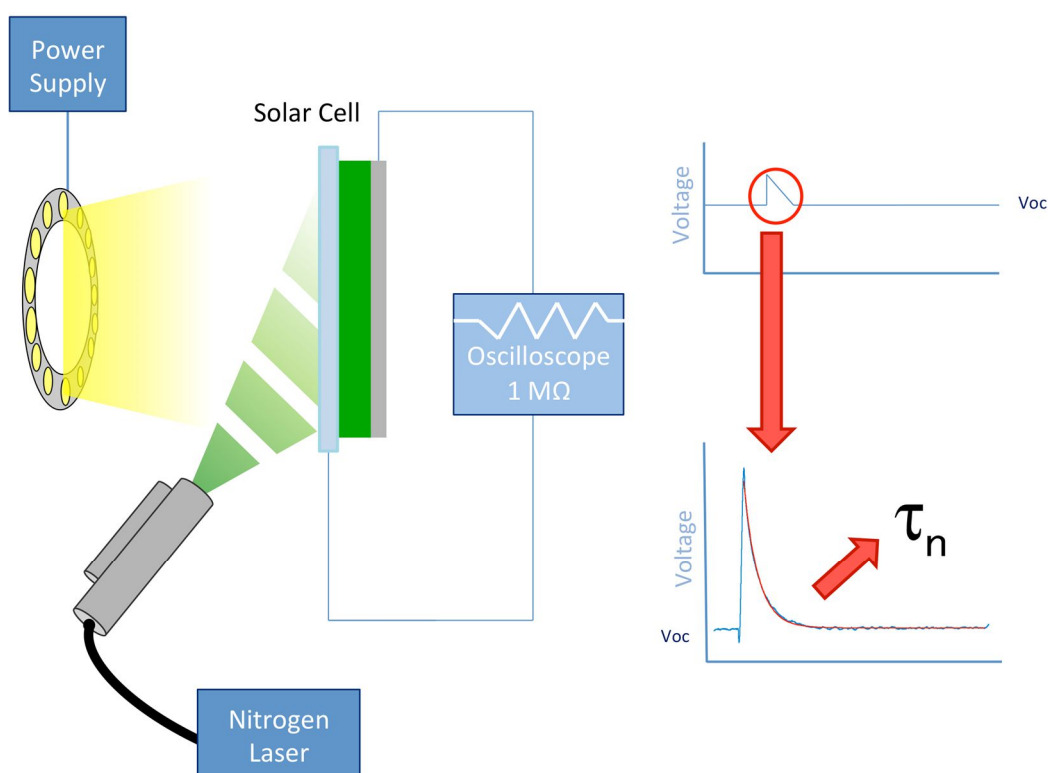
Figure 11. Scheme of a Photo-Induced Transient PhotoVoltage setup.

Photo-Induced Transient PhotoCurrent (PIT-PC)

Photo-induced Transient PhotoCurrent (PIT-PC) is a technique used to obtain the charges produced in the device by a certain laser pulse. **Figure 12** shows a scheme where the PIT-PC setup is explained.
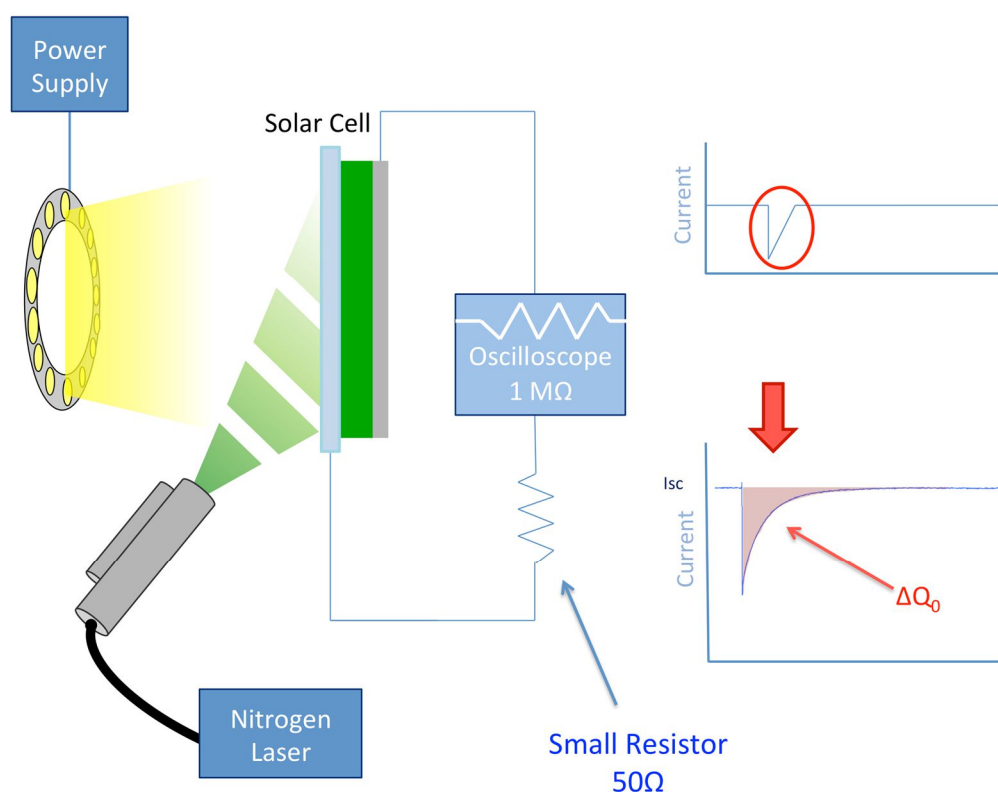
Figure 12. Scheme of a Photo-Induced Transient PhotoCurrent setup.

In this technique, the cell is connected to the oscilloscope going through by a known low resistance resistor while the cell is short-circuited.

The illumination of the cells is not as important in this technique as in the other ones, because if there is no electric fields, i.e. there are no negligible losses at shorcircuit, the result must be the same, no matter the illumination of the solar cell. Also, as there are no negligible losses at short-circuit, and the system is at short-circuit, all charges are extracted without recombination.

When the laser hits on the device, this creates a perturbation in the current, which can be integrated to obtain the charge created by the laser pulse, ΔQ_0.

A typical PIT-PC at dark and at 1 sun are plotted in **Figure 13**, where it is possible to see that even when the illumination intensities are different, the PIT-PC shows the same shape. Notice that both PIT-PC baseline have been subtracted to level them to $I_{sc}=0$ for proper comparison.
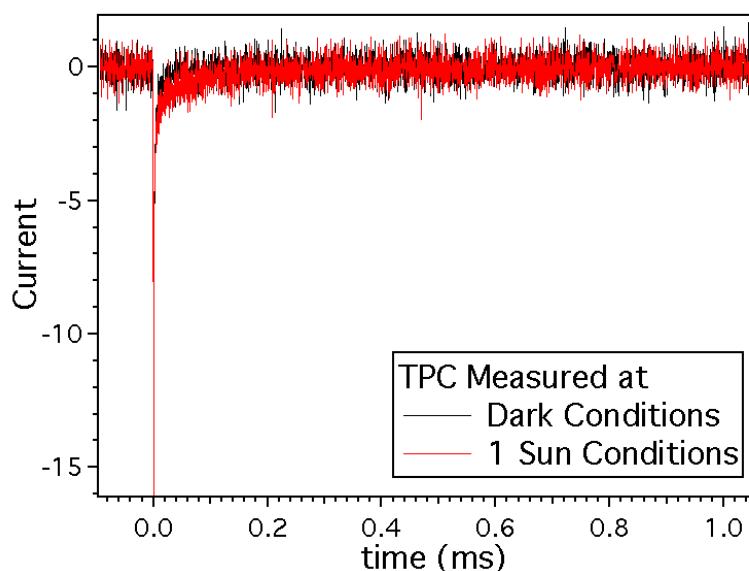
Figure 13. Plot of PIT-PC made at 1 sun (red line) and at dark (black line) conditions of a mp-TiO$_2$/Perovskite/OMeTAD solar cell. Both PIT-PCs baseline have been subtracted to maintain $I_{sc}=0$

Photo-Induced Differential Charging (PIDC)

Photo-Induced Differential Charging is a method that combines PIT-PC and PIT-PV in order to obtain the capacitance of photovoltaic devices where the PICE extraction is slower or in the same range than PIT-PV, what makes impossible the extraction of the total charges before they recombine.

To do this technique, three rules must be followed, to be sure that there will be no losses at short-circuit and all the charges will be extracted.

- PIT-PC decay must be the same under various light intensities. This means that there are no electric fields in the device.

- PIT-PC decay must be faster than PIT-PV at 1 sun.

UNIVERSITAT ROVIRA I VIRGILI
SOLUTION PROCESSED INORGANIC SEMICONDUCTOR SOLAR CELLS
José Manuel Marín Beloqui
Dipòsit Legal: T 68-2016

PhD Thesis   **Chapter 1**

-      A linear relationship between J_{sc} and light intensity must exist (α=1).

If only one of these assumptions is not true, the differential charging cannot be used to obtain the charge in the device.

Differential Charge is based in the **Equation 21** where the usual capacitance formula was translated in terms of values that can be calculated with PIT-PV and PIT-PC. In **Equation 21** ΔQ_0 is the charge calculated in PIT-PC that remains constant when the V is changed. ΔV_0 is the amplitude of the PIT-PV signal at certain V_{oc} obtained with the same laser intensity that PIT-PC was performed. With the different amplitudes for different voltages, the capacitance distribution with the voltage is obtained.

$$\text{Cap}(V_{oc}) = \frac{dQ}{dV} \approx \frac{\Delta Q_0}{\Delta V_0(V_{oc})} \quad \textbf{Equation 21}$$

Transient Absorption Spectroscopy

Transient Absorption Spectroscopy (TAS) is a time-solved spectroscopic technique that measures the changes of optical density (Δ O.D.), making possible to detect different transient species and their kinetics.

A typical TAS setup is shown in **Figure 14**. The sample is illuminated with a laser with a wavelength (λ_2) to excite our sample in order to generate the transient specie Ψ_1, called *excitation wavelength*. Meanwhile, a monochromatic light of a proper wavelength (λ_1) called *probe wavelength* that goes through the sample. This light comes from a lamp that goes through a monochromator where this wavelength can be selected. Also, the light goes through a monochromator after the sample in order to improve the selectivity of the measurement. This wavelength is selected to excite the transient specie Ψ_1 to the next excited state Ψ_2 (**Figure 15**). The variation of the absorbance of the Ψ_1 specie with time is what will be measured by TAS.
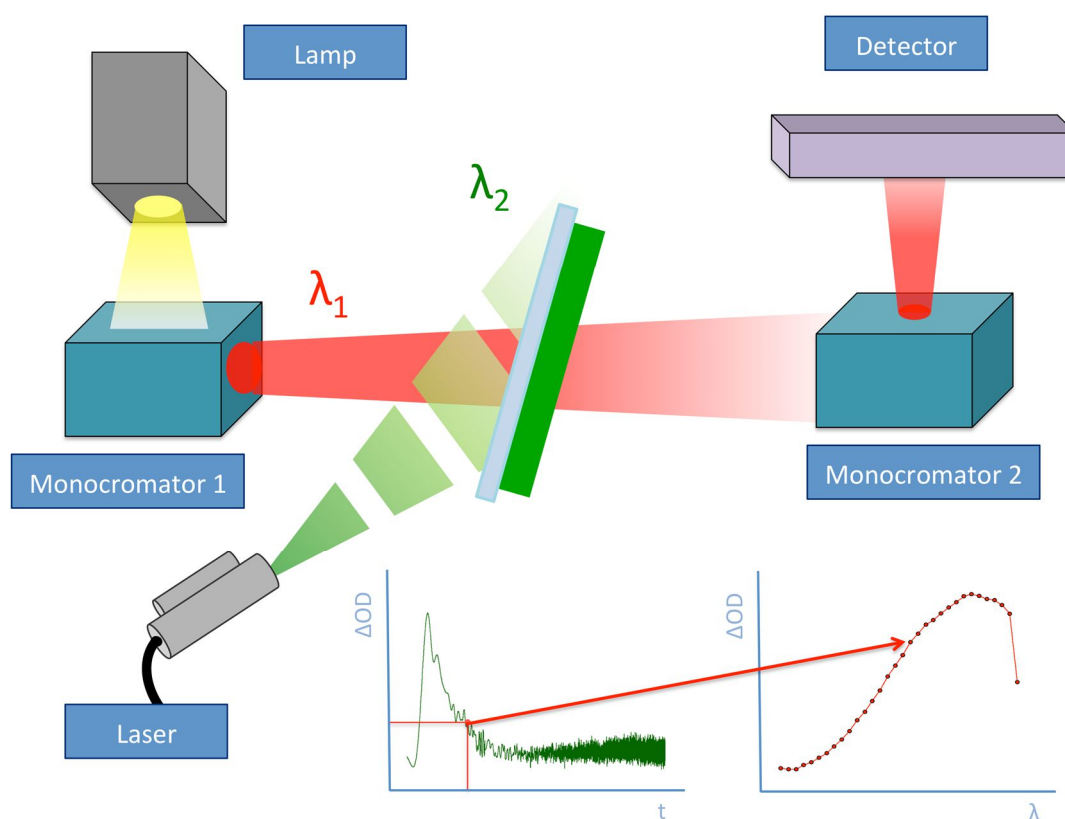
Figure 14. Scheme of a Transient Absorption Spectroscopy setup.

To obtain a spectrum of the excited specie Ψ_1, TAS decay will be performed in a wide range of wavelengths. Then the value of Δ O.D. at each wavelength at the same time is plotted against the wavelength, as depicted in the bottom right **Figure 14**.
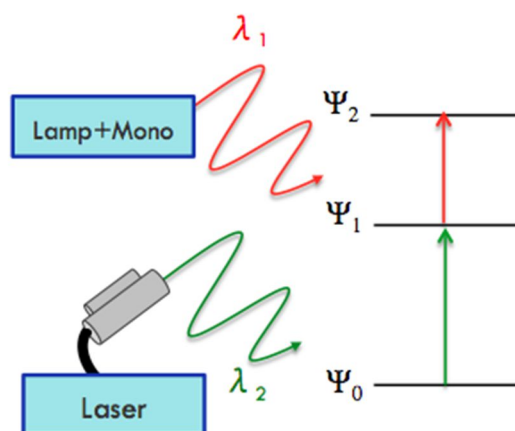
Figure 15. Scheme of the different excitations that occurs in the sample with the two different wavelengths used in the TAS.

The value of change in transient absorption spectrum can be positive or negative. It can be negative if there is a ground state bleaching or stimulated emission, and positive due to the product absorption. The bleaching occurs when the ground state disappears due to the excitation of the sample. The TAS signal also becomes negative if it is measured at the emission wavelength of the ground state. On the other hand, signal will be positive if a new transient specie that absorbs at that wavelength is created.

The shape of the TAS decay gives information about the number of processes involved at certain wavelength and the duration of these processes.

With this technique is possible to follow the kinetics of certain transient species as excitons, polarons, etc. For example, it has been widely used to calculate the injection of dyes in the mp-TiO_2 in DSSCs, the recombination rate in OSCs, etc. In a solar cell, the excitation wavelength (λ_1) excites the sample, and different processes can be followed selecting different probing wavelengths.

References

1   D. Credgington, Y. Kim, J. Labram, T. D. Anthopoulos and J. R. Durrant, *J. Phys. Chem. Lett.*, 2011, **2**, 2759–2763.

2   L. J. A. Koster, V. D. Mihailetchi, H. Xie and P. W. M. Blom, *Appl. Phys. Lett.*, 2005, **87**, 203502.

3   J. Tang and E. H. Sargent, *Adv. Mater.*, 2011, **23**, 12–29.

4   A. Maurano, C. G. Shuttle, R. Hamilton, A. M. Ballantyne, J. Nelson, W. Zhang, M. Heeney and J. R. Durrant, *J. Phys. Chem. C*, 2011, **115**, 5947–5957.

Chapter 2

Inorganic Semiconductor Nanocrystals

UNIVERSITAT ROVIRA I VIRGILI
SOLUTION PROCESSED INORGANIC SEMICONDUCTOR SOLAR CELLS
José Manuel Marín Beloqui
Dipòsit Legal: T 68-2016

PhD Thesis   **Chapter 2**

Quantum Dots (QDs) or semiconductor nanocrystals (NCs) are quasi-zero dimensional crystalline nanomaterials in which carrier motion is restricted in the three spatial dimensions[1]. This quantum confinement confers to the QDs a unique energetic structure that is between molecular and bulk semiconductor energetics, as seen in **Figure 1**. Molecules have discrete energy levels (molecular orbitals) as a result of the combination of energy levels of each atom in the molecule (atomic orbitals), with the bandgap being the difference between the HOMO (Highest Occupied Molecular Orbital) and the LUMO (Lowest Unoccupied Molecular Orbital). In the bulk semiconductor, there are two continuous energy bands separated by the band gap, with the valence band being the one with less energy, which is filled with the electrons of the material, and the conduction band to where the electrons are promoted. These bands are the junction of a large amount of energy levels of the semiconductor. However, QDs have size dependent discrete energy levels separated by the bandgap due to the quantum confinement.
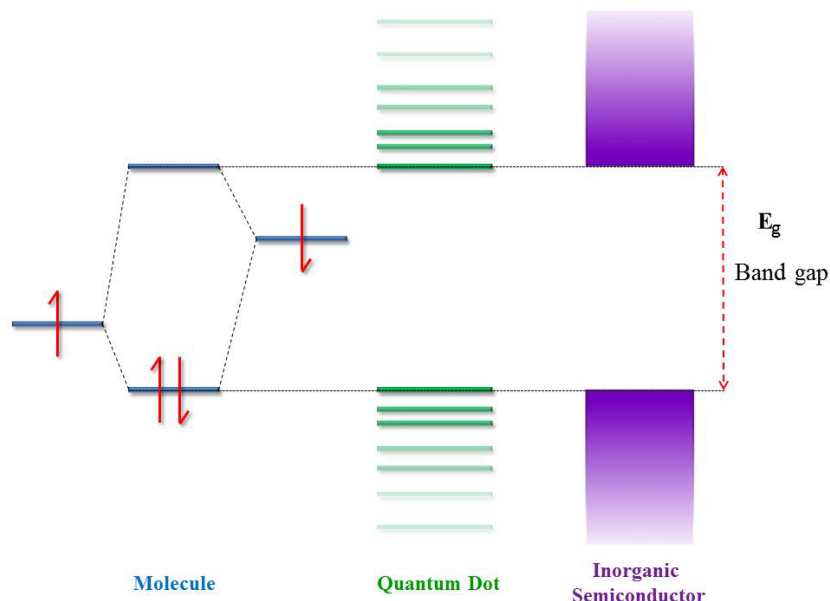
Figure 1. Scheme of energy levels in discrete molecules, Quantum Dots and
Inorganic Semiconductors.

The boundary between QDs, molecules and semiconductors is not well
defined and is material dependent. As a fast approximation, it is possible to say that
the limits are 100 to 10,000 atoms per nanocrystal. The lower limit is the proper
crystalline stability of the material with respect the isomerization into a molecular
structure. The upper limit is given by the size where separation between discrete
energy levels becomes the thermal energy kT (where k is the Boltzmann constant and
T the temperature), and they form a semiconductor band[2,3].

This energetic structure between molecular and semiconductor can be
explained using quantum chemistry[4]. The energetic of the transition, and
consequently the absorbance spectrum, the **Equation 1**:

$$E_{nml} = E_g - \frac{R_y^*}{n^2} + \frac{h^2 \chi_{ml}^2}{8M\pi^2 a^2} \quad \textbf{Equation 1}$$

where E_{nml} is the energy of the transition of the electron, and it is quantized by n, l and
m. Being n the first quantic number, l and m are the quantic numbers related with the
angular and magnetic moment, respectively. E_g is the minimal energy to create an

electron-hole pair, χ_{ml} is the quantized factor by l and m. a is the radius of the nanocrystals and R_y^{*} is the Rydberg constant, that is the ionization energy of the lower state (**Equation 2**).

$$R_y = \frac{e^2}{2a_B} \quad \textbf{Equation 2}$$

Thus, in **Equation 1** there is a constant E_g, a quantized value that depends on the radius of the nanoparticle a, and another value that depends of the exciton Bohr radius a_B.

In a system with considerable quantum confinement $a_B >> a$ and the quantized value will be bigger than the a_B-dependent one. As the value is quantized, several transitions allowed in a bulk semiconductor will be forbidden depending of the conservation of the angular and magnetic moment. Then, these systems will exhibit discrete absorption spectra (**Figure 2**) and will be strongly size-dependent, because the energy will be dependent of a^{-2} from a_B^{-1} when there is no quantum confinement.
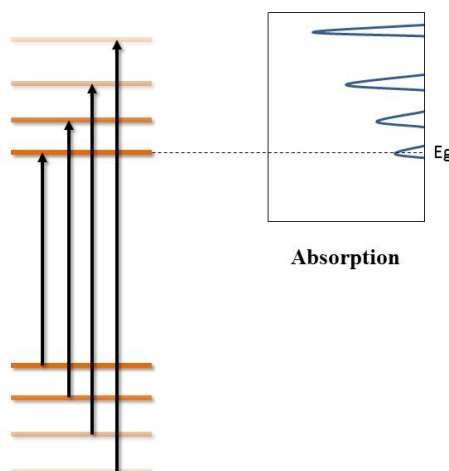
Figure 2. Scheme illustrating the correlation between electronic transitions and absorption spectrum in a QD.

With this effect it is possible to change the electronic and optical properties of the QD by only varying its size. With this property it is possible to vary the optical bandgap by changing the QD size during synthesis by more than 1 eV[5]. By tuning the

size of CdSe QDs it is possible to obtain different nanoparticles with different bandgaps to cover the whole visible spectrum, from green (500 nm) to deep red (700 nm)[6], as seen in **Figure 3**. By tuning the size of PbS QDs, the bandgap changes resulting in the QD absorbing in different parts of the infrared spectrum, from 1800 mm (with a 7.6 nm size) to 800 nm (with a 2.5 nm size)[7].
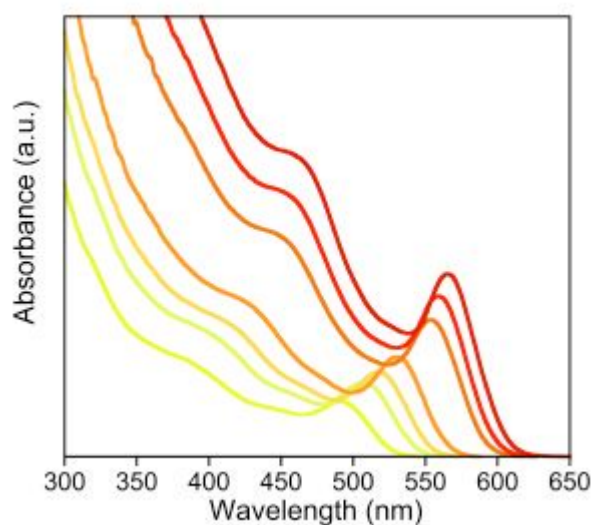
Figure 3. Absorption spectra of CdSe QDs with several sizes, covering the visible region of the spectrum. All CdSe have been synthesized in ICIQ.

Another interesting electronic property of QDs derived from their discrete energy levels is that they can undergo Multiple Exciton Generation (MEG)[3]. Usually, photon-energy conversion mechanism involves a photon and one electron-hole pair, but with MEG it is possible to generate more than one e-h with each absorbed photon. The mechanism is illustrated in **Figure 4**, where the material absorbs a photon with 2 times E_g energy. Then the electron relaxes to a lower energy level transferring this energy to another electron, which is also promoted. Finally, two promoted electrons have been obtained from only one absorbed photon, increasing the internal quantum efficiency over the 100%.

UNIVERSITAT ROVIRA I VIRGILI
SOLUTION PROCESSED INORGANIC SEMICONDUCTOR SOLAR CELLS
José Manuel Marín Beloqui
Dipòsit Legal: T 68-2016

PhD Thesis   **Chapter 2**
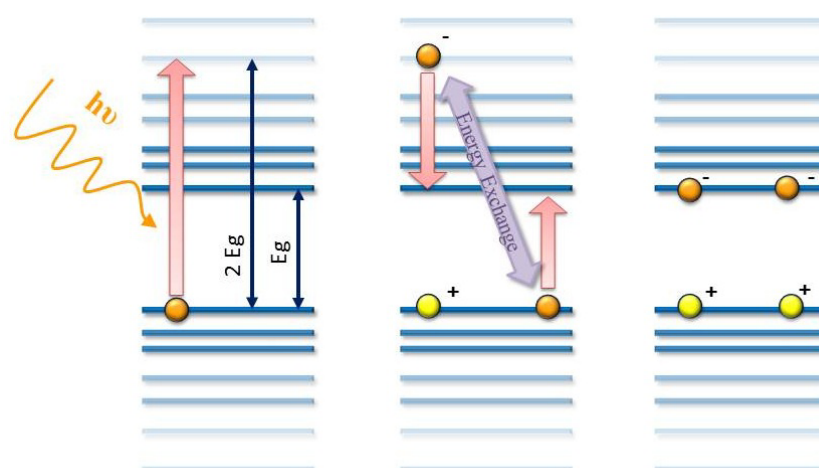
Figure 4. Multiple Exciton Generation (MEG) scheme.

QDs Synthesis

In initial works, the synthesis of QDs was carried out inside a glass matrix. In this way the size dispersion could be optimized, but the growth of the QD depends of the matrix used and its dimensions. However, the main problem with this kind of synthesis is that the amount of QD obtained was very small because it was determined by the total size of the matrix. Other sol-gel synthesis methods were used to obtain this kind of material but they had several problems relating to size control.

However, in 1993 Murray et al[8] developed a new system of synthesis where nucleation step was separated from the growth step resulting in better size control. A metal precursor is synthesized creating an organometallic compound with the metal of the QD and a long organic ligand. Then, the other precursor is injected swiftly into the organometallic hot solution, leading to a quick saturation of monomers. The faster the injection, the narrower the size dispersion will be, yielding very good size distributions results.

The synthesis is carried out in an organic solvent, such as 1-Octadecene (ODE), because they allow a good range of temperatures being the long ligand of the QD and the precursor the responsible of the solubility. The wide range of temperatures provided by the use of organic solvents the synthesis of the QDs can be

tuned to obtain different sizes and shapes[9]. Besides, the solvent controls the reaction speed as it has the ability to bind to the precursor in a reversible way.

The ligand used in this kind of synthesis should be ambipolar, with a polar head and a non-polar long alkyl chain tail. The polar head joins to the metal precursor to control the reaction speed and the dimensions of the final QD whereas the ligand tail controls the diffusion of the precursor and solubilizes it.

After synthesis, the QD is surrounded by a huge quantity of long ligands, that although it increases the stability and solubility of the QD, they decrease the electronic performance when present in solar cells. Because of this, usually an extra step involving the exchange of this ligand with a smaller one is done after the synthesis, where the QD is heated and stirred for several hours until all of the ligands surrounding the QD have been exchanged by the new one.

By tuning the temperature and the amount of ligand, and also the ratio of the precursors used it is possible to tune the size of the QD, as shown in **Figure 5**.
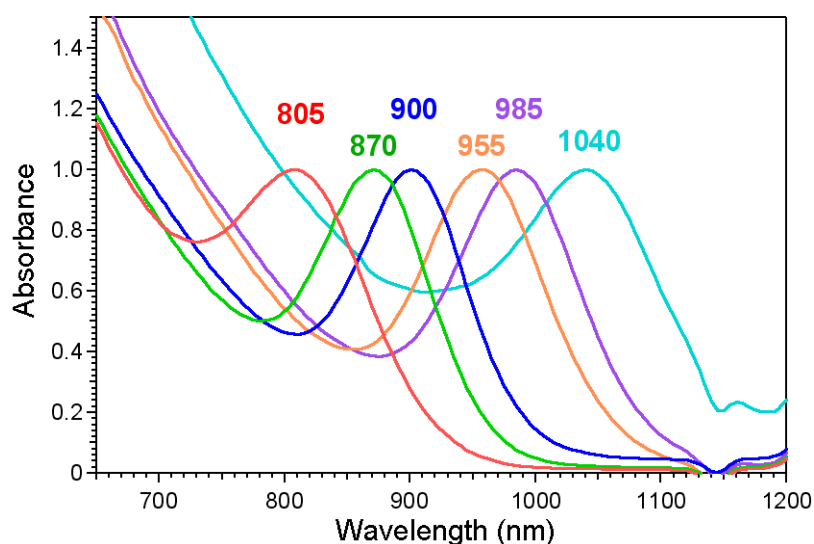
Figure 5. Absorption Spectra of several PbS QDs synthesized during this thesis. Numbers above de curves reflects the maximum absorbance wavelength in nanometres.

References

1   A. P. Alivisatos, *Science.*, 1996, **271**, 933–937.

2   V. I. Klimov, *J. Phys. Chem. B*, 2000, **104**, 6112–6123.

3   V. I. Klimov, *J. Phys. Chem. B*, 2006, **110**, 16827–45.

4   S. V. Gaponenko, *Optical Properties of Semiconductor Nanocrystals*, 1998.

5   V. I. Klimov, *Annu. Rev. Phys. Chem.*, 2007, **58**, 635–73.

6   D. J. Norris, A. Sacra, C. B. Murray and M. G. Bawendi, *Phys. Rev. Lett.*, 1994, **72**, 2612–2615.

7   B.-R. Hyun, Y.-W. Zhong, A. C. Bartnik, L. Sun, H. D. Abruña, F. W. Wise, J. D. Goodreau, J. R. Matthews, T. M. Leslie and N. F. Borrelli, *ACS Nano*, 2008, **2**, 2206–12.

8   C. B. Murray, D. J. Norris and M. G. Bawendi, *J. Am. Chem. Soc.*, 1993, **115**, 8706–8715.

9   L. Manna, E. C. Scher and A. P. Alivisatos, *J. Am. Chem. Soc.*, 2000, **122**, 12700–12706.

Chapter 3

Charge Recombination in Inorganic Semiconductor Nanocrystals

A hybrid organic-inorganic approach is promising as it offers the possibility of maximizing the benefits of each material as well as minimizing the drawbacks and limitations of each respective compound. OSCs, *for e.g.,* have now exceeded power conversion efficiencies of 11% and are edging closer to the production line. However, some limitations still exist, with one being their inability to obtain very high photocurrent due to their intrinsic low exciton diffusion lengths. Furthermore, it is difficult to have efficient organic semiconductors that can extend their absorption far into the NIR, limiting their ability to cover the entire spectrum.

Colloidal quantum dot (CQD) based solar cells however, can extend their absorption further into the NIR with PbS or PbSe nanocrystals and have recently shown high efficiencies[1–3] CQDs have several advantages over organic semiconductors in particular their optical properties, with the ability to tune their absorption characteristics simply by changing the nanocrystal size[4,5], and also posses the capability of multiple

exciton generation[6]. Another advantage is that they have higher dielectric constants meaning in comparison to organic semiconductors, allowing spontaneous generation of free charge carriers under light irradiation. Several approaches have already been demonstrated in the literature utilizing quantum dots such as Schottky devices[7], depleted heterojunctions[8], quantum dot sensitized solar cells (QDSSC)[9], bulk heterojunction (BHJ) QD:polymer[10], and bilayer CQD/small molecule solar cells[11].

Pb-based nanocrystals have shown the best device efficiencies due to the their excellent optical properties in that they posses the characteristic of being panchromatic with the ability to extend their absorption into the infrared through increasing their diameter[5,12], allowing a larger portion of the solar spectrum to be harvested compared to Cd-based CQDs *for e.g*; this leads to devices with extremely high photocurrents[2]. However, the further one wishes to extend the absorption of the CQDs into the NIR, the lower the band-gap becomes, which in turn affects the open-circuit voltage (V_{OC})[13]. The device architecture can also limit the V_{OC}, *for e.g.*, the maximum achievable V_{OC} for a Schottky or depleted heterojunction device is limited by the work functions of the electrodes. A method to decouple the influence of the contacts on the V_{OC} is to employ a donor-acceptor type-II heterojunction where the V_{OC} is instead determined by the difference in the donor HOMO (valence band) and the acceptor LUMO (conduction band) of the organic (inorganic) semiconductors. The V_{OC} is simply the point at which no-net current flows in a device, where the flux of charge generation is equal to the flux of charge recombination. PbS CQD devices have also used this heterojunction approach with PbS acting as the donor, and either a metal oxide (ZnO)[14], inorganic semiconductors (Bi_2S_3)[15], or organic (C_{60})[11], acting as the acceptor. Hybrid inorganic CQD/organic devices are particularly interesting, especially considering the difficulty in designing efficient NIR chromophores that can absorb at wavelengths beyond 800 nm. Using CQDs together with organic semiconductors therefore offers exciting prospects for single junction solar cells with absorption extending much further into the NIR than is possible using a pure organic active layer. Furthermore, this approach also opens the door to tandem solar cells.

Previously we have studied the charge transfer kinetics and non-geminate charge recombination dynamics for a number of QDSSC and QD:polymer solar cells through the use of transient optical and optoelectronic techniques[16–19], and we now extend the

analysis to bilayer PbS quantum dot/C_{60} devices to quantify the rate of non-geminate recombination with respect to the charge density in the device, and to use this information to understand the role non-geminate recombination has on the V_{OC} in these devices. An added advantage of choosing a bilayer architecture is that we can control the interface rather than have a disordered BHJ morphology that is common for QD:polymer devices. We employ transient optoelectronic techniques, namely photo-induced charge extraction (PICE) and photo-induced transient photovoltage (PIT-PV), to quantify the charge density and non-geminate recombination rate, of PbS/C_{60} planar heterojunction solar cells under working conditions (device architecture and typical energy levels of the materials are shown in **Figure 1**, while device fabrication and PbS CQD synthesis are described in the experimental section). Correlating the charges present in the device with the charge carrier lifetime allows us to accurately reconstruct the experimental current-voltage curve using the model introduced for organic solar cells[20], which to the best of our knowledge is the first time it has been reported for hybrid organic-inorganic solar cells based on CQDs.
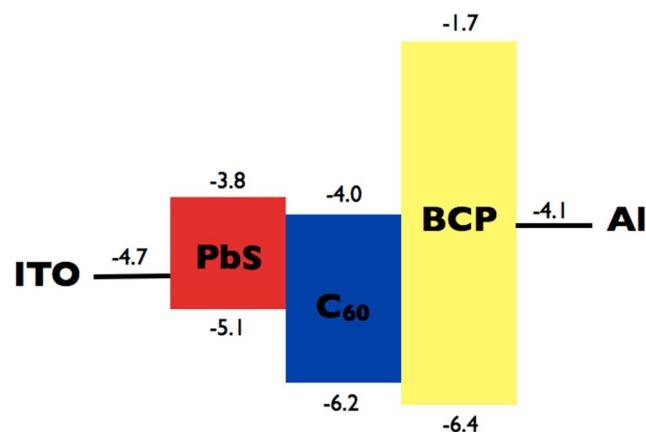
Figure 1. Energy levels for the materials used in these devices PbS (15 nm)/C60(40 nm)/BCP(10 nm)/Al(100 nm).

Results and Discussions

The current/voltage (J-V) curve of the device under various light intensities measured using a calibrated solar simulator (AM 1.5 G, 100 mW/cm^2) is shown in

UNIVERSITAT ROVIRA I VIRGILI
SOLUTION PROCESSED INORGANIC SEMICONDUCTOR SOLAR CELLS
José Manuel Marín Beloqui
Dipòsit Legal: T 68-2016

Chapter 3   **PhD Thesis**

Figure 2. The device shows a short circuit current, J_{SC}, of 8.26 mA/cm^2, a V_{OC} of 0.38 V and FF of 0.64, corresponding to a power conversion efficiency, $\eta = 2.04\%$ at 1 Sun.
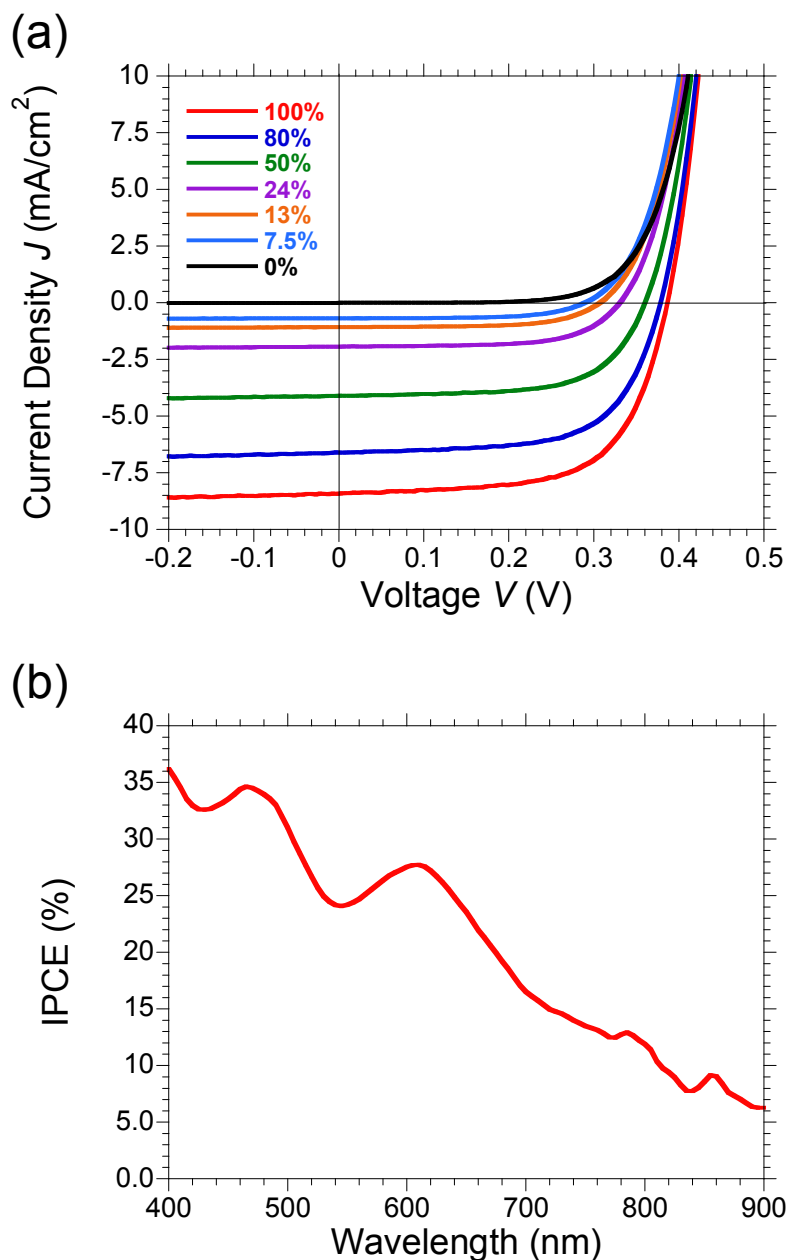
Figure 2. Current/voltage curves (a) for devices measured under standard AM 1.5 G conditions (100 mW/cm2), where the intensity of irradiance was fixed using neutral density filters. The legend shows the % of irradiance with respect to 1 Sun illumination, calculated using a calibrated silicon diode. IPCE for the corresponding device is shown in (b).

Figure 3(a) shows the relationship between J_{SC} and light intensity (LI), which has a power law behavior with the relationship $P \propto LI^{\alpha}$, with $\alpha = 1.01$, signifying that non-geminate recombination at short circuit is negligible and also that there is no significant space charge buildup[21,22]. The correlation between V_{OC} with LI is also shown in **Figure 3(b)**, showing a linear increase of V_{OC} with the logarithmic of LI. The slope of the curve in an ideal diode would correspond to the thermal voltage k_BT, the deviation from ideal behavior is termed the ideality factor and is calculated from the following equation:

$$n_{id} = \frac{e}{k_BT}\frac{dV_{oc}}{dln(LI)} \quad \textbf{Equation 1}$$

where, e is the elementary charge, k_BT is the thermal energy, with $n_{id} = 1.47$. Generally, the ideality factor ranges from 1 to 2 and it provides information on the origin of the charge recombination that occurs in a device. An ideality factor increasing from 1 indicates the presence of trap states, with higher values corresponding to the presence of deeper and more abundant traps. The ideality factor also gives an indication of what process is determining the charge carrier recombination dynamics, $n_{id} = 1$ signifying bimolecular recombination and $n_{id} = 2$ indicating Shockley-Read-Hall (SRH) recombination[13,23]. Therefore, the rather high value obtained for PbS/C$_{60}$ suggests that there is a significant concentration of trap states, which will affect the non-geminate recombination dynamics. In related studies, trap states (mid-gap states) have been shown to affect non-geminate recombination and furthermore the V_{OC} in PbS/methano-fullerene bilayer, although no relationship with charge carrier density was shown[24].

UNIVERSITAT ROVIRA I VIRGILI
SOLUTION PROCESSED INORGANIC SEMICONDUCTOR SOLAR CELLS
José Manuel Marín Beloqui
Dipòsit Legal: T 68-2016

Chapter 3   **PhD Thesis**

(a)

(b)
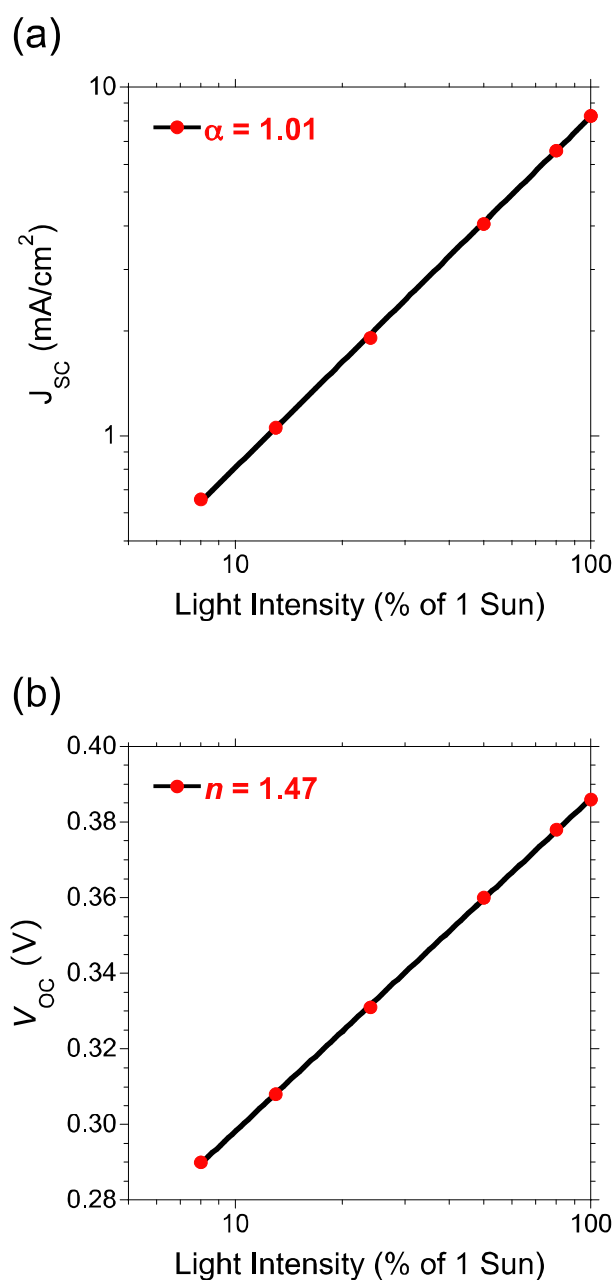
Figure 3. J_{SC} (a) and V_{OC} (b) plotted versus light intensity. In (a) α corresponds to the power law fit where $P \propto LI^{\alpha}$ and in (b) n corresponds to the ideality factor obtained from Equation (1).

To quantify the charge present in the device under illumination, we employed the photo-induced charge extraction technique, as used in previous publications by our group as well as others[25,26]. For this experiment, the device is held at open-circuit by applying either a light or electrical bias through a set of LEDs or external power source until steady state is reached (1-2 s) and then switched from open circuit to short circuit while simultaneously switching off the LEDs. Sweeping the bias from values higher

than V_{OC} at 1 sun (V_{OC}=0.38V at 1 sun in this case) to dark conditions allows a good estimate of the charge present in the device under working conditions to be obtained. **Figure 4** shows the charge density plotted *versus* light bias, which increases linearly to begin with before becoming exponential at higher applied bias (red curve). The geometrical capacitance was calculated by carrying out PICE measurements in the dark and under negative bias, as reported before[21], and was found to be 83 nF/cm^2. The linear dependence of charge *versus* bias at low light intensity is similar to the geometrical charges signifying that there is very little chemical charge built up in the active layer at low light bias, with the charges mostly present at the electrodes. At increased forward bias the charges in the device begin to increase exponentially to values higher than the corresponding capacitive charges. The charges can therefore be related to excess charge carriers generated in the photoactive region. This exponential increase has been previously attributed to the splitting of the quasi-Fermi levels in donor and acceptor molecules in organic bulk-heterojunction solar cells[10]. We can fit the data in **Figure 2** according to the following equation that correlates the charges in the device with the V_{OC}:

Figure 4. Photo-nduced charge extraction data for the same device measured under light bias and applied bias (dark and 1 Sun illumination). Charge losses during extraction are accounted for.
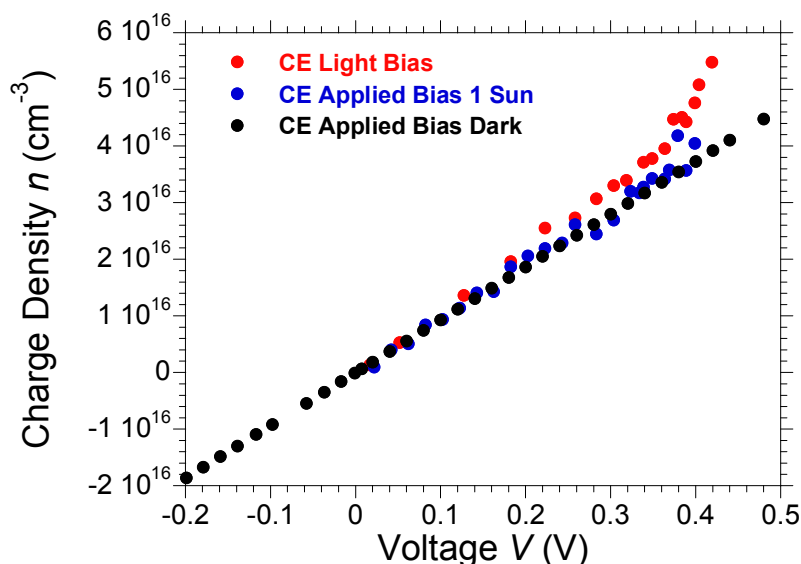
$$n = n_0 e^{\gamma V} \quad \textbf{Equation 2}$$

where, $n_0 \sim 2.77 \times 10^{15}$ carriers/cm^3 and $\gamma \sim 7.12$ V-1, if we consider the total charge in the device. The parameter γ provides an estimate of the tail of the density of states (DOS), and is considerably lower than an ideal semiconductor ($\gamma < 19$ V -1 for 2kT). This points towards the system having a high density of trap states and is consistent with the ideality factor measured from **Figure 3b**[27]. Our observations here of a low number of carriers and a low γ is similar to previous charge extraction measurements of planar heterojunction solar cells[21,26,28], and is due to the thin nature of the films and high energetic disorder[20,29].

PIT-PV measurements provide a measurement of the charge carrier lifetimes in the device. The PIT-PV experiment consists of holding the device at open-circuit under steady state conditions by applying a light bias via a ring of LEDs, akin to PICE. Next a small perturbation is applied to the device by, in this case, a laser. The small perturbation (5-10 mV) generates extra charges in the device that cannot be extracted, as the system is being held at open-circuit, forcing the charges to recombine. An added advantage of this technique is that the small excess charge generated decay mono-exponentially making it easy to calculate the excess charge carrier lifetime:

$$\Delta n = \Delta n_0 e^{-t/\tau_{\Delta n}} \quad \textbf{Equation 3}$$

where is the time, Δn_0 is the photogenerated charge at t = 0 and $\tau_{\Delta n}$ is the lifetime of the transient. For each point on the current-voltage curve we can obtain a specific lifetime. Plotting the measured small perturbation lifetimes, $\tau_{\Delta n}$ as a function of V_{OC} is shown in **Figure 5**, which shows a non-linear relationship between charge carrier lifetime and applied bias. The charge carriers in fact decay exponentially with bias with the function

UNIVERSITAT ROVIRA I VIRGILI
SOLUTION PROCESSED INORGANIC SEMICONDUCTOR SOLAR CELLS
José Manuel Marín Beloqui
Dipòsit Legal: T 68-2016

PhD Thesis   **Chapter 3**
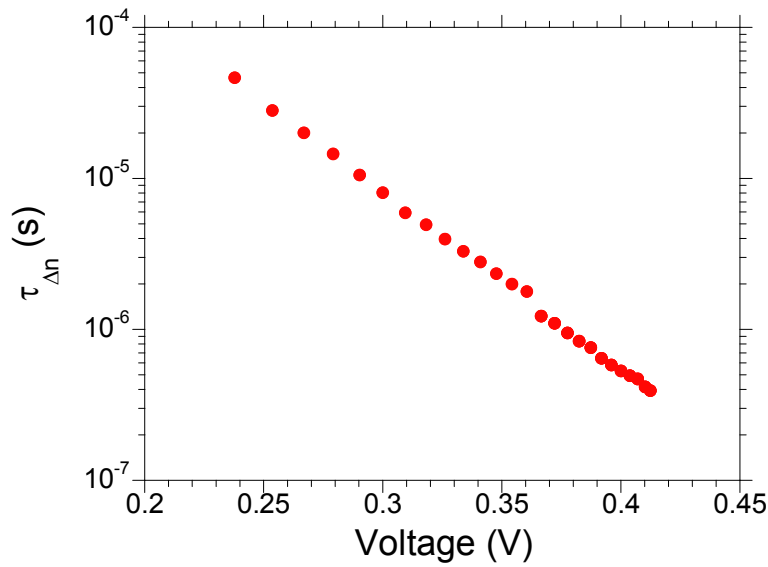
Figure 5. Small perturbation lifetime *versus* lifetime obtained from PIT-PV measurements.

$$\tau_{\Delta n} = \tau_{\Delta n_0} e^{-\beta V_{oc}} \quad \textbf{Equation 4}$$

where, $\tau_{\Delta n_0} \sim 0.012$ s, and β, the decay constant, is ~ 24.94 V^{-1}. This exponential decay is consistent with the behavior of organic solar cells. At 1 Sun conditions $\tau_{\Delta n}$ is < 1 μs; these lifetimes are very short in comparison to higher V_{OC} OSCs, which already suggests the reason for the low device V_{OC}.

Having now obtained the relationship between $\tau_{\Delta n}$ and applied bias as well as the behavior of n with applied bias, we can correlate $\tau_{\Delta n}$ with n by interpolating the applied bias with the exponential fit obtained from PICE under light bias. **Figure 6** shows the lifetime *versus* charge density, which displays a power law behavior:

UNIVERSITAT ROVIRA I VIRGILI
SOLUTION PROCESSED INORGANIC SEMICONDUCTOR SOLAR CELLS
José Manuel Marín Beloqui
Dipòsit Legal: T 68-2016

Chapter 3   **PhD Thesis**
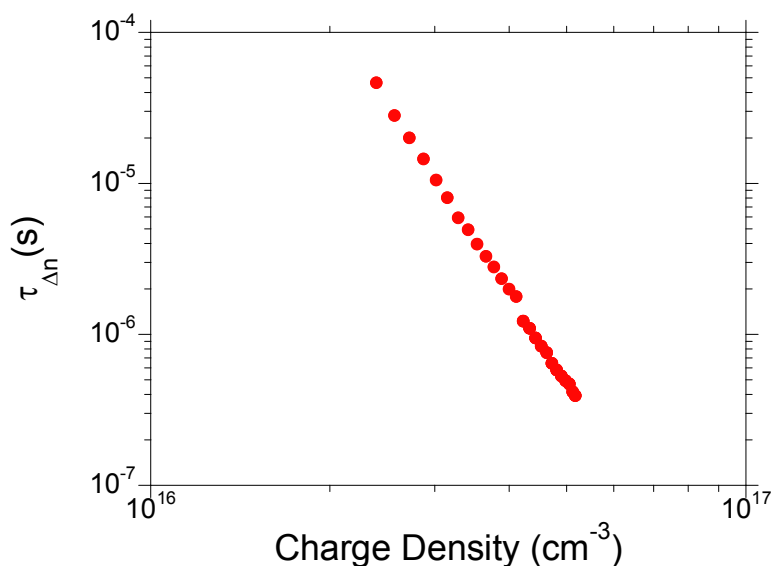
Figure 6. Small perturbation *versus* charge density, using the exponential relationship between charge density and bias obtained from PICE under light bias.

$$\tau_{\Delta n} \propto n^{-\lambda} \quad \textbf{Equation 5}$$

The power law, λ, can also be calculated simply by considering the exponential decay of $\tau_{\Delta n}$ *versus* bias (β) and the exponential growth of charge density *versus* bias (γ): β/γ = λ. This thus provides us with a relationship between charge density and the small perturbation charge carrier lifetime, as opposed to the total charge carrier lifetime, τ_n. Correcting for this is rather simple and has been shown to apply to both OSCs and dye-sensitized solar cells, with the total charge carrier lifetime:

$$\tau_n = \tau_{\Delta n}(\lambda + 1) \quad \textbf{Equation 6}$$

It has been shown for organic solar cells that the relationship between *n* and τ_n gives the empirical reaction order, Φ (Φ = λ+1) of the free charge carriers, with some values suggesting bimolecular recombination[20,30,31]. For the measured PbS/C$_{60}$ devices here, we obtain an empirical reaction order of 5.8. This is simply too high to be related to bimolecular recombination, but is not uncommon for such a thin active layer. For OSCs, many devices have shown high reaction orders too and in particular when the active layer thickness is very thin[32,33]. One of the reasons for the high values of Φ is due to a large gradient in carrier concentration[32], due to energetic disorder, surface recombination and trap-assisted recombination. What is important here however is that the relationship still gives us accurate information on the rate at which the charges are

recombining within the device, even though the origin of the recombination is not clear, and is most likely a convolution of different events occurring at the PbS/C$_{60}$ interface, within each respective layer, or at the contacts.

Having determined the correlation between charge density and charge carrier lifetime in the active layer, we attempt to reconstruct the *J-V* behavior of the hybrid PbS/C$_{60}$ device under 1 Sun conditions. Durrant and coworkers have shown that using a simple model that takes into account the flux of photo-generated charges (J_{gen}) and the flux of non-geminate recombination (J_{loss}) that it is possible to reconstruct the *J-V* curve accurately[33], using the relationship:

$$J = J_{gen} + J_{loss} \quad \textbf{Equation 7}$$

$$J_{loss} = \frac{edn}{\tau_n} \quad \textbf{Equation 8}$$

where *d* is the thickness of the active layer, *n* is the charge density and τ_n the charges lifetime. In this approximation it is assumed that the loss processes are simply due to non-geminate recombination and are negligible close to short-circuit. Increasing the bias closer to V_{OC}, the non-geminate recombination begins to increase significantly and at V_{OC} the flux of non-geminate recombination equals that of J_{gen}, Carrying out CE under 1 Sun illumination conditions (**Figure 4**) and applied electrical bias allows *n* to be calculated each point across the *J-V* curve. To reconstruct the *J-V* curve to the experimental one shown at 1 Sun in **Figure 2**, we allow $J_{gen} = J_{SC}$, and calculate J_{loss} using Equation 8. An additional correction to account for the small photoshunt is also applied using the experimental *J-V* data. This correction does not affect the calculated V_{OC} and any non-geminate recombination causing it can be ruled out based on the relationship between J_{SC} and LI having a power law = 1.01 (see **Figure 3a**). The voltage in cell is corrected for considering: $V_{cell} = V_{appl} - IR_s$, where R_s is the series resistance. The experimental and reconstructed *J-V* curves are shown in **Figure 7** and are in good agreement, with the reconstructed $V_{OC} = 0.383$ mV exactly matching the experimental V_{OC} of 0.383 mV. In other similar devices that we measured there was a small fluctuation between the calculated V_{OC} and the experimental V_{OC}, consistent with the trend observed for a range of different organic solar cells[34]. The fact that the 1 Sun *J-V* behavior can be reproduced using this simple relationship between generation and

recombination signifies that the origin the V_{OC} in these devices is field-independent and is controlled by non-geminate recombination. Knowing that non-geminate recombination is the key loss mechanism affecting the V_{OC} thus provides a route towards optimizing device performance further. Reducing the concentration of trap states is perhaps the most significant step with regards to optimization. CQDs in particular tend to have a high distribution of mid-gap states that trap charges and thus push the ideality factor higher; reducing these trap states will see more ideal diode behavior, longer charge carrier lifetime and thus higher V_{OC}. Recently, CQD solar cells have seen improvements in V_{OC} with either a reduction in trap states or through doping the transition metal acceptor. It will be interesting to see if the same procedure to reconstruct the *J-V* curve can be applied to other CQD-based solar cells such as depleted heterojunction devices, which have different working mechanism but like organic semiconductors tend to have a large degree of energetic disorder, unlike their bulk material properties.
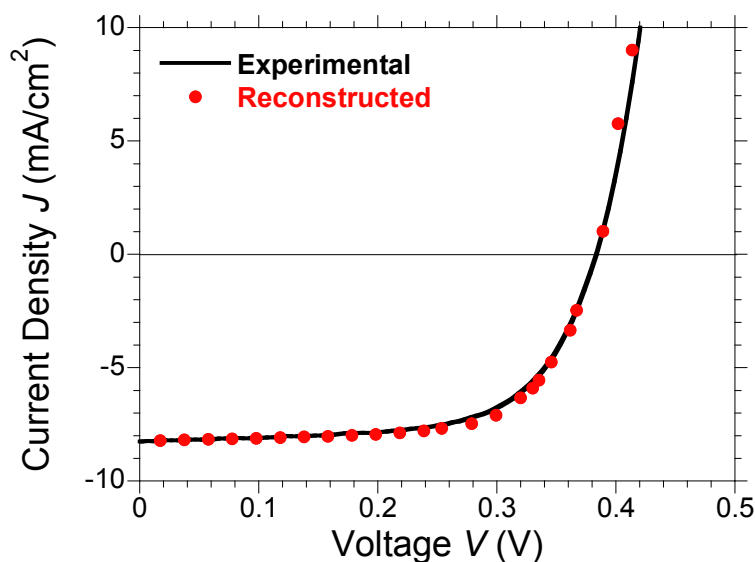
Figure 7. Comparison between the reconstructed *JV* curve using Equation 7 and the experimental *JV* curve as presented in **Figure 2**.

Conclusions

In summary, we have studied the optoelectronic performance of PbS/C_{60} devices through both steady state *J-V* characterization and transient optoelectronic measurements. From the data obtained we see that the open-circuit voltage increases linearly with the logarithm of LI, evidence for the increased splitting of quasi-Fermi levels with LI and correlated their relationship to obtain an ideality factor of 1.47, meaning that there is quite a large density of traps that affect non-geminate recombination. Furthermore, based on the relationship between J_{SC} and LI, non-geminate recombination is negligible at short circuit, suggesting that the origin of the photoshunt is a field dependent generation process. The charge carrier lifetime in the films is short, on the order of 1×10^{-6} s, with a steep decay order of 24.94, meaning charge carrier lifetime decreases rapidly with increasing bias. The charge density in the active layer is very low, as seen for similar organic bilayer devices, with most of the charges residing at the electrodes under low bias conditions, and increasing exponentially close to V_{OC}. Using the relationship between J_{gen} and J_{loss} we could accurately reconstruct the *J-V* curve proving that V_{OC} here is field independent and can be improved by reducing the rate of non-geminate recombination. More important, our results clearly demonstrate that increasing the lifetime of the charge carriers through reducing the trap states present at the PbS/C_{60} interface will lead to higher V_{OC} and thus improved efficiencies. Thus, the biggest room for improvement lies with the PbS CQD synthesis and choice of ligands/passivation layer.

UNIVERSITAT ROVIRA I VIRGILI
SOLUTION PROCESSED INORGANIC SEMICONDUCTOR SOLAR CELLS
José Manuel Marín Beloqui
Dipòsit Legal: T 68-2016

Chapter 3 - References   **PhD Thesis**

References

1   I. J. Kramer and E. H. Sargent, *ACS Nano*, 2011, **5**, 8506–14.

2   A. H. Ip, S. M. Thon, S. Hoogland, O. Voznyy, D. Zhitomirsky, R. Debnath, L. Levina, L. R. Rollny, G. H. Carey, A. Fischer, K. W. Kemp, I. J. Kramer, Z. Ning, A. J. Labelle, K. W. Chou, A. Amassian and E. H. Sargent, *Nat. Nanotechnol.*, 2012, **7**, 577–82.

3   A. J. Labelle, S. M. Thon, S. Masala, M. M. Adachi, H. Dong, M. Farahani, A. H. Ip, A. Fratalocchi and E. H. Sargent, *Nano Lett.*, 2015, **15**, 1101–8.

4   A. P. Alivisatos, *Science (80-.).*, 1996, **271**, 933–937.

5   I. Moreels, K. Lambert, D. Smeets, D. De Muynck, T. Nollet, J. C. Martins, F. Vanhaecke, A. Vantomme, C. Delerue, G. Allan and Z. Hens, *ACS Nano*, 2009, **3**, 3023–30.

6   O. E. Semonin, J. M. Luther, S. Choi, H.-Y. Chen, J. Gao, A. J. Nozik and M. C. Beard, *Science*, 2011, **334**, 1530–3.

7   J. Tang, X. Wang, L. Brzozowski, D. A. R. Barkhouse, R. Debnath, L. Levina and E. H. Sargent, *Adv. Mater.*, 2010, **22**, 1398–402.

8   A. G. Pattantyus-Abraham, I. J. Kramer, A. R. Barkhouse, X. Wang, G. Konstantatos, R. Debnath, L. Levina, I. Raabe, M. K. Nazeeruddin, M. Grätzel and E. H. Sargent, *ACS Nano*, 2010, **4**, 3374–80.

9   P. K. Santra, P. V. Nair, K. George Thomas and P. V. Kamat, *J. Phys. Chem. Lett.*, 2013, **4**, 722–729.

10   Y. Zhou, M. Eck, C. Veit, B. Zimmermann, F. Rauscher, P. Niyamakom, S. Yilmaz, I. Dumsch, S. Allard and U. Scherf, *Sol. Energy Mater. Sol. Cells*, 2011, **95**, 1232–1237.

11   E. J. D. Klem, C. W. Gregory, G. B. Cunningham, S. Hall, D. S. Temple and J. S. Lewis, *Appl. Phys. Lett.*, 2012, **100**, 173109.

12   J. Tang and E. H. Sargent, *Adv. Mater.*, 2011, **23**, 12–29.

13   K. Szendrei, W. Gomulya, M. Yarema, W. Heiss and M. A. Loi, *Appl. Phys. Lett.*, 2010, **97**, 203501.

14   J. J. Choi, Y.-F. Lim, M. B. Santiago-Berrios, M. Oh, B.-R. Hyun, L. Sun, A. C. Bartnik, A. Goedhart, G. G. Malliaras, H. D. Abruña, F. W. Wise and T. Hanrath, *Nano Lett.*, 2009, **9**, 3749–55.

UNIVERSITAT ROVIRA I VIRGILI
SOLUTION PROCESSED INORGANIC SEMICONDUCTOR SOLAR CELLS
José Manuel Marín Beloqui
Dipòsit Legal: T 68-2016

PhD Thesis   **Chapter 3 - References**

15   A. K. Rath, M. Bernechea, L. Martinez, F. P. G. de Arquer, J. Osmond and G. Konstantatos, *Nat. Photonics*, 2012, **6**, 529–534.

16   J. Albero, Y. Zhou, M. Eck, F. Rauscher, P. Niyamakom, I. Dumsch, S. Allard, U. Scherf, M. Krüger and E. Palomares, *Chem. Sci.*, 2011, **2**, 2396.

17   E. Martínez-Ferrero, I. M. Seró, J. Albero, S. Giménez, J. Bisquert and E. Palomares, *Phys. Chem. Chem. Phys.*, 2010, **12**, 2819–21.

18   M. Shalom, J. Albero, Z. Tachan, E. Martínez-Ferrero, A. Zaban and E. Palomares, *J. Phys. Chem. Lett.*, 2010, **1**, 1134–1138.

19   T. Zewdu, J. N. Clifford, J. P. Hernández and E. Palomares, *Energy Environ. Sci.*, 2011, **4**, 4633.

20   C. G. Shuttle, R. Hamilton, B. C. O'Regan, J. Nelson and J. R. Durrant, *Proc. Natl. Acad. Sci. U. S. A.*, 2010, **107**, 16448–52.

21   D. Credgington, Y. Kim, J. Labram, T. D. Anthopoulos and J. R. Durrant, *J. Phys. Chem. Lett.*, 2011, **2**, 2759–2763.

22   L. J. A. Koster, V. D. Mihailetchi, H. Xie and P. W. M. Blom, *Appl. Phys. Lett.*, 2005, **87**, 203502.

23   C. van Berkel, M. J. Powell, A. R. Franklin and I. D. French, *J. Appl. Phys.*, 1993, **73**, 5264.

24   N. Zhao, T. P. Osedach, L.-Y. Chang, S. M. Geyer, D. Wanger, M. T. Binda, A. C. Arango, M. G. Bawendi and V. Bulovic, *ACS Nano*, 2010, **4**, 3743–52.

25   G. F. A. Dibb, T. Kirchartz, D. Credgington, J. R. Durrant and J. Nelson, *J. Phys. Chem. Lett.*, 2011, **2**, 2407–2411.

26   A. Sánchez-Díaz, L. Burtone, M. Riede and E. Palomares, *J. Phys. Chem. C*, 2012, **116**, 16384–16390.

27   A. Maurano, C. G. Shuttle, R. Hamilton, A. M. Ballantyne, J. Nelson, W. Zhang, M. Heeney and J. R. Durrant, *J. Phys. Chem. C*, 2011, **115**, 5947–5957.

28   A. Foertig, A. Wagenpfahl, T. Gerbich, D. Cheyns, V. Dyakonov and C. Deibel, *Adv. Energy Mater.*, 2012, **2**, 1483–1489.

29   J. Bisquert and G. Garcia-Belmonte, *J. Phys. Chem. Lett.*, 2011, **2**, 1950–1964.

30   A. Maurano, R. Hamilton, C. G. Shuttle, A. M. Ballantyne, J. Nelson, B. O'Regan, W. Zhang, I. McCulloch, H. Azimi, M. Morana, C. J. Brabec and J. R. Durrant, *Adv. Mater.*, 2010, **22**, 4987–92.

UNIVERSITAT ROVIRA I VIRGILI
SOLUTION PROCESSED INORGANIC SEMICONDUCTOR SOLAR CELLS
José Manuel Marín Beloqui
Dipòsit Legal: T 68-2016

Chapter 3 - References   **PhD Thesis**

31   C. G. Shuttle, B. O'Regan, A. M. Ballantyne, J. Nelson, D. D. C. Bradley and J. R. Durrant, *Phys. Rev. B*, 2008, **78**, 113201.

32   T. Kirchartz and J. Nelson, *Phys. Rev. B*, 2012, **86**, 165201.

33   D. Credgington and J. R. Durrant, *J. Phys. Chem. Lett.*, 2012, **3**, 1465–1478.

34   J. Tang, L. Brzozowski, D. A. R. Barkhouse, X. Wang, R. Debnath, R. Wolowiec, E. Palmiano, L. Levina, A. G. Pattantyus-Abraham, D. Jamakosmanovic and E. H. Sargent, *ACS Nano*, 2010, **4**, 869–78.

Chapter 4

Double Heterojunction Solar Cells. The Methylammonium Lead Iodide Perovskite

UNIVERSITAT ROVIRA I VIRGILI
SOLUTION PROCESSED INORGANIC SEMICONDUCTOR SOLAR CELLS
José Manuel Marín Beloqui
Dipòsit Legal: T 68-2016

PhD Thesis   **Chapter 4**

Perovskite is a mineral compound, $CaTiO_3$, named by Lev Perovski with a (usually distorted) cubic crystal structure where Calcium, the bigger cation, is in the middle of the unit cell (A), the Titanium is in the vertex (B) and the Oxigen is in octahedral coordination of the Ti, occupying the middle of the edges of the unit cell (X), as shown in **Figure 1**.

Perovskite is also the name of the minerals category that share the same crystal unit cell ABX_3 (**Figure 1**). These materials have been widely used for electronic applications, but the perovskite oxides were the most used due to their ferroelectricity and superconductivity properties[1], they also have been studied as promising anodes[2]. However in the last few years the halide perovskite have attracted so much attention because of their photovoltaic properties.

UNIVERSITAT ROVIRA I VIRGILI
SOLUTION PROCESSED INORGANIC SEMICONDUCTOR SOLAR CELLS
José Manuel Marín Beloqui
Dipòsit Legal: T 68-2016

Chapter 4   **PhD Thesis**
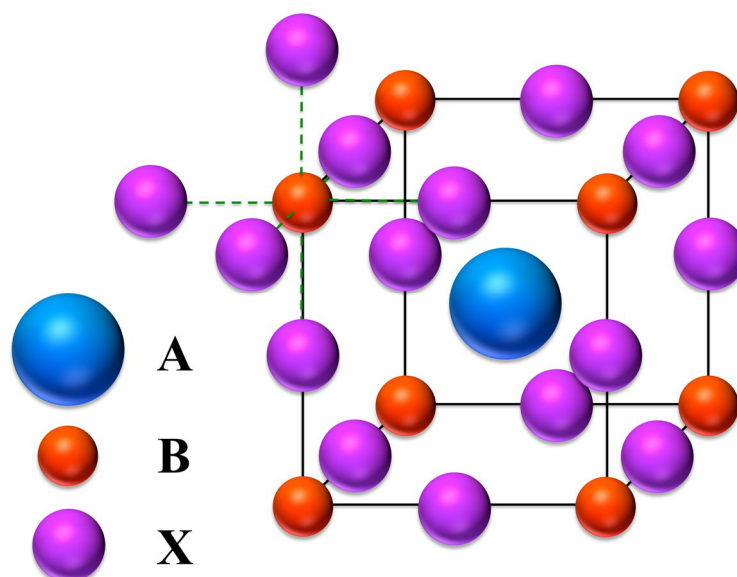
Figure 1. Diagram where is shown the unit cell of the perovskite crystal structure. A (blue ball) is the bigger cation, B (red ball) the smaller cation and X the anion of the compound. Green dashed lines show the octahedral coordination of X with B.

The tolerance t and the octahedral μ factors dictate the crystallographic structure and stability of the material[3]. **Equation 1** defines the tolerance factor, being R_X, R_A and R_B the ionic radii of the material components.

$$t = \frac{R_A + R_X}{\sqrt{2}\,R_B + R_X} \qquad \textbf{Equation 1}$$

The value of μ is calculated by **Equation 2**

$$\mu = \frac{R_B}{R_X} \qquad \textbf{Equation 2}$$

For halide perovskites (X=F, Cl, Br, I), these values have shown to be $0.81 < t < 1.11$ and $0.44 < \mu < 0.90$. But only for t values between the 0.89 and 1.0 the cubic structure is obtained, instead of the distorted ones, tetragonal or orthorhombic.

The most interesting material for photovoltaic applications, the one presented in this thesis, is the halide perovskite ABX_3 where A is an organic cation, being the methylammonium (MA, $CH_3NH_3^+$) the most usual one, with R_A= 0.18 nm[4], but formamidinium (FA, $NH_2CH=NH_2^+$) has also given good results[5], with a stimated

radium of 0.19 - 0.22 nm [6]. For efficient cells, the B has to be Lead, Pb, with $R_B=$ 0.119 nm. Still, Tin, Sn ($R_B=0.110$ nm), is a possible substitute for Lead, due to its lower toxicity and theoretically more ideal bandgaps[7], but when Sn is used the perovskite is easily degradated by the oxidation of Sn to SnI_4. The halogen can be Iodine ($R_X= 0.220$ nm), in the most of the cases, Bromine ($R_X= 0.196$ nm), or Chlorine ($R_X= 0.181$ nm).

$CH_3NH_3MX_3$ was firstly reported by Weber in 1978[8,9], where the metal was Pb or Sn, and the halogen was I, Br and Cl. Weber reported the cubic unit cell parameters, being, the arista of the cube, *a*, 0.568, 0.592 and 0.627 nm for perovskites where the X was Cl, Br, and I respectively. As seen, the cubic unit cell size increased with the size of the halide.

The crystalline structure of the perovskite strongly influences its optical properties. Usual $CH_3NH_3PbI_3$ has a bandgap around 1.55 eV, calculated from its IPCE, that is not enough for a panchromatic light absorption as it is limited to 800 nm. The perovskite bandgap could be modified changing the elements in the perovskite crystal structure in order to extend its absorption limit to longer wavelengths, being carefully enough to not diminish its absorption coefficient. Introducing other organic cation we modify the B-X-B bond length and angle and this modify the bandgap maintaining the valence band maximum[10]. Replacing the MA cation by FA, the bandgap is reduced by 0.07 eV, increasing the absorption of the perovskite 40 nm[11]. If Lead is replaced by Tin, the B-X bond is modified, decreasing the bandgap from 1.55 to 1.17 eV[12], depending of the amount of Sn in the crystal structure, as the bandgap will decrease as increases the amount of Sn. This modification of the B-X bond will affect both, the valence and the conduction band of the perovskite[13]. However, the substitution of Pb by Sn decreases the absorption coefficient, being necessary an equilibrium of Pb/Sn ratio in order to enhance the absorption limit without losing much absorption coefficient. The change of the halogen also changes the optical bandgap, being these bandgaps 1.55 (1.55), 1.78 (2.00) and 1.55 (3.11) for I, Br and Cl perovskites respectively with tetragonal and cubical (between parenthesis) structures.

Moreover, electric properties are also linked with the perovskite crystal structure. Giant dielectric constant observed in perovskites under illumination,

especially at low frequencies, is related with the molecular orientation of the MAI cation[14]. Furthermore, the higher electrical conductivity of Sn-based perovskites is attributed to the infinite linear I-Sn-I chains in the perovskite structure[15].

The attention that has brought perovskite solar cells has been unseen in any other photovoltaic technology, exponentially increasing the publications, going from 14 papers in 2012, 52 in 2013, 438 in 2014 to 469 in the first six months of 2015 (**Figure 2)**. Besides, citations have also enhanced in a similar way in only few years (**Figure 2**).
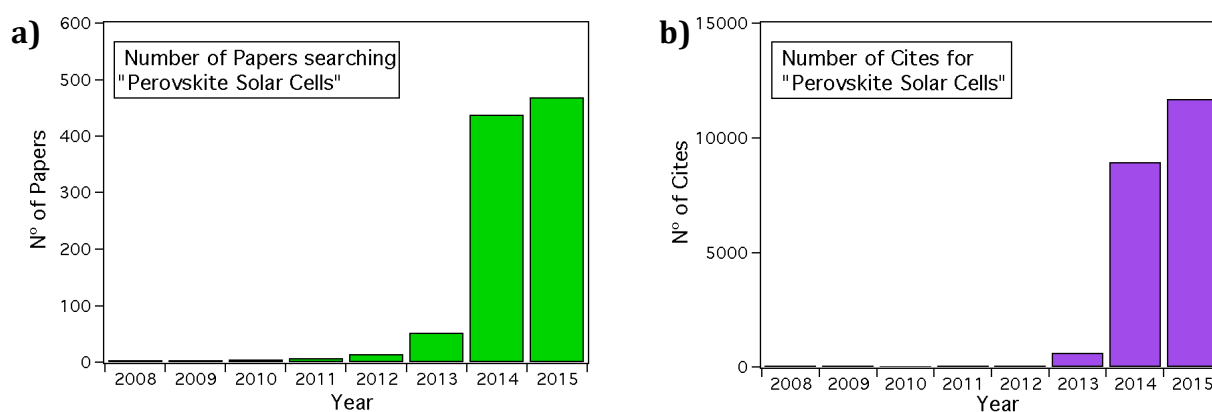
Figure 2. Number of publications **a)** and cites **b)** by year obtained when "Perovskite Solar Cells" was searched on ISI Web of Knowledge on July the 1st.

This can be only explained by the fast enhancement in efficiency in last few years overcoming other more well-known technologies such as DSSCs, QDSCs or OSCs, as seen in **Figure 3**.

Despite the fact that perovskite materials have been used for more than a century in different kind of devices[16], the first time that this organic-inorganic halide perovskite were used as a component in different devices was in the 90's by Mitzi[17,18], who used perovskite in transistors and LEDs. However, their photovoltaic effect was not really studied, even when it was anticipated[17].
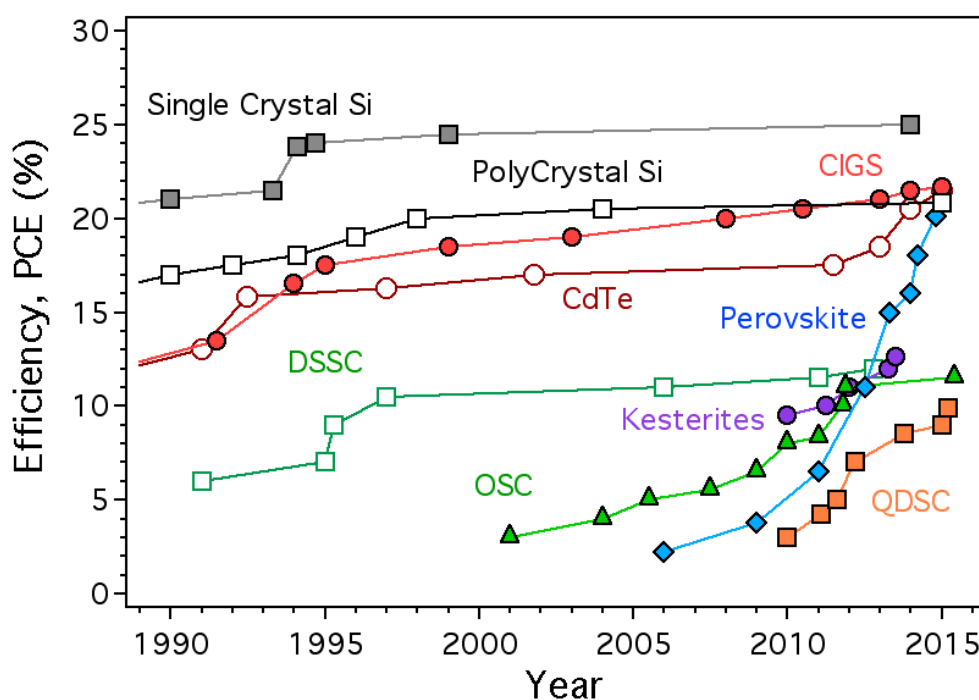
Figure 3. Efficiency evolution from 1990 to 2015 with the values presented in NREL chart in www.nrel.gov/ncpv.

Miyasaka was the first, in 2006, who reported an actual device using perovskite in a conference obtaining a 2.2% of efficiency with methylammonium lead bromine (MAPBr), acting as a dye in a DSSC[19]. Later in 2009, he obtained a 3.8% changing bromine by iodine[20].
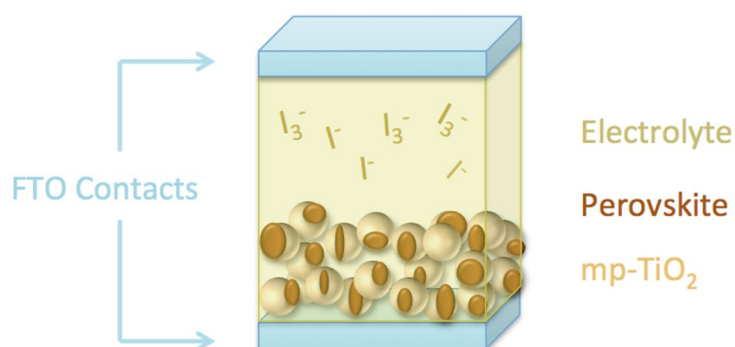
Figure 4. Device architecture where perovskite was used in an usual DSSC configuration with liquid electrolyte.

UNIVERSITAT ROVIRA I VIRGILI
SOLUTION PROCESSED INORGANIC SEMICONDUCTOR SOLAR CELLS
José Manuel Marín Beloqui
Dipòsit Legal: T 68-2016

Chapter 4   **PhD Thesis**

In 2011, Nam-Gyu Park used a thinner mp-TiO$_2$ layer obtaining a 6.5% of efficiency[21]. In this case, perovskite was deposited as hemispherical nanoparticles over the TiO$_2$, exhibiting better absorption than N719 films of the same thickness. But perovskite was still used as a dye in a DSSC and liquid electrolyte dissolved the perovskite making these cells very unstable.

The real breakthrough was performed in 2012 changing the previously reported DSSC architecture into a Solid State Dye-Sensitized Solar Cell (SS-DSSC), replacing the liquid electrolyte by a solid one, the 2,2',7,7'-tetrakis(N,N-di-p-methoxyphenulamine)-9-9'-spirobifluorene, called spiro-OMeTAD[22]. Not only the efficiency increased, reaching almost 10%, also, the stability was really good, maintaining the efficiency over 500 hours.
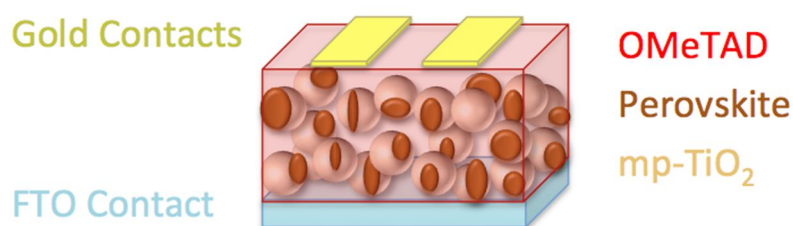
Figure 5. Device architecture where solid electrolyte was replaced by the solid one (spiro-OMeTAD).

At the same time but in a independent way, Snaith's group[23] reported a 10.9% efficiency using a mixed halide instead the pure iodine perovskite, where PbCl$_2$ was used instead the PbI$_2$ obtaining the CH$_3$NH$_3$I$_{3-x}$Cl$_x$ perovskite. The amount of Chlorine was thought to be stoichiometric (x=1)[23], but further studies was found that the Chlorine was present in little amount[24] in the perovskite. However, the effect of the chlorine is still under debate, but it seems that improves the morphology of the film[25]. Another important breakthrough was the use of of the insulating Al$_2$O$_3$ scaffold instead the electron acceptor mesoporous TiO$_2$ layer. Proving that the perovskite was able to transport both holes and electrons and confirming that perovskite was not a dye.
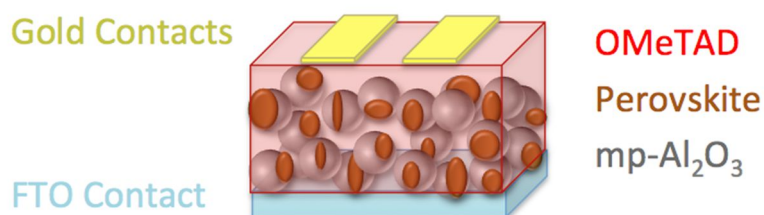
Figure 6. Device where an insulating Al_2O_3 layer replaced the usual TiO_2.

Another step ahead in efficiency was performed by Gratzel group including a perovskite capping layer over the mesoporous layer in order to decrease the recombination in the device obtaining a 12.0%[26].
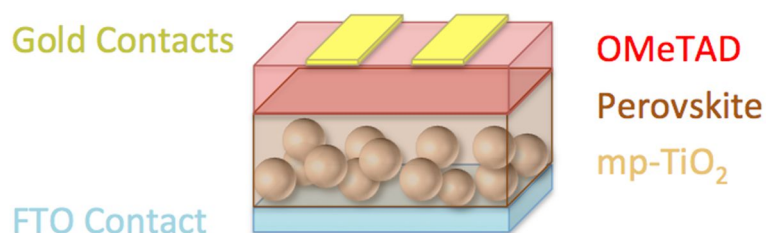
Figure 7. Scheme where the device configuration of a mesoporous TiO_2 with a capping perovskite layer is shown.

Afterwards, Seok group increased efficiency with a mixed Bromine Iodine perovskite to a 12.3%[27]. Best efficiencies were obtained when Bromine levels were low (<10%), but with higher Bromine content (>20%) higher moisture stability was obtained. This effect was explained in the paper due to the pseudo cubic structure for smaller Br radius.

Later, Gratzel´s group published a work improving the morphology of the perovskite layer using a two-step process of deposition obtaining a 15% of efficiency[28]. Snaith group was also dedicated to improve the morphology of the perovskite changing the deposition method. In this case, a device without any scaffold (flat device) depositing the mixed perovskite by two-source evaporation, obtaining 15.4%[29]. Evaporation method has the advantage that increased a lot the smoothness

and improved morphology of the perovskite layer, decreasing the pinholes that contacted HTM with the d-TiO$_2$ that decrease the efficiency.

Next, it was Yang Yang's who increased efficiency doping the d-TiO$_2$ with Yttrium of a flat solar cell (without any scaffold) to improve the charge extraction of the device[30]. However, this result was not certified.

Recently, formamidinium has proven to be a better alternative to methylammonium because they increase the t factor and push the perovskite to a symmetric cubic structure. Seok's group used this organic cation and DMSO as solvent, instead the usual DMF, reporting a certified 20.1%[31].

Besides there are several papers that did not supposed a breakthrough in efficiency, but they were helpful in the understanding of the working conditions of the cell or in the future applicability of these devices.

PSC and the rest of third generation solar cells have some applications that are not possible with Silicon or other photovoltaic technologies, for example flexible and transparent solar cells. Flexible solar cells are useful for indoor applications as they can be used as different energy providers for electronic devices, as for example laptop and tablet chargers that are already for sale. Transparency in solar devices is a very interesting property as they can be used as windows in every building providing energy as well as different colors.

For flexible solar cells, substrates have to be changed from rigid glass/FTO to a flexible polymeric substrate, forbidding high temperature steps as the annealing of the TiO$_2$ layers. In order to improve this, solar cells with ZnO layers have been used to remove the high temperature steps from the fabrication process, still obtaining good efficiencies, 15.7%[32]. In fact, there are some reported cases of efficient perovskite solar cells on flexible substrates[24,33].

As previously said, transparent devices are a very interesting due to its use as a window, like in the EPFL campus (Switzerland) where DSSC are actually being used as windows using transparent electrodes. Snaith and coworkers published efficient and transparent solar cells that are suitable for solar windows, depositing the perovskite as isolates islands, allowing the light to trespass the light, but with the

UNIVERSITAT ROVIRA I VIRGILI
SOLUTION PROCESSED INORGANIC SEMICONDUCTOR SOLAR CELLS
José Manuel Marín Beloqui
Dipòsit Legal: T 68-2016

PhD Thesis   **Chapter 4**

necessary amount of perovskite to absorb the light. Also, in order to make this application more attractive changing the brown color of the perovskite devices, Míguez in collaboration with Snaith prepared different photonic mesoporous layer in order to set different colors[34].

Following applicability issues, stability is a major aspect to take into account in perovskite solar cells. Even though these cells have shown better stability than other third generation solar cells[35–37], it is still far away the desired for commercial use. The main cause for this lack of stability of the devices is the moisture and oxygen that degrades the perovskite. Water breaks the ionic bond between the ionic species reverting the crystallization reaction of perovskite, giving as subproducts MAI and PbI_2, as indicates the yellow colour of the perovskite when it is degraded. However, the oxygen harms the perovskite in its superoxide form (O_2^-) that is formed by the reaction between the oxygen and the photoexcited perovskite. Then, the superoxide reacts with the perovskite, deprotonating the MA cation, creating water in the process that accelerates the degradation of the perovskite[38].

Besides, HTM, due to its inorganic nature, is also responsible of the lack of the device stability. In order to improve this, organic HTM have been changed by an inorganic HTM obtaining higher stability but lower efficiencies. Kamat and co-workers published 6.0% efficiency perovskite devices changing the OMeTAD by CuI[39]. Later a 12.4% was obtained with CuSCN acting as a hole transporting material[40]. Additionaly, the HTM was removed by Gratzel, that used TiO_2 and ZrO_2 as scaffolds and a Carbon layer to deposit the perovskite obtaining 12.8% stable devices for more than 1000 hours[35]. As well as some examples with lower efficiency of HTM-free devices have been published[41].

As said before, there are some publications that have help to understand the working conditions of the actual solar device. Snaith[42] and Gratzel[43] groups published at the same time in Science, being both papers consecutively printed, a Photoluminiscence study where the exciton diffusion length was calculated quenching the fluorescence with a hole and an electron quencher. They calculated the mixed halide perovskite diffusion length to be one order of magnitude higher than pure iodine one.

Other interesting paper that is also related with this thesis is the one published by Mosser et al in Nature Photonics[44]. In this paper they identified by Transient Absorption Spectroscopy (TAS) all the process lifetimes that occur in perovskite solar cells depositing perovskite over Al_2O_3 and TiO_2 with and without a HTM layer (OMeTAD). Perovskite injection of electrons in TiO_2 was found to be in the picosecond time scale, the perovskite hole regeneration in the nanosecond scale, and recombination between electrons in TiO_2 and holes in HTM in the microsecond time scale.

Bisquert´s group also published several papers of Impedance Spectroscopy (IS)[14,45,46] in order to dilucidate the inner electrical phenomena in perovskite devices. They found that MAPI perovskite exhibit a huge dielectric constant and the polarization in the device is amplified by an external voltage and illumination. Moreover, an extremely uncommon very slow V_{oc} decay, corresponding to a slow dynamic process increasing the capacitance at low frequency that gives origin to the hysteresis. However, the impedance spectroscopy studies have to go further to get a common model to match the impedance measurements.

One of the most interesting ability of perovskites is their suitability for tandem solar cells use, highly increasing their theoretical maximum efficiency combining the high Voc of perovskite solar cells and the current of a CIGS or a Si solar cell. McGehee[47] published a tandem joining perovskite with CIGS and Silicon solar cell demonstrating the suitability of these kind of devices in order to overcome the efficiency of the raw CIGS and Silicon solar cells.

One thought that has to be in mind is that efficiencies are not the same at lab scale, where solar cells are of little size (between 1 and 0.01 cm^2) far from the sizes needed for its future use in the daily life. For perovskite solar cells, IMEC recently published a panel of 16 cm^2 that reach a 11% of efficiency[48] still far from the 20% obtained at lab-scale.

Hysteresis

One of the most studied effects in PSC unseen in the previously reported third-generation cells is the hysteresis shown in these devices when the J-V curve is measured. This effect is seen when the J-V curve shows different shape when the direction of the sweep is from short-circuit to open-circuit (forward scan, FS) and open-circuit to short-circuit (reverse scan, RS) (**Figure 8a**). This phenomenon affects the J-V parameters, (Jsc, Voc, FF and PCE), being fill factor the most influenced. But, this dependence of the shape of the J-V curve is not only dependent of the sweep direction of the measurement, also of the scanning parameters such as the time that the cell is left since the voltage is applied and the current point is measured (delay time), the time that current point is measured (integration time) and time that voltage is applied before measurement of the current point (**Figure 8b**). Also, it depends of the preconditions of the measurements; the J-V curve will be different if voltage is applied to the device before the measurement.

However, this effect was also seen in other photovoltaic technologies like CIGS, CdTe and amorphous silicon where high internal capacitances were showed. In these cases hysteresis was attributed to charge carrier charge accumulation in the depletion layer, the existence of defect states and ion movement inside the crystal structure[20,22,23].

a)

b)
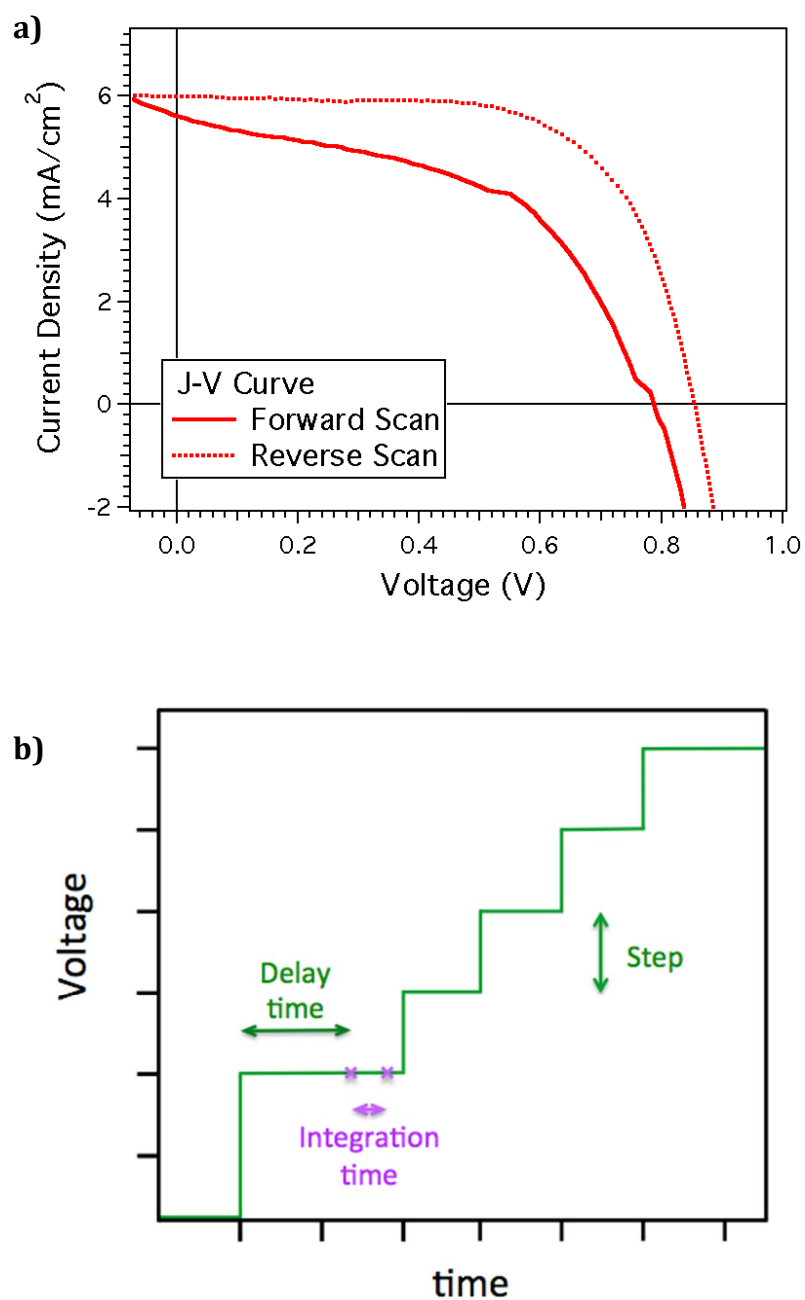
Figure 8. a) J-V curve showing hysteresis b) Scheme where the different parameters
to measure the J-V curve are shown.

Although this effect is present in all perovskite devices, still in some of them hysteresis is almost negligible, it will depend of different factors. The structure of the device has shown to be a determining factor for hysteresis, being the flat devices (those with any scaffold where perovskite is deposited over d-TiO$_2$) and mesosuperstructured (when Al$_2$O$_3$ is used as scaffold) the ones where this effect is

more severe. Nonetheless, when mp-TiO$_2$ or planar[49] (PEDOT and PCBM) architectures are used hysteresis becomes almost suppressed. Crystal size has shown to be also a critical factor that affects the hysteresis in the device, decreasing the hysteresis as higher the crystal size[50]. Additionally, the cell contacts have an enormous effect in hysteresis[51], and the different processes that occurs in the interfaces between the perovskite and the contacts

Most of the papers discussing this matter use different time solved J-V experiments[52,53] in order to identify the time scale of the changes in the inner device system that turn into the hysteresis. It has been seen that there is a fast process, in the microsecond scale, that generates the photocurrent, and a slow process, in the millisecond-second scale, that defines the rest of conditions, including the hysteresis [54,55].

Several publications have shown Impedance Spectra (IS) studies where devices with higher hysteresis show lower capacitance at lower frequencies C$_{LF}$, increases with the crystal size and with the presence of the mp-TiO$_2$[52]. This capacitance has been identified as responsible of the hysteresis being related to the relaxation of polarization[14,46] and correspond with the slow process of the J-V hysteresis.

Despite of the many examples of research about this phenomenon in perovskite solar cells, the actual origin of it remains unclear and still causes some controversy. In bibliography is possible to see papers where this circumstance it is explained by trapping/de-trapping of charge carriers[52,56,57], changes in absorber or contact conductivity[58], ferroelectricity[11,56,59–61] and ion migration[56,59,62–64]

The trapping-detrapping mechanism suggests that charges could be accumulate in inner perovskite trap states or more likely, in the perovskite surface and interfaces. Under forward bias working conditions, electron and holes get trapped inside this large amount of traps, when reverse bias is applied, these charges are released from the traps obtaining higher efficiencies[56,59]. This is in accordance with the fact that hysteresis disappears at fast sweep rates, as the charges have no time to get detrapped. However, the time of this trap/detrapping mechanism could not be in

the same range than sweep rate, and the amount of necessary charges to cause the hysteresis is calculated to be around 30 mC/cm^2, which is unrealistically high[55].

On other hand, the methylammonium iodide (MAI) is highly rotationally mobile inside the perovskite structure. The variation of the orientation of the MAI$^+$ originates ordered domains resulting in an inner polarization inside the perovskite. This polarization causes a field that changes with the direction of the external voltage, causing differences in the J-V curve measured at reverse and forward conditions. This hypothesis identifies the slow process as the changes of ferroelectric structure, and the fast to the carrier distribution[65].

But the most feasible responsible of the hysteresis effect regarding the last articles published, is the ion migration inside the perovskite structure by the iodine ion. This effect was previously seen in PbI$_2$[66], where halide vacancies are created after the compound is excited by light. The enhancement of halide vacancies enables the ion migration obtaining high ionic conductivity in the material.

In this case, the iodine migration to the vacancies improves the charge collection of the perovskite under the effect of an electric field. A built-in electric field caused by the difference in the work functions of the contacts is present in the perovskite layer at short-circuit. This field causes the migration of iodine to the contacts, screening the field caused by the applied voltage. If the cell is measure in reverse conditions, a forward bias is applied that dissipates the ionic charge in the contacts. This enhances the collection of the charges as it disappears the screening of the built-in field[53].

The ion conductivity is very sensitive to the stoichiometry, the degree of crystallinity as well with the crystal size. All these factors will highly affect the number of vacancies in the perovskite. This huge dependence in many factors could cause the disparity in hysteresis results obtained in different groups.

Future Commercialization

First barrier to pass trough for perovskite solar cells to be commercialized is the low stability of perovskite, that is damaged by water and oxygen as described before in the introduction. This problem could be palliated with encapsulation, but it increases the prize of the manufacturing and the fabrication of these cells.

Although they have proved to be stable after the equivalent to 100 hours at 1 sun[67], or more than 500 hours in dark conditions[22], their moisture and oxygen sensibility is a problem for further commercialization. Perovskite lack of stability makes these devices to require a more expensive encapsulation than their more near competitor (CdTe). However, some investigation to avoid the humidity with overlayers[68], obtaining good efficiencies even after watering the cells, as well new cheap encapsulation methods[33] have been performed.

Another issue to take in account for further commercialisation is the toxicity of these kind of cells due to the presence of Pb, a toxic heavy metal. The European Restriction of Hazardous Substances (RoHS) makes a restriction near 0.1% of Pb by weight in a so-called homogeneous layer, which is defined by RoHS as a "uniform composition through-out" or a layer "that cannot be… separated into different materials by mechanical actions such as unscrewing, cutting, crushing, grinding and abrasive processes"[69]. Most of the perovskite solar cells are far for compliance these requirements, but ETA and sensitized perovskite devices where the mp-TiO_2 pores are filled with OMeTAD, the Pb amount is only about a 0.4-0.5%, which overcomes the limit of RoHS, but not appreciably. Also, the major competitor of perovskite solar cells, CdTe devices, doesn't satisfy the RoHS limit either (0.01% in the case of Cd). However, the RoHS makes an exception in the case of the photovoltaic modules, at least for large, stationary, professionally installed systems. Still, this legislation can change in the few years and new approaches have to be done in order to avoid future problems with the lead toxicity. One of these approaches is to exchange the Pb by a less toxic perovskite such as $CH_3NH_3SnI_3$[70,71].

Concerning the price of the devices, there is not an actual real price for module, even though Prof. Snaith predicts to be "something like 30 cents per Watt peak"[72]. Again, we can compare it with the CdTe as they have very similar structure

UNIVERSITAT ROVIRA I VIRGILI
SOLUTION PROCESSED INORGANIC SEMICONDUCTOR SOLAR CELLS
José Manuel Marín Beloqui
Dipòsit Legal: T 68-2016

Chapter 4   **PhD Thesis**

and efficiencies. In 2013 the fabrications costs of a CdTe module were reported to be 0.54 $ per Watt or 72 $ m^{-2} [73], being predicted to be decreased to 68$ m^{-2} in 2017[74]. The fabrication should be similar to the perovskite, because the main cause of the price are shared materials such as FTO-glass.

But the major advantage of the perovskite solar cells in order to get commercialised is their use in tandem solar cells where efficiencies over 30% could be achieved.

UNIVERSITAT ROVIRA I VIRGILI
SOLUTION PROCESSED INORGANIC SEMICONDUCTOR SOLAR CELLS
José Manuel Marín Beloqui
Dipòsit Legal: T 68-2016

PhD Thesis   **Chapter 4 - References**

References

1   Y. Maeno, H. Hashimoto, K. Yoshida, S. Nishizaki, T. Fujita, J. G. Bednorz and F. Lichtenberg, *Nature*, 1994, **372**, 532–534.

2   J. Macías, A. A. Yaremchenko, D. P. Fagg and J. R. Frade, *Phys. Chem. Chem. Phys.*, 2015, **17**, 10749–58.

3   C. Li, X. Lu, W. Ding, L. Feng, Y. Gao and Z. Guo, *Acta Crystallogr. B.*, 2008, **64**, 702–7.

4   N. K. McKinnon, D. C. Reeves and M. H. Akabas, *J. Gen. Physiol.*, 2011, **138**, 453–66.

5   N. J. Jeon, J. H. Noh, W. S. Yang, Y. C. Kim, S. Ryu, J. Seo and S. Il Seok, *Nature*, 2015, **517**, 476–480.

6   M. A. Green, A. Ho-Baillie and H. J. Snaith, *Nat. Photonics*, 2014, **8**, 506–514.

7   P. Umari, E. Mosconi and F. De Angelis, *Sci. Rep.*, 2014, **4**, 4467.

8   D. Weber, *Naturforsch*, 1978, **33b**, 862–865.

9   D. Weber, *Naturforsch*, 1978, **33b**, 1443–1445.

10   W. Geng, L. Zhang, Y.-N. Zhang, W.-M. Lau and L.-M. Liu, *J. Phys. Chem. C*, 2014, **118**, 19565–19571.

11   C. C. Stoumpos, C. D. Malliakas and M. G. Kanatzidis, *Inorg. Chem.*, 2013, **52**, 9019–38.

12   F. Hao, C. C. Stoumpos, R. P. H. Chang and M. G. Kanatzidis, *J. Am. Chem. Soc.*, 2014, **136**, 8094–9.

13   T. Umebayashi, K. Asai, T. Kondo and A. Nakao, *Phys. Rev. B*, 2003, **67**, 155405.

14   E. J. Juarez-Perez, R. S. Sanchez, L. Badia, G. Garcia-Belmonte, Y. S. Kang, I. Mora-Sero and J. Bisquert, *J. Phys. Chem. Lett.*, 2014, **5**, 2390–2394.

15   K. Yamada, T. Matsui, T. Tsuritani, T. Okuda and S. Ichiba, *Zeitschrift für Naturforsch. A*, 1990, **45**.

16   H. Töpsoe, *Zeitschrift für Krist.*, 1884, **8**, 246–296.

17   D. B. Mitzi, S. Wang, C. A. Feild, C. A. Chess and A. M. Guloy, *Science*, 1995, **267**, 1473–6.

UNIVERSITAT ROVIRA I VIRGILI
SOLUTION PROCESSED INORGANIC SEMICONDUCTOR SOLAR CELLS
José Manuel Marín Beloqui
Dipòsit Legal: T 68-2016

Chapter 4 - References   **PhD Thesis**

18   D. B. Mitzi, K. Chondroudis and C. R. Kagan, *IBM J. Res. Dev.*, 2001, **45**, 29–45.

19   T. Miyasaka, in *Proc. 210th ECS Meeting*, 2006.

20   A. Kojima, K. Teshima, Y. Shirai and T. Miyasaka, *J. Am. Chem. Soc.*, 2009, **131**, 6050–6051.

21   J.-H. Im, C.-R. Lee, J.-W. Lee, S.-W. Park and N.-G. Park, *Nanoscale*, 2011, **3**, 4088.

22   H.-S. Kim, C.-R. Lee, J.-H. Im, K.-B. Lee, T. Moehl, A. Marchioro, S.-J. Moon, R. Humphry-Baker, J.-H. Yum, J. E. Moser, M. Grätzel and N.-G. Park, *Sci. Rep.*, 2012, **2**, 1–7.

23   M. M. Lee, J. Teuscher, T. Miyasaka, T. N. Murakami and H. J. Snaith, *Science (80-.).*, 2012, **338**, 643–647.

24   J. You, Z. Hong, Y. M. Yang, Q. Chen, M. Cai, T.-B. Song, C.-C. Chen, S. Lu, Y. Liu, H. Zhou and Y. Yang, *ACS Nano*, 2014, **8**, 1674–80.

25   S. Dharani, H. A. Dewi, R. R. Prabhakar, T. Baikie, C. Shi, D. Yonghua, N. Mathews, P. P. Boix and S. G. Mhaisalkar, *Nanoscale*, 2014, **6**, 13854–60.

26   J. H. Heo, S. H. Im, J. H. Noh, T. N. Mandal, C.-S. Lim, J. A. Chang, Y. H. Lee, H. Kim, A. Sarkar, M. K. Nazeeruddin, M. Grätzel and S. Il Seok, *Nat. Photonics*, 2013, **7**, 486–491.

27   J. H. Noh, S. H. Im, J. H. Heo, T. N. Mandal and S. Il Seok, *Nano Lett.*, 2013, **13**, 130321112645008.

28   J. Burschka, N. Pellet, S.-J. Moon, R. Humphry-Baker, P. Gao, M. K. Nazeeruddin and M. Grätzel, *Nature*, 2013, **499**, 316–9.

29   M. Liu, M. B. Johnston and H. J. Snaith, *Nature*, 2013, **501**, 395–8.

30   H. Zhou, Q. Chen, G. Li, S. Luo, T. -b. Song, H.-S. Duan, Z. Hong, J. You, Y. Liu and Y. Yang, *Science (80-.).*, 2014, **345**, 542–546.

31   W. S. Yang, J. H. Noh, N. J. Jeon, Y. C. Kim, S. Ryu, J. Seo and S. I. Seok, *Science (80-.).*, 2015, **348**, 1234–1237.

32   D. Liu and T. L. Kelly, *Nat. Photonics*, 2013, **8**, 133–138.

33   J. Troughton, D. Bryant, K. Wojciechowski, M. J. Carnie, H. Snaith, D. A. Worsley and T. M. Watson, *J. Mater. Chem. A*, 2015, **3**, 9141–9145.

34   W. Zhang, M. Anaya, G. Lozano, M. E. Calvo, M. B. Johnston, H. Miguez and H. J. Snaith, *Nano Lett.*, 2015, **15**, 1698–1702.

35   A. Mei, X. Li, L. Liu, Z. Ku, T. Liu, Y. Rong, M. Xu, M. Hu, J. Chen, Y. Yang, M. Gratzel and H. Han, *Science (80-.).*, 2014, **345**, 295–298.

36   K. Zilberberg, H. Gharbi, A. Behrendt, S. Trost and T. Riedl, *ACS Appl. Mater. Interfaces*, 2012, **4**, 1164–8.

37   K. Kawano, R. Pacios, D. Poplavskyy, J. Nelson, D. D. C. Bradley and J. R. Durrant, *Sol. Energy Mater. Sol. Cells*, 2006, **90**, 3520–3530.

38   N. Aristidou, I. Sanchez-Molina, T. Chotchuangchutchaval, M. Brown, L. Martinez, T. Rath and S. a. Haque, *Angew. Chemie Int. Ed.*, 2015, n/a–n/a.

39   J. a. Christians, R. C. M. Fung and P. V. Kamat, *J. Am. Chem. Soc.*, 2014, **136**, 758–764.

40   P. Qin, S. Tanaka, S. Ito, N. Tetreault, K. Manabe, H. Nishino, M. K. Nazeeruddin and M. Grätzel, *Nat. Commun.*, 2014, **5**, 3834.

41   A. Dymshits, A. Rotem and L. Etgar, *J. Mater. Chem. A*, 2014, **2**, 20776–20781.

42   S. D. Stranks, G. E. Eperon, G. Grancini, C. Menelaou, M. J. P. Alcocer, T. Leijtens, L. M. Herz, A. Petrozza and H. J. Snaith, *Science*, 2013, **342**, 341–344.

43   G. Xing, N. Mathews, S. Sun, S. S. Lim, Y. M. Lam, M. Grätzel, S. Mhaisalkar and T. C. Sum, *Science*, 2013, **342**, 344–7.

44   A. Marchioro, J. Teuscher, D. Friedrich, M. Kunst, R. van de Krol, T. Moehl, M. Gratzel and J.-E. Moser, *Nat Phot.*, 2014, **8**, 250–255.

45   H.-S. Kim, I. Mora-Sero, V. Gonzalez-Pedro, F. Fabregat-Santiago, E. J. Juarez-Perez, N.-G. Park and J. Bisquert, *Nat. Commun.*, 2013, **4**, 2242.

46   R. S. Sanchez, V. Gonzalez-Pedro, J. Lee, N. Park, Y. S. Kang, I. Mora-Sero and J. Bisquert, *J. Phys. Chem. Lett.*, 2014, **5**, 2357–2363.

47   C. D. Bailie, M. G. Christoforo, J. P. Mailoa, A. R. Bowring, E. L. Unger, W. H. Nguyen, J. Burschka, N. Pellet, J. Z. Lee, M. Grätzel, R. Noufi, T. Buonassisi, A. Salleo and M. D. McGehee, *Energy Environ. Sci.*, 2014, 956–963.

48   I. makes 11% P. Module, http://www.pv-magazine.com/news/details/beitrag/imec-perovskite-breakthrough-yields-119-efficiency_100020211/#axzz3kfNqq3OF .

49   C.-G. Wu, C.-H. Chiang and Z.-L. Tseng, *J. Mater. Chem. A*, 2014, **2**, 15897–15903.

UNIVERSITAT ROVIRA I VIRGILI
SOLUTION PROCESSED INORGANIC SEMICONDUCTOR SOLAR CELLS
José Manuel Marín Beloqui
Dipòsit Legal: T 68-2016

Chapter 4 - References   **PhD Thesis**

50   H.-S. Kim and N.-G. Park, *J. Phys. Chem. Lett.*, 2014, **5**, 2927–2934.

51   A. K. Jena, H.-W. Chen, A. Kogo, Y. Sanehira, M. Ikegami and T. Miyasaka, *ACS Appl. Mater. Interfaces*, 2015, **7**, 9817–9823.

52   H.-S. Kim and N.-G. Park, *J. Phys. Chem. Lett.*, 2014, **5**, 2927–2934.

53   C. Eames, J. M. Frost, P. R. F. Barnes, B. C. O'Regan, A. Walsh and M. S. Islam, *Nat. Commun.*, 2015, **6**, 7497.

54   B. C. O'Regan, P. R. F. Barnes, X. Li, C. Law, E. Palomares and J. M. Marin-Beloqui, *J. Am. Chem. Soc.*, 2015, **137**, 5087–5099.

55   W. Tress, N. Marinova, T. Moehl, S. M. Zakeeruddin, N. Mohammad K. and M. Grätzel, *Energy Environ. Sci.*, 2015, **8**, 995–1004.

56   H. J. Snaith, A. Abate, J. M. Ball, G. E. Eperon, T. Leijtens, N. K. Noel, S. D. Stranks, J. T.-W. Wang, K. Wojciechowski and W. Zhang, *J. Phys. Chem. Lett.*, 2014, **5**, 1511–1515.

57   T. Heiser and E. R. Weber, *Phys. Rev. B*, 1998, **58**, 3893–3903.

58   D. L. Staebler and C. R. Wronski, *J. Appl. Phys.*, 1980, **51**, 3262.

59   A. Dualeh, T. Moehl, N. Tétreault, J. Teuscher, P. Gao, M. K. Nazeeruddin and M. Grätzel, *ACS Nano*, 2014, **8**, 362–73.

60   J. M. Frost, K. T. Butler, F. Brivio, C. H. Hendon, M. van Schilfgaarde and A. Walsh, *Nano Lett.*, 2014, **14**, 2584–90.

61   F. Brivio, A. B. Walker and A. Walsh, *APL Mater.*, 2013, **1**, 042111.

62   I. Lyubomirsky, V. Lyakhovitskaya, R. Triboulet and D. Cahen, *Appl. Phys. Lett.*, 1995, **67**, 3132.

63   J. MIZUSAKI, K. ARAI and K. FUEKI, *Solid State Ionics*, 1983, **11**, 203–211.

64   K. Yamada, *Solid State Ionics*, 1995, **79**, 152–157.

65   J. M. Frost, K. T. Butler and A. Walsh, *APL Mater.*, 2014, **2**, 081506.

66   J. F. Verwey, *J. Phys. Chem. Solids*, 1970, **31**, 163–168.

67   R. K. Misra, S. Aharon, B. Li, D. Mogilyansky, I. Visoly-Fisher, L. Etgar and E. A. Katz, *J. Phys. Chem. Lett.*, 2015, **6**, 326–330.

68   S. N. Habisreutinger, T. Leijtens, G. E. Eperon, S. D. Stranks, R. J. Nicholas and H. J. Snaith, *Nano Lett.*, 2014, **14**, 5561–5568.

69   *Directive 2001/65/EU of the European Parliament and of the Council of 8 June 2011 on the restriction of the use of certain hazardous substances ion electrical and electronic equipment (recast).*, .

70   N. K. Noel, S. D. Stranks, A. Abate, C. Wehrenfennig, S. Guarnera, A.-A. Haghighirad, A. Sadhanala, G. E. Eperon, S. K. Pathak, M. B. Johnston, A. Petrozza, L. M. Herz and H. J. Snaith, *Energy Environ. Sci.*, 2014, **7**, 3061–3068.

71   F. Hao, C. C. Stoumpos, D. H. Cao, R. P. H. Chang and M. G. Kanatzidis, *Nat. Photonics*, 2014, **8**, 489–494.

72   R. the cost of perovskite solar Cells, http://www.rsc.org/chemistryworld/2013/04/cheap-perovskite-solar-cells-al2o3

73   M. Widmar, 2014. *First Solar Q4'2 Earnings Call*

74   T. De Jong, *Firt Solar Manufacturing Update*.

Chapter 5

Charge Recombination in Double Heterojunction Solar Cells

Photovoltaic cells constructed from methylammonium lead iodide, $CH_3NH_3PbI_3$ (MAPI), and related materials have generated much interest in the last 2 years. The energy conversion efficiency has been increasing very rapidly since their first description at 3.8%[1] to the current reports ranging from 15% to 18%[2–4]. At the same time, there is much debate about the optoelectronic mechanisms that allow this low temperature material to deliver such high efficiencies. Debate concerns the possible roles of crystal size, stoichiometry, defects, and ferroelectric domains. There is debate about where in the cell the voltage is generated, the type of recombination, importance of traps, doping levels, and more. There is also debate about how to correctly measure the recombination and transport times, the charge density, and even the correct measurement of efficiency[5–9].

In this chapter, we examine the measurement of charge density and recombination in cells that does not exhibit significant hysteresis. Previous authors

UNIVERSITAT ROVIRA I VIRGILI
SOLUTION PROCESSED INORGANIC SEMICONDUCTOR SOLAR CELLS
José Manuel Marín Beloqui
Dipòsit Legal: T 68-2016

Chapter 5   **PhD Thesis**

have used photoinduced transient photovoltage (PIT-PV), impedance, microwave absorption, and luminescence to examine recombination in MAPI cells[5,10–12]. However, there is no consensus on the recombination lifetime or on the correct model for cell operation. In part, this may be because it has been assumed that when impedance is performed in the dark, with any preconditioned step, or relaxed condition of the cell does not change with time and voltage. How to characterize cells preconditioning the cell or a steady state is still not fully understood, not the least because of the short lifetime of these states in many cells. Here, cells with mesoporous TiO_2 layers of perovskite have been fabricated, and measurements such as photoinduced transient photovoltage (PIT-PV), photoinduced transient photocurrent (PIT-PC) and photoinduced charge extraction (PICE) have been performed. Frequency domain measurements at applied voltage or V_{oc} can take too long to give a picture of the partially preconditioned or relaxed states, because the cell state will be evolving during the measurement. Our results highlight some important differences between MAPI cells and other related technologies such as dye-sensitized solar cells (DSSCs) and polymer/C_{60} cells. We also demonstrate that careful evaluation of the PIT-PV lifetimes and charge densities is required and self-consistency checks are imperative when assigning kinetic features in new and complicated solar cell materials.
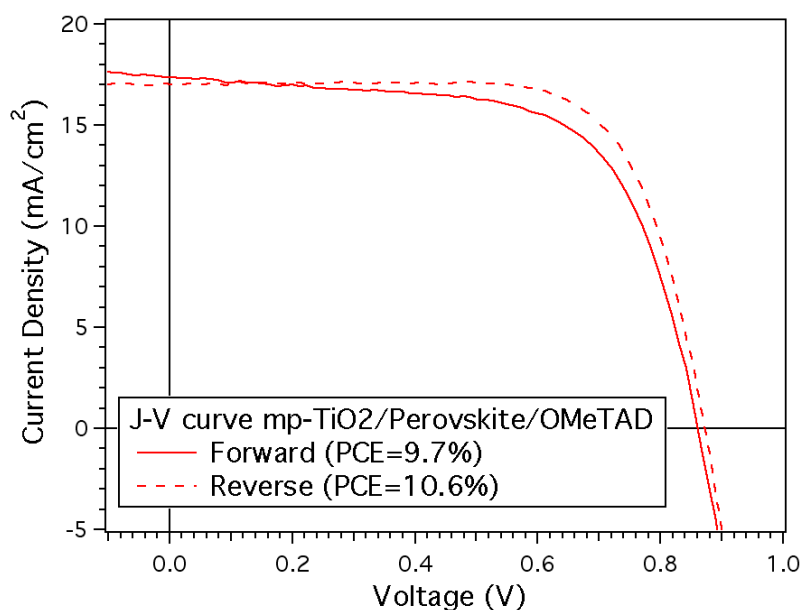

Figure 1. J-V curve of a d-TiO_2/mp-TiO_2/Perovskite/OMeTAD/Au measured from in forward (solid line), from negative to positive bias and in reverse (dashed line) direction.

In this work, the device structure was FTO/dTiO$_2$/mp-TiO$_2$/MAPI/OMeTAD/Au, where FTO is fluorine-doped tin oxide, dTiO$_2$ indicates dense-TiO$_2$, mpTiO$_2$ is mesoporous TiO$_2$, and OMeTAD was Spiro-OMeTAD. Most cells were made by the 1:3 ratio PbCl$_2$ and methylammonium iodide recipe. We will call this the MAPIC synthesis route; however, we refer to the product as MAPI cells throughout, since there is debate whether any significant chloride remains in the cells.

Charge obtained by PICE

Critical to understanding the physics of MAPI cells is measurement of the charge density under various conditions. In DSSCs and polymer cells, the photoinduced charge extraction (PICE) measurement has been found to be accurate and useful (see Chapter 0 for details)[13–15]. **Figure 2a** shows the photoinduced charge extraction current collected after the cell was switched from 1 sun OC to dark SC. Although the photoinduced charge extraction current decay in **Figure 2a** looks complete at 200 µs, closer inspection shows that it is not (**Figure 2b**). There is a second portion of the decay with a maximum current of 100 µA/cm^2 that decays exponentially with a lifetime close to 1 ms. Although the current is 1000 times lower than that of the fast component, the time is sufficiently long that the integrated charge collected is about 50 times higher, $\square 3.6 \times 10^{-5}$ C/cm^2. The two very disparate time scales give some clue that there are least two ways in which photogenerated charge is stored in this system. Charge obtained by PICE for perovskite solar cells is in the same range than normalised charge obtained for DSSC. The charge stored in a DSSC is known to be mixed ionic/electric charge, where electrons in TiO$_2$ are charge balanced by ions in solution inside the mesoporous TiO$_2$ network. One might speculate that the charge in the MAPI cell is also electrons in TiO$_2$ and mobile ions in MAPI. However, if there are moving ions in the MAPI/OMeTAD, they should be moving much slower than those in the electrolyte of a DSSC. There are additional problems with assigning the photoinduced charge extraction results to "electrons in TiO$_2$", as we detail below.
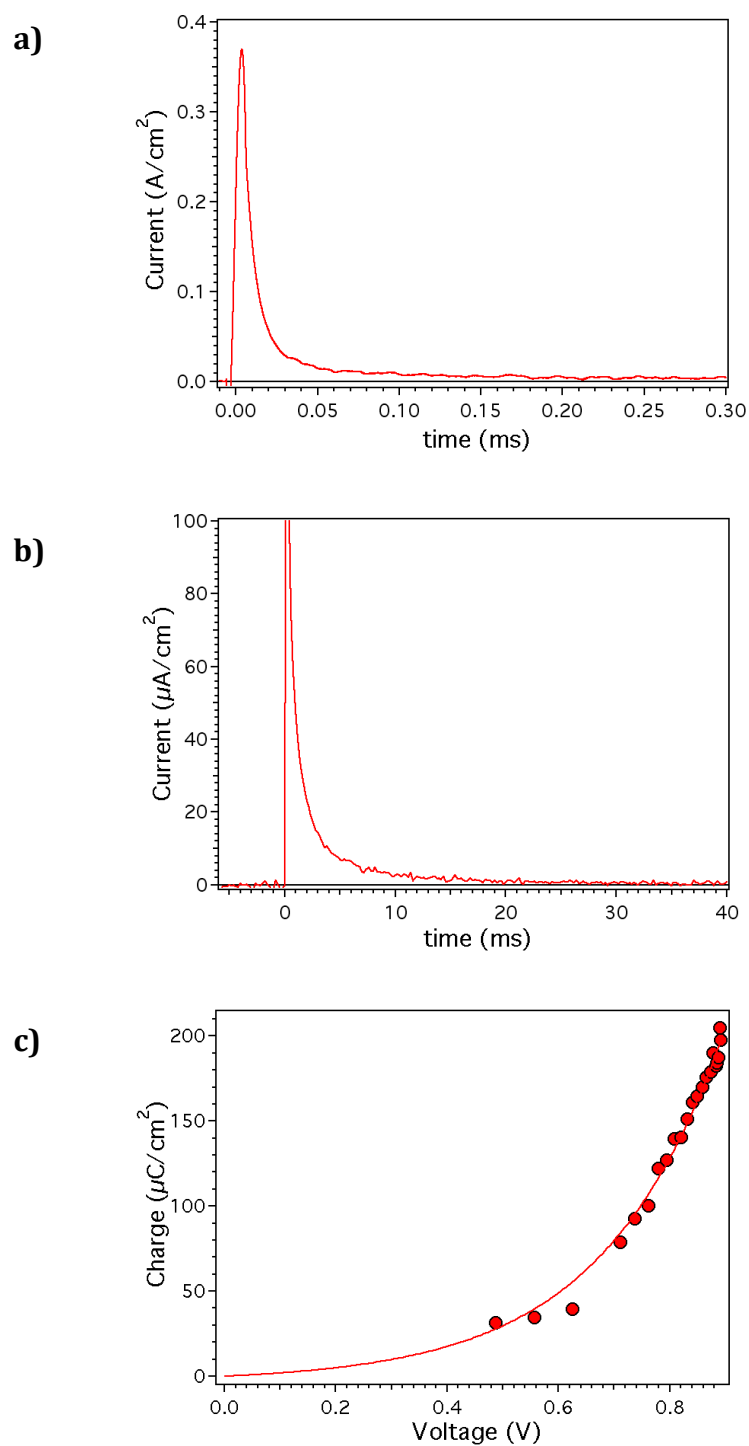
Figure 2. a) PICE decay at 1 sun V_{oc}=0.86 V obtained at short times. **b)** The same charge extraction transient viewed at a longer time scale. **c)** Charge obtained by PICE vs V_{oc}.

UNIVERSITAT ROVIRA I VIRGILI
SOLUTION PROCESSED INORGANIC SEMICONDUCTOR SOLAR CELLS
José Manuel Marín Beloqui
Dipòsit Legal: T 68-2016

PhD Thesis   **Chapter 5**

Charge obtained by Differential Charging

PhotoInduced Differential Charging (PIDC) is another technique that has been used to measure capacitance and thus charge density in both DSSCs and polymer/PCBM solar cells. It was found in both these cell types that the photoinduced differential charging method gives essentially the same stored charge as the photoinduced charge extraction method[13,15,16]. We show herein that this is not true for mpTiO$_2$/MAPI cells. The differential capacitance can be measured by combining photoinduced transient photovoltage (PIT-PV) and photoinduced transient photocurrent (PIT-PC) results to find $C = dQ/dV_0$. **Figure 3a** shows representative PIT-PV transient taken using a laser pulse (600 nm) at different bias light intensities. The laser used for PIT-PV creates a perturbation with an intensity of dV_0, that decrease as increase the background illumination. In order to find the dQ value for the pulse, we use the photocurrent transients. **Figure 3b** shows photocurrent transients at short-circuit made using the same laser pulse, with bias light intensities of 1 sun and dark conditions. The area under the curve of the PIT-PC is used as an estimate of the charge generation flux using the same pulse at OC. The estimate is reasonable under the following assumptions: **(i)** that their are no significant collection losses at short circuit and **(ii)** that charge generation efficiency is similar at short circuit and open circuit. Either of these assumptions could be wrong. However, for the measurements presented here, we can show (below) that any corrections required would not change the main conclusions drawn from the data. We note that a better way to find dQ during PIT-PV is to measure the transient absorption (TA) of the charges simultaneously with the PIT-PV[17]. The TA can then be converted to charge if the absorption coefficient is known. However, these data are not available yet for the MAPI system.

UNIVERSITAT ROVIRA I VIRGILI
SOLUTION PROCESSED INORGANIC SEMICONDUCTOR SOLAR CELLS
José Manuel Marín Beloqui
Dipòsit Legal: T 68-2016

Chapter 5   **PhD Thesis**

a)

b)
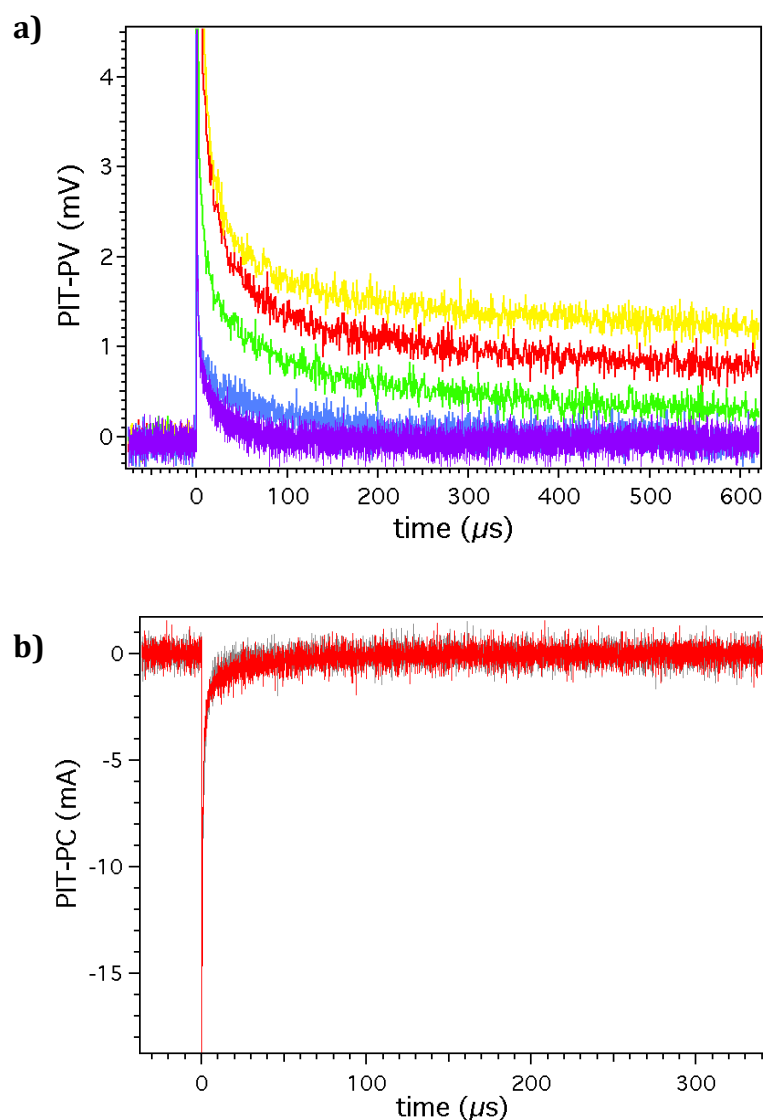
Figure 3. a) PIT-PV decay obtained at several light illuminations increasing
lifetimes and amplitude as the light intensity was lower. **b)** PIT-PC decay obtained at
dark conditions (grey line) and at 1 sun (red line) conditions.

Figure 4a shows the differential capacitance at V_{oc} for a range of light levels
from dark to above 1 sun. Integration of the capacitance vs voltage gives the charge
stored (**Figure 4b**). In **Figure 4b**, the red circles are the integral of the full
capacitance and the green square symbols are the integral of the part of the
capacitance above the flat baseline between 0 and 0.3 V. Assuming that the flat
baseline represents the charge on the contact electrodes, the green squares symbols
represent the charge stored in the bulk of the solar cell, including at the internal
interfaces.

UNIVERSITAT ROVIRA I VIRGILI
SOLUTION PROCESSED INORGANIC SEMICONDUCTOR SOLAR CELLS
José Manuel Marín Beloqui
Dipòsit Legal: T 68-2016

PhD Thesis   **Chapter 5**
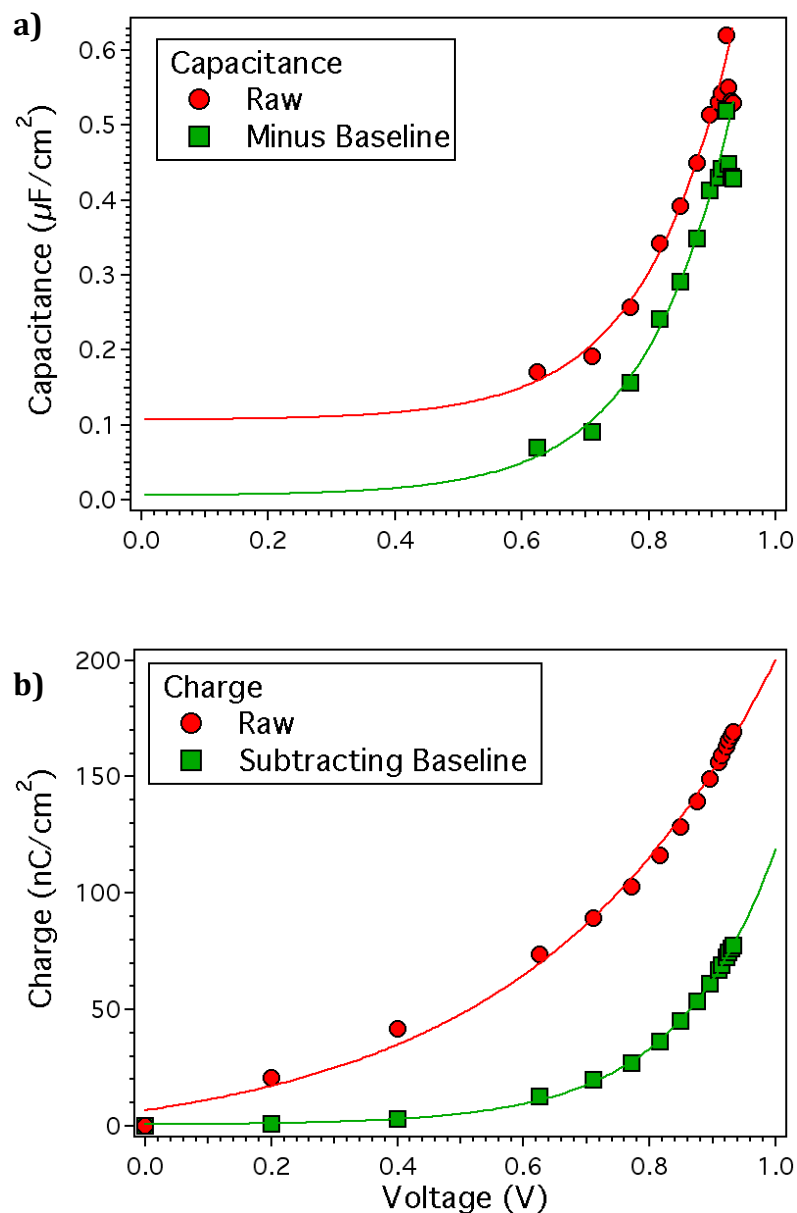
Figure 4. a) Capacitance vs Voc obtained by PIDC at each Voc. **b)** PIT-PC Charge
obtained integrating the area under the capacitance curve.

There is a notable features of **Figure 4a, b**. The first is the magnitude of the capacitive charge relative to the charge measured by photoinduced charge extraction. The total capacitive charge stored at 1 sun is $\square$48 nC/cm^2. This is 3000 times smaller than the 170 μC/cm^2 measured in the photoinduced charge extraction experiment (**Figure 2c**). Thus, unlike in DSSCs and polymer cells, differential capacitance and photoinduced charge extraction gave very different results in MAPI cells. Interestingly, the capacitance in **Figure 4a** is also about 3000 times less than would be expected for a solid-state dye-sensitized cell using a similar mpTiO$_2$ film

thickness[18,19]. This implies either that the traps in the TiO_2 are passivated by the MAPI or they are not all accessible at a given potential. The latter is a reasonable result for a p-i-n structure where the potential drops across the MAPI and $mpTiO_2$/MAPI layers. At any $V_{oc} < V_{bi}$ (where V_{bi} is the built in potential), the Fermi level will be farther below the TiO_2 conduction band edge for positions farther from the FTO contact. Thus, only the TiO_2 electron states near the FTO will be filled to the level implied by the V_{oc}.

On the other hand, we have performed some initial measurements of capacitance for MAPI cells with different $mpTiO_2$ thickness. There appears to be a trend for larger capacitance with thicker $mpTiO_2$, indicating that mesoporous layer is involved in the charge generation, **Figure 5**.
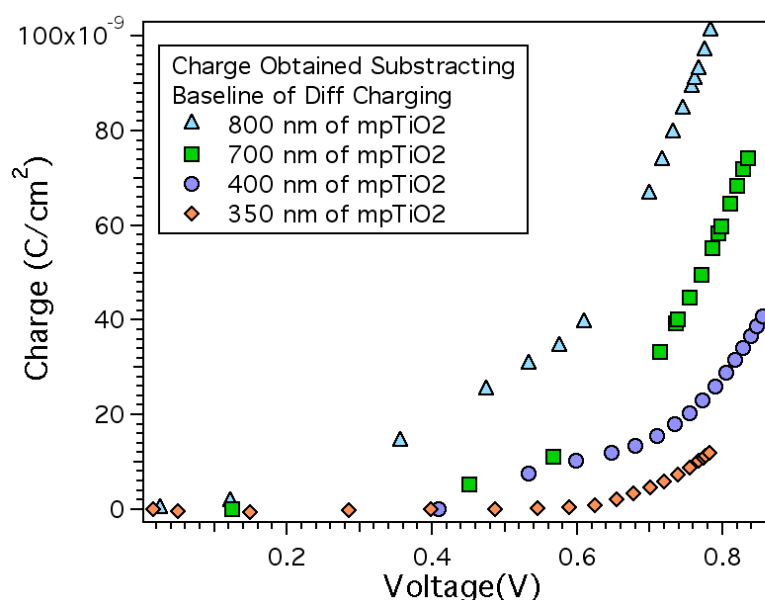
Figure 5. Capacitance vs Voc measured by differential charging for a set of mp-TiO_2/MAPI/OMeTAD with different mp-TiO_2 thickness.

Recombination Lifetime

We now turn to the decay dynamics of the photovoltage transients and their possible interpretation as recombination time constants. **Figure 6a** shows the PIT-PV decay under 1 sun bias light. This decay is strongly double exponential. Figure 6a shows the double exponential fit. The fast part has a lifetime lower than 1 μs and the slow part 50 μs. **Figure 6a** highlights the double exponential nature of the decay and

UNIVERSITAT ROVIRA I VIRGILI
SOLUTION PROCESSED INORGANIC SEMICONDUCTOR SOLAR CELLS
José Manuel Marín Beloqui
Dipòsit Legal: T 68-2016

PhD Thesis   **Chapter 5**

the poor quality of a single exponential fit. This is in agreement with several previous reports of PIT-PV decays on MAPI cells[8,20]. **Figure 6b** shows the two PIT-PV lifetimes as a function of cell charge. The fast and slow lifetimes differ by a factor of □50.
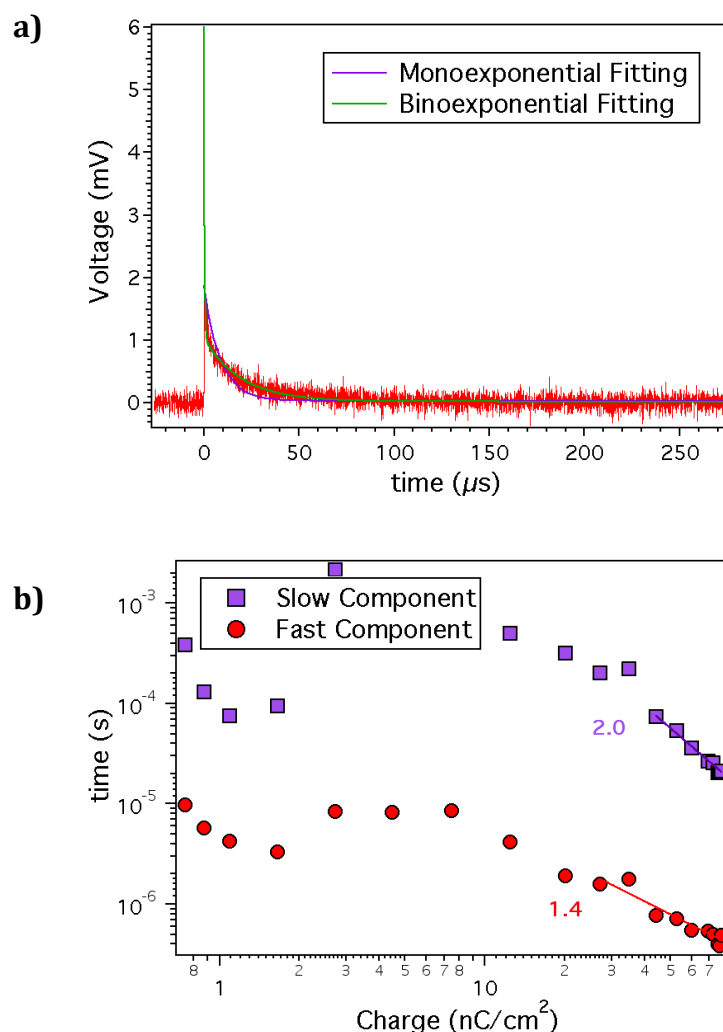
Figure 6. a) PIT-PV decay at 1 sun with monoexponential (purple) and biexponential (green) fit. **b)** PIT-PC Fast (red circles) and slow (purple squares) lifetimes obtained from PIT-PV represented against charge, obtained by PIDC.

Our data show that at 1 sun, >70% of the photoinduced transient photovoltage decays with a lifetime of □1 µs. This result falls at the short end of what has been reported in the literature. Bisquert et al. recently reported 1 sun PIT-PV lifetimes that varied from 100 to 2 µs, depending on the material (MAPI or formamadinium lead iodide) and the fabrication procedure (single or two step)[5]. They came to the conclusion that these decay times could not be associated with electron/hole recombination. Most other papers using transients or impedance have found a 90–200

µs characteristic time, which they have assigned to charge recombination. Unfortunately only one of the PIT-PV based papers presented raw transient data. In that paper, the photovoltage transient had a 20 µs rise time that would have obscured any fast decay components that might have been present[8].

Implied Recombination Flux at Voc

In a new technology such as perovskites cells, it is risky to assume, without verification, that a given impedance signal or photovoltage decay lifetime corresponds to a particular process. We propose here that the 1 µs lifetime that we observe in PIT-PV is a result of the predominant electron/hole recombination channel, and thus the average charge lifetime, at the 1 sun V_{oc}, is close to 1 µs in these cells. In the paragraphs below, we test this assignment for consistency with the photocurrent and charge density. We do so by combining the PIT-PV lifetimes in **Figure 5b** with the charge in **Figure 4b** to find the implied "recombination current" inside the cell. The recombination current (J_{rec}, with units mA/cm^2) is calculated with **Equation 1**.

$$J_{rec} = \frac{Q(V_{oc})}{(\tau(V_{oc}) \times OF)} \quad \textbf{Equation 1}$$

where Q is the charge in the cell, τ is the PIT-PV lifetime, and OF is the order factor. An OF is required if the recombination lifetime varies with charge density (i.e., the effective order of the process is not 1). The OF is given by ($-S + 1$) where S is the slope of $\log(\tau)$ vs $\log(Q)$ in **Figure 5b**[21,22]. We can make this calculation for the short and long lifetimes and total or above baseline charge (**Table 1**). If the implied recombination current is not physically reasonable, then the specific PIT-PV decay is unlikely to be a measure of recombination in the cell. For example, at 1 sun V_{oc}, using the fast lifetime (0.9 µs, **Figure 5b**) and the "charge above baseline" (48 nC/cm^2, **Figure 4b**) with an order factor of 1.4 (from **Figure 5b**), we calculate a recombination current of 38 mA/cm^2 (see **Table 1**).

UNIVERSITAT ROVIRA I VIRGILI
SOLUTION PROCESSED INORGANIC SEMICONDUCTOR SOLAR CELLS
José Manuel Marín Beloqui
Dipòsit Legal: T 68-2016

PhD Thesis   **Chapter 5**

Charge Method	Charge (nC/cm^2)	TPV component	Decay Lifetime (μs)	Order Factor	Jrec (mA/cm^2)
C	48	Fast	0.9	1.4	38
		Slow	54	2.0	0.4
T	135	Fast	0.7	2.8	69
		Slow	54	4.5	0.6
CE	170000	Fast	0.7	1.1	220000
		Slow	54	2.4	1300

Table 1. Charge in the Device, Photo-Induced Photovoltage (PIT-PV) Lifetime, and Calculated Recombination Current (J_{rec}) at V_{oc}. With T as Total Charge obtained by differential charging, C as Cell Charge obtained subtracting the baseline and CE the charge obtained by PICE

In **Table 1**, we give the recombination current calculation using other combinations of τ and charge. On the other hand, the J_{rec} calculated for the fast lifetime, with the total capacitive charge, is 69 mA/cm^2. that is clearly not physically reasonable. The implication is thus that the charges held in the baseline capacitance do not participate in the fast recombination process.

Last lines of **Table 1** show the recombination current calculated using the fast or slow PIT-PV lifetime and the charge measured by photoinduced charge extraction (170 μC/cm^2, **Figure 2c**). The implied recombination currents are 220 and 1.3 A/cm^2, respectively, which are both >100 times the maximum possible charge generation current. We can conclude that the charge measured by photoinduced charge extraction does not contribute to the PIT-PV decays shown in **Figure 5** and is thus almost certainly not electronic in nature. It must instead be due to moving ions or reorienting dipoles.

Other Possible Sources of Fast PIT-PV Decays

In the above discussion, we have asserted that the fast component of the PIT-PV decay represents the main loss of charge in the cell. However, before accepting this assignment we should examine the alternatives. The only way that the pulse can

UNIVERSITAT ROVIRA I VIRGILI
SOLUTION PROCESSED INORGANIC SEMICONDUCTOR SOLAR CELLS
José Manuel Marín Beloqui
Dipòsit Legal: T 68-2016

Chapter 5   **PhD Thesis**

create a voltage signal is by causing a net separation of positive and negative charge along a vector normal to the cell contacts. The decay of the voltage corresponds to the decay of the net separation. However, the decay does not have to be recombination. There are (at least) three ways that the PIT-PV pulse could establish a voltage that would decay by a mechanism different from recombination. These are as follows: **(1)** Illumination that is strongly absorbed on one side of the active layer can create charges that separate because of unequal mobility. In this case, equilibration of the charge distributions can cause decay of the photovoltage without recombination. **(2)** In the "bulk photovoltaic effect", the absorption of light in a non-centrosymmetric material can result in a net separation of charges along some directions in the crystal. The voltage can again decay by equilibration of the charge distributions without recombination. **(3)** A photo-"isomerization" effect can turn dipoles or shifts ionic charges rather than electronic charges. In this case, the photovoltage decay occurs by rotation or movement of atomic charges rather than recombination of electronic charge. For all three of these possibilities, we believe it is possible to show that they are not the source for the fast component of the PIT-PV decays measured on our cells.

With respect to mechanism 1, the photovoltage decay occurs by charge transport. The hole and electron mobilities in MAPI are reported to be in the 2–20 cm^2/(V s) range[12,23,24]. At the 1 sun V_{oc} ($\square$0.85 V), there will remain a built in field of perhaps 0.3 V. Under this field, the transit time of electrons and holes across the film is only a few nanoseconds. Thus, any voltage decay that depends on charge transport rather than recombination should fall in the <20 ns time scale. Consistent with this, when using a 20 ns laser pulse, >80% of the voltage rise occurs within the pulse. The fast component of the PIT-PV decay is 1 μs at 1 sun. This is at least 50 times longer than the apparent charge transport times, indicating that the fast PIT-PV decay is not due to mechanism 1 in the previous paragraph. Further, the optical density of our films at 650 nm is about 1. This means that only about twice as many photons are absorbed in the front half of the film. This absorption is a bit weak to cause a voltage signal by mechanism 1.

With regard to the bulk photovoltaic effect, we can ask whether there are enough photons in the pulse to create the observed voltage increase during the first 2 μs of the pulse. The bulk photovoltaic effect occurs when absorption of light directly

creates a separation of electrons and holes. The separation is said to be limited to at most a few mean free paths. In **Figure 3a**, the first 2 µs of the pulse results in absorption of $\square 4 \times 10^{10}$/cm^2 photons and creates a voltage increase of 4 mV. Using a relative dielectric constant of 20, the electron/hole separation per photon would have to be 10 nm[25]. Although this is probably too large, it might be possible. However, the argument from the proceeding paragraph holds here as well. Given the published values for the mobility, it should take only a few nanoseconds for these charges to re-equilibrate after the end of the pulse, instead of the 1 µs measured. With respect to mechanism 3, we assume that each absorbed photon can rotate at most one methylammonium (MA) dipole. The partial charge on the MA dipole is about 0.3q. During the first 2 µs of the pulse, rotation of $\square 4 \times 10^{10}$ MA dipoles in the film volume, again using a dielectric constant of 20, should give rise to a voltage signal of only $\square 0.2$ mV. Although this is too small relative to the fast component of the PIT-PV decay, it is similar to the magnitude of the slow phase.

Conclusions

We have demonstrated that in mpTiO$_2$/MAPI cells there are two kinds of extractable charge stored when the cell is held at V_{oc}: a capacitive electronic charge ($\square 50$ nC/cm^2) and another, much larger charge (170 µC/cm^2), which could be the result of dipole realignment or the effect of mobile ions. The capacitive charge is $\square 10$ times smaller than that in mpTiO$_2$/dye/HTM cells with similar mpTiO$_2$ thickness. In mpTiO$_2$/MAPI cells, the photoinduced transient photovoltage decays are strongly double exponential with two time constants that differ by a factor of 50, independent of bias light intensity. The fast decay (lower than 1µs at 1 sun) can be assigned to the predominant charge recombination pathway in the cell. Calculation of recombination flux at V_{oc} shows that charge generation is not a function of applied bias.

If the 0.7 and 50 µs PIT-PV decays (at 1 sun) account for all of the electronic recombination in the cell, as seems likely from **Table 1**, then all these slower processes are chemical in nature. By "chemical", we mean they involve the movement of atoms (dipoles or ions) instead of, or in addition to, electrons.

UNIVERSITAT ROVIRA I VIRGILI
SOLUTION PROCESSED INORGANIC SEMICONDUCTOR SOLAR CELLS
José Manuel Marín Beloqui
Dipòsit Legal: T 68-2016

Chapter 5 - References   **PhD Thesis**

References

1   A. Kojima, K. Teshima, Y. Shirai and T. Miyasaka, *J. Am. Chem. Soc.*, 2009, **131**, 6050–6051.

2   K. Wojciechowski, S. D. Stranks, A. Abate, G. Sadoughi, A. Sadhanala, N. Kopidakis, G. Rumbles, C.-Z. Li, R. H. Friend, A. K.-Y. Jen and H. J. Snaith, *ACS Nano*, 2014, **8**, 12701–9.

3   J. Burschka, N. Pellet, S.-J. Moon, R. Humphry-Baker, P. Gao, M. K. Nazeeruddin and M. Grätzel, *Nature*, 2013, **499**, 316–9.

4   N. J. Jeon, J. H. Noh, Y. C. Kim, W. S. Yang, S. Ryu and S. Il Seok, *Nat. Mater.*, 2014, **13**, 897–903.

5   R. S. Sanchez, V. Gonzalez-Pedro, J. Lee, N. Park, Y. S. Kang, I. Mora-Sero and J. Bisquert, *J. Phys. Chem. Lett.*, 2014, **5**, 2357–2363.

6   D. Bi, L. Yang, G. Boschloo, A. Hagfeldt and E. M. J. Johansson, *J. Phys. Chem. Lett.*, 2013, **4**, 1532–1536.

7   Y. Zhao, A. M. Nardes and K. Zhu, *J. Phys. Chem. Lett.*, 2014, **5**, 490–494.

8   V. Roiati, S. Colella, G. Lerario, L. De Marco, A. Rizzo, A. Listorti and G. Gigli, *Energy Environ. Sci.*, 2014, **7**, 1889.

9   V. W. Bergmann, S. A. L. Weber, F. Javier Ramos, M. K. Nazeeruddin, M. Grätzel, D. Li, A. L. Domanski, I. Lieberwirth, S. Ahmad and R. Berger, *Nat. Commun.*, 2014, **5**, 5001.

10   E. Guillén, F. J. Ramos, J. A. Anta and S. Ahmad, *J. Phys. Chem. C*, 2014, **118**, 22913–22922.

11   A. Dualeh, T. Moehl, N. Tétreault, J. Teuscher, P. Gao, M. K. Nazeeruddin and M. Grätzel, *ACS Nano*, 2014, **8**, 362–73.

12   T. J. Savenije, C. S. Ponseca, L. Kunneman, M. Abdellah, K. Zheng, Y. Tian, Q. Zhu, S. E. Canton, I. G. Scheblykin, T. Pullerits, A. Yartsev and V. Sundström, *J. Phys. Chem. Lett.*, 2014, **5**, 2189–2194.

UNIVERSITAT ROVIRA I VIRGILI
SOLUTION PROCESSED INORGANIC SEMICONDUCTOR SOLAR CELLS
José Manuel Marín Beloqui
Dipòsit Legal: T 68-2016

PhD Thesis   **Chapter 5 - References**

13   B. C. O'Regan, S. Scully, A. C. Mayer, E. Palomares and J. Durrant, *J. Phys. Chem. B*, 2005, **109**, 4616–4623.

14   N. . Duffy, L. . Peter, R. M. . Rajapakse and K. G. . Wijayantha, *Electrochem. commun.*, 2000, **2**, 658–662.

15   C. G. Shuttle, A. Maurano, R. Hamilton, B. O'Regan, J. C. de Mello and J. R. Durrant, *Appl. Phys. Lett.*, 2008, **93**, 183501.

16   P. R. F. Barnes, K. Miettunen, X. Li, A. Y. Anderson, T. Bessho, M. Gratzel and B. C. O'Regan, *Adv. Mater.*, 2013, **25**, 1881–922.

17   A. Y. Anderson, P. R. F. Barnes, J. R. Durrant and B. C. O'Regan, *J. Phys. Chem. C*, 2010, **114**, 1953–1958.

18   P. Chen, J. H. Yum, F. De Angelis, E. Mosconi, S. Fantacci, S.-J. Moon, R. H. Baker, J. Ko, M. K. Nazeeruddin and M. Grätzel, *Nano Lett.*, 2009, **9**, 2487–92.

19   N. Cai, S.-J. Moon, L. Cevey-Ha, T. Moehl, R. Humphry-Baker, P. Wang, S. M. Zakeeruddin and M. Grätzel, *Nano Lett.*, 2011, **11**, 1452–6.

20   J.-W. Lee, T.-Y. Lee, P. J. Yoo, M. Grätzel, S. Mhaisalkar and N.-G. Park, *J. Mater. Chem. A*, 2014, **2**, 9251.

21   B. C. O'Regan, J. R. Durrant, P. M. Sommeling and N. J. Bakker, *J. Phys. Chem. C*, 2007, **111**, 14001–14010.

22   J. Bisquert, *J. Phys. Chem. B*, 2004, **108**, 2323–2332.

23   Q. Wang, Y. Shao, H. Xie, L. Lyu, X. Liu, Y. Gao and J. Huang, *Appl. Phys. Lett.*, 2014, **105**, 163508.

24   T. Leijtens, S. D. Stranks, G. E. Eperon, R. Lindblad, E. M. J. Johansson, I. J. McPherson, H. Rensmo, J. M. Ball, M. M. Lee and H. J. Snaith, *ACS Nano*, 2014, **8**, 7147–55.

25   F. Brivio, A. B. Walker and A. Walsh, *APL Mater.*, 2013, **1**, 042111.

Chapter 6

Photo-Induced Charge Recombination Kinetics in MAPbI$_{3-x}$Cl$_x$ Perovskite-like Solar Cells Using Low Band-Gap Polymers as Hole Conductors

Hybrid inorganic/organic double heterojunction solar cells have been the focus of intense research mainly to replace the liquid red/ox electrolyte in mesoscopic TiO_2 dye sensitized solar cells (DSSC)[1]. In most cases, the same sensitizer is used for both architectures but the liquid electrolyte is replaced by a solution process hole transport material (HTM), generally either the spiro-OMeTAD[2] (chemical name: 2,2',7,7'-tetrakis(N,N-di-p-methoxyphenylamine) or a semiconductor polymer such as P3HT (chemical name: Poly(3-hexylthiophene)[3,4]. However, the light-to-energy conversion efficiency (η) of these, so called, solid-state DSSCs have been generally below the efficiency values of their liquid counterparts mainly due to the lower photocurrent produced in the thinner mesoporous TiO_2 layers needed for solid-state DSSCs or the desorption of the sensitizer after the spin-coating of the HTM which frequently requires organic solvents such as chlorobenzene.

A breakthrough in the double heterojunction was reported in 2013 by several research groups[5–9] working independently by replacing the sensitizer using an organolead halide, either $CH_3NH_3PbI_3$ or $CH_3NH_3PbI_{3-x}Cl_x$ ($MAPbI_3$ or $MAPbI_{3-x}Cl_x$), and using spiro-OMeTAD as the hole conductor with outstanding efficiencies surpassing 15% under standard measurement conditions.

These results fuelled the interest of many research groups devoted to the study of DSSC and OSC (organic solar cells) and many different device configurations have been studied with published efficiencies ranging from 10% for thin-film approaches that avoid the use of HTM (see **Scheme 1**) to over 16% for those device structures that use HTM.
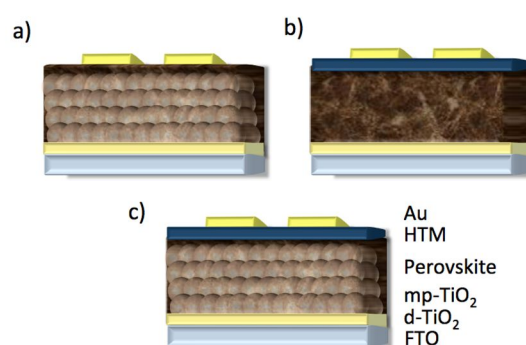

Scheme 1. Different device structures for MAPbI or MAPbICl based solar cells. (a) Thin-film approach without the use of a HTM. (b) Thin-film approach without the use of mp-TiO₂ and (c) the meso-structured approach using both mp-TiO₂ and HTM.

Most studies have focussed on replacing the spiro-OMeTAD HTM material with alternative HTM molecules with great success but studies on the photo-induced interfacial charge recombination reactions in these novel solar cells are more scarce[10,11]. However, the study of the charge recombination processes under operation conditions are paramount to advance towards the theoretical maximum efficiency of $MAPbI_{3-x}Cl_x$ solar cells[12] by minimizing the interfacial losses, as for example the charge recombination reaction between the photo-injected electrons at the TiO_2 and the oxidised HTM (reaction 3 in **Scheme 2**).

In this communication we have fabricated efficient mp-TiO₂/$MAPbI_{3-x}Cl_x$ devices using as HTM materials two semiconductor low-band gap polymers, PTB1 and PTB7, that show excellent hole mobility in OPV devices (4.5 10^{-4} cm²V⁻¹S⁻¹ and

$5.8 \cdot 10^{-4}$ $cm^2V^{-1}s^{-1}$ for PTB1 and PTB7 respectively). **Figure 1** shows the IV curves for both type of solar cells and the standard solar cell using spiro-OMeTAD for comparison purposes.
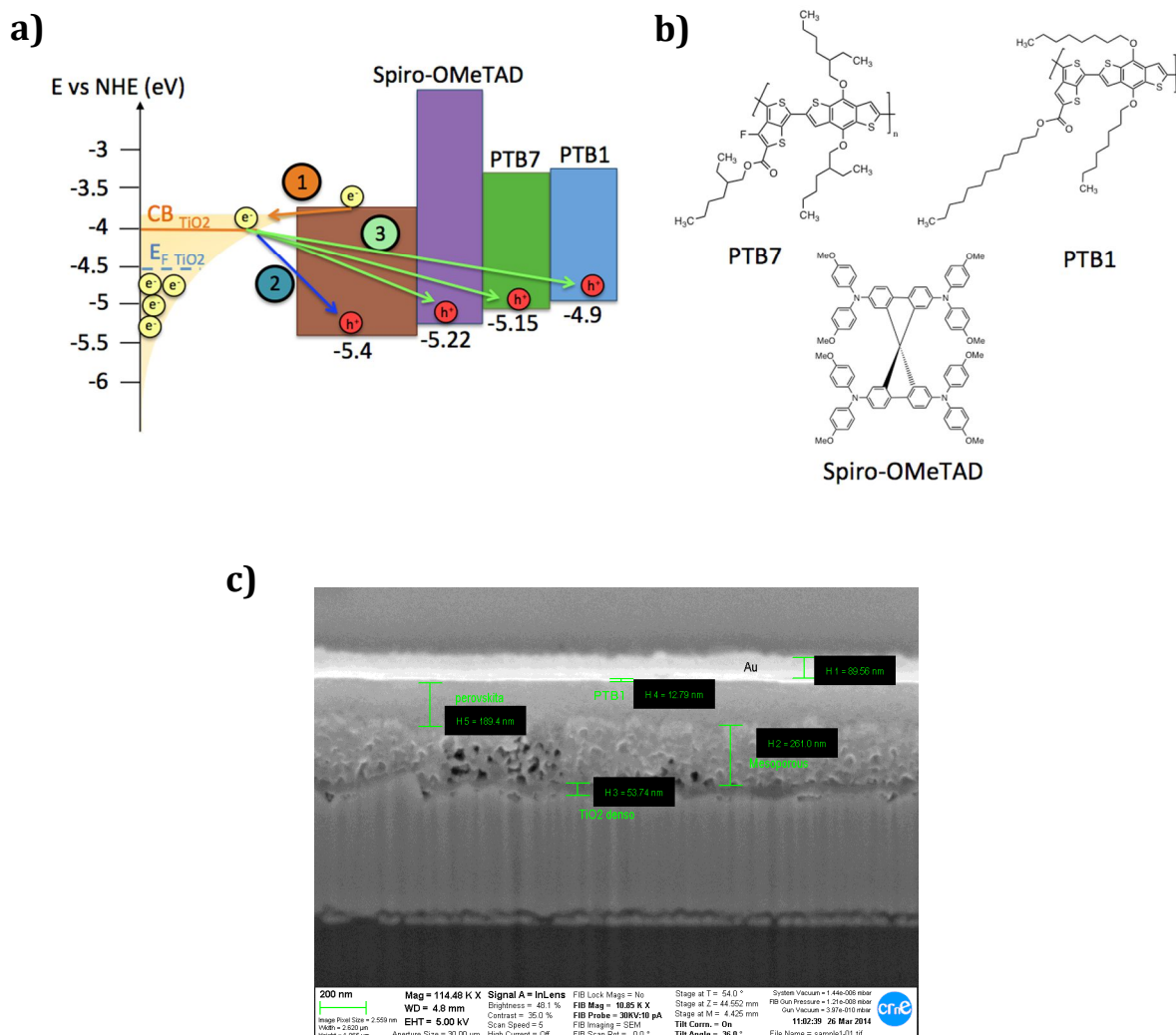
Scheme 2. a) Energy diagram for the materials used in our devices (energy numbers in eV). The arrows correspond to the interfacial charge transfer reactions occurring during working conditions: (1) charge injection, (2) charge recombination between the photo-injected electrons in the TiO_2 and the holes in the perovskite material, (3) as in (2) but the recombination reaction occurs with the oxidised HTM. **b)** Molecular structure of the HTM materials used in our study. **c)** High resolution scanning electron microscopy image of the sections of our PTB1 based solar cell. H_1= Gold contact (thickness: 89.6nm), H_2=mp-TiO_2 (thickness: 261.0nm), H_3=d-TiO_2 (thickness: 53.7nm), H_4= PTB1 (thickness: 12.8nm), H_5= perovskite (thickness: 189.4nm).

To simplify our discussion the use of chemical additives such as 1,8 di-iodooctane (DIO), 4-tert-Butyl Pyridine (tBuPyr) or Lithium Bis(Trifluoromethanesulfonyl)Imide (LiTFSI) on the semiconductor polymers was avoided. Nonetheless, efficiencies as high as the ones reported for other

semiconductor polymers in similar device structures have been achieved as listed in **Table 1**.
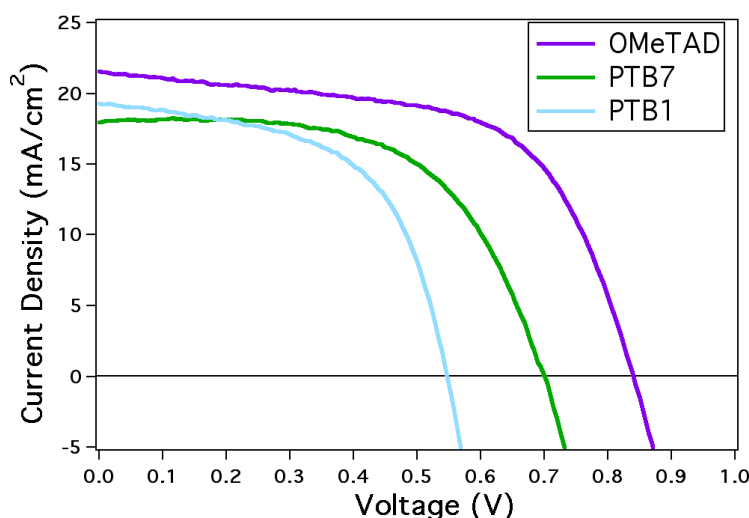

Figure 1. Photocurrent vs voltage (IV curves) measured at 1 sun (100mW/cm^2 1.5 AM G sun-simulated light) for our best devices using the different HTMs.

Table 1. IV curve parameters for our best devices.

HTM	Jsc (mA/cm^2)	Voc (mV)	FF (%)	PCE, η (%)
Spiro-OMeTAD	21.6	839	60.5	10.9
PTB1	19.3	543	57.2	6.0
PTB7	18.0	699	59.8	7.5
PCPDTBT	10.3	770	66.7	5.3*
PCDTBT	10.5	920	43.7	4.2*

Jsc= Device short-circuit photocurrent density. Voc= Open circuit photovoltage. FF = Fill factor. PCE, η= Solar cell efficiency. * From Reference 13[13].

It is important to note that the devices were stable during the time necessary to characterize the recombination kinetics using PIT-PV and L-TAS as shown in the ESI.

The devices were fabricated using a 50 nm thick layer of dense TiO$_2$ (d-TiO$_2$) and a 300 nm thick mesoporous TiO$_2$ (mp-TiO$_2$) layer all deposited onto FTO

(fluorine doped Tin Oxide) glass with a resistance of $8\Omega/cm^2$ following previous literature. The $CH_3NH_3PbI_{3-x}Cl_x$ was afterwards deposited on the mp-TiO_2 spin-coating a $PbCl_2$:CH_3NH_3I solution in DMF with a molar ratio of 1:3. The deposition of the metal oxide layers were carried out under ambient conditions but the subsequent deposition of the $MAPbI_{3-x}Cl_x$ was carried out in a glove box ([H_2O] < 0.1 ppm and [O_2] < 100 ppm content). Each semiconductor polymer was spin-coated onto the FTO/d-TiO_2/mp-TiO_2/$MAPbI_{3-x}Cl_x$ at 2000rpm for 60 s from a solution of chlorobenzene (10 mg/mL). The devices made using spiro-OMeTAD as HTM were fabricated using an identical protocol. **Scheme 2c** shows the cross-sectional scanning electron microscopy image for a PTB1 device. **Figure 2** shows the different L-TAS transient decays for the films upon excitation using our nanosecond Nd-YAG laser system (see ESI).
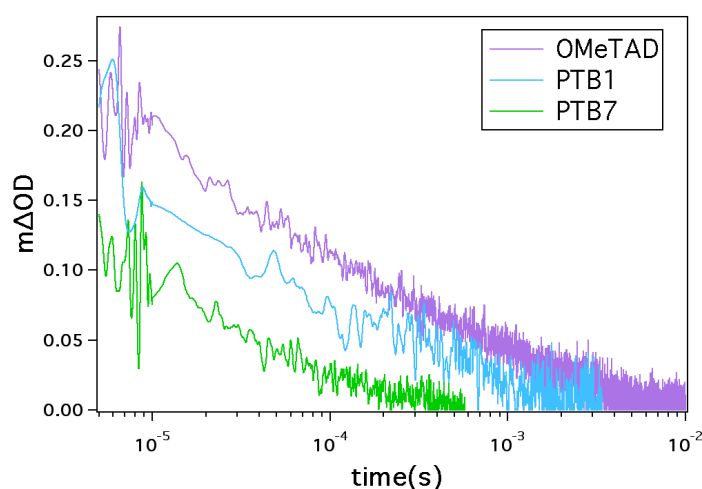

Figure 2. L-TAS decays, under ambient conditions, for the FTO/d-TiO_2/mp-TiO_2/$MAPbI_{3-x}Cl_x$/HTM films exciting at λ_{ex}=500nm for the spiro-OMeTAD films and λ_{ex}=700m for both semiconductor polymer films. The probe wavelengths were λ_{pr}=1400nm for the spiro-OMeTAD, λ_{pr}= 1100nm for the PTB7 and λ_{pr}= 980nm for the PTB1 films.

As can be seen, the signal amplitude for the spiro-OMeTAD and the PTB1 films are greater than that for the PTB7 film and, moreover, the decay lifetime for the spiro-OMeTAD is also slower, which implies that the back-electron transfer from the photo-injected electrons in the TiO_2 to the oxidised spiro-OMeTAD (reaction 3 in **Scheme 2**) is much slower than for the polymers. This can help explain why spiro-OMeTAD based devices are more efficient. We could estimate qualitatively the efficiency on the regeneration of the perovskite ground state from these signal

amplitudes. However, the unknown molar absorption coefficient of the HTM$^+$ polarons for both spiro-OMeTAD and the semiconductor polymers makes it difficult to ensure that the larger signal amplitude for spiro-OMeTAD corresponds to a better regeneration of the pervoskite ground state. Further work is in progress regarding this. Nonetheless, additional data using Time Correlated Single Photon Counting (TCSPC) shows differences in luminescence quenching of the perovskite for the different HTM materials in perfect agreement with the L-TAS signal amplitude **(Figure 3)**.
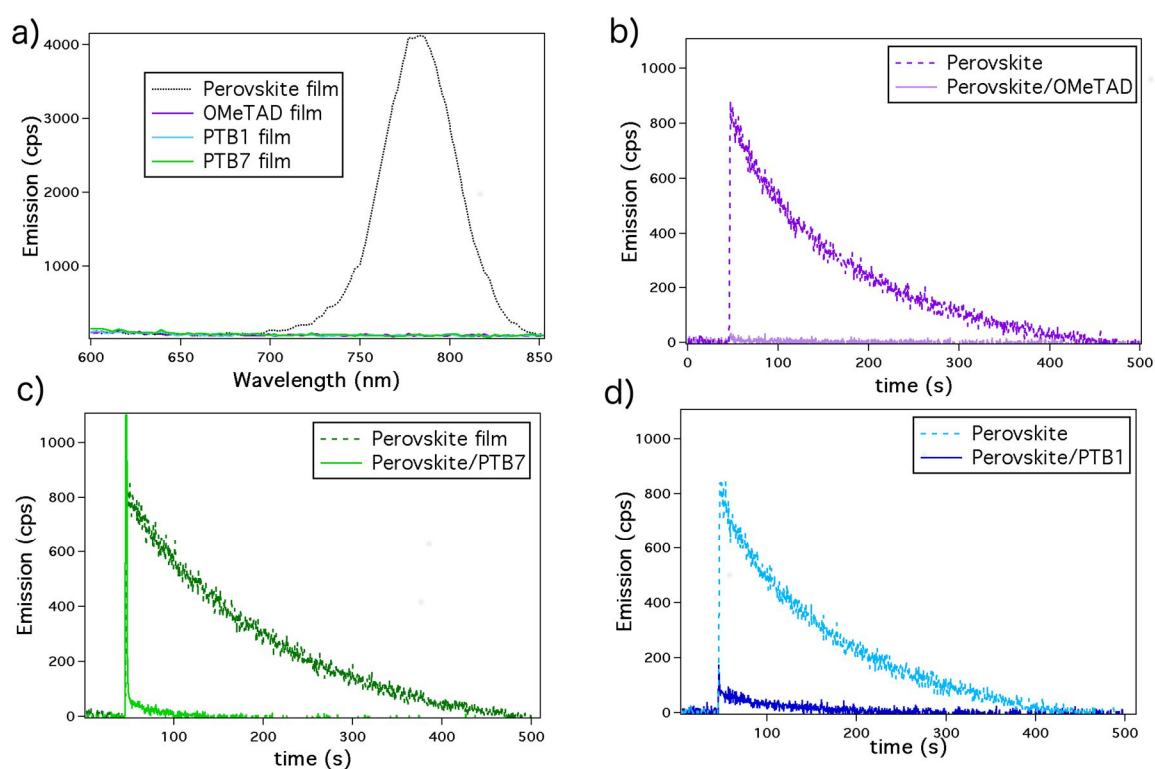

Figure 3. a) Photoluminiscence spectrum with λ_{ex}=470 nm of the different materials used in this communication deposited over a glass film following the same procedure of the actual devices. Comparison between the photoluminiscence decay (with λ_{ex}=470 nm and λ_{pr}=780 nm) of the raw perovskite film (dashed line) and the one with perovskite/HTM (solid line) being the HTMs **b)** OMeTAD, **c)** PTB7 and **d)** PTB1. From the integrals of these decays was possible to obtain the percentage of the regeneration of the perovskite with these HTMs. These regeneration percentages were 100% for OMeTAD, 96% for PTB1 and 98% for PTB7. In the case of perovskite/PTB7 there is a high peak with a very short lifetime (~30 ns) that correspond to a feature of the laser with this sample, and has been subtracted for the regeneration percentage calculations. All these measurements were carried out in a Time Correlated Single Photon Counting (TCSPC) instrument under ambient conditions..

In order to validate our hypothesis that the L-TAS signal corresponds to the recombination between the photo-injected electrons and the oxidised HTM, we carried out PIT-PV measurements in complete devices and compare the PIT-PV

decay with the L-TAS decay (**Figure 4**). This assumption cannot be done without the combination of both time-resolved techniques.
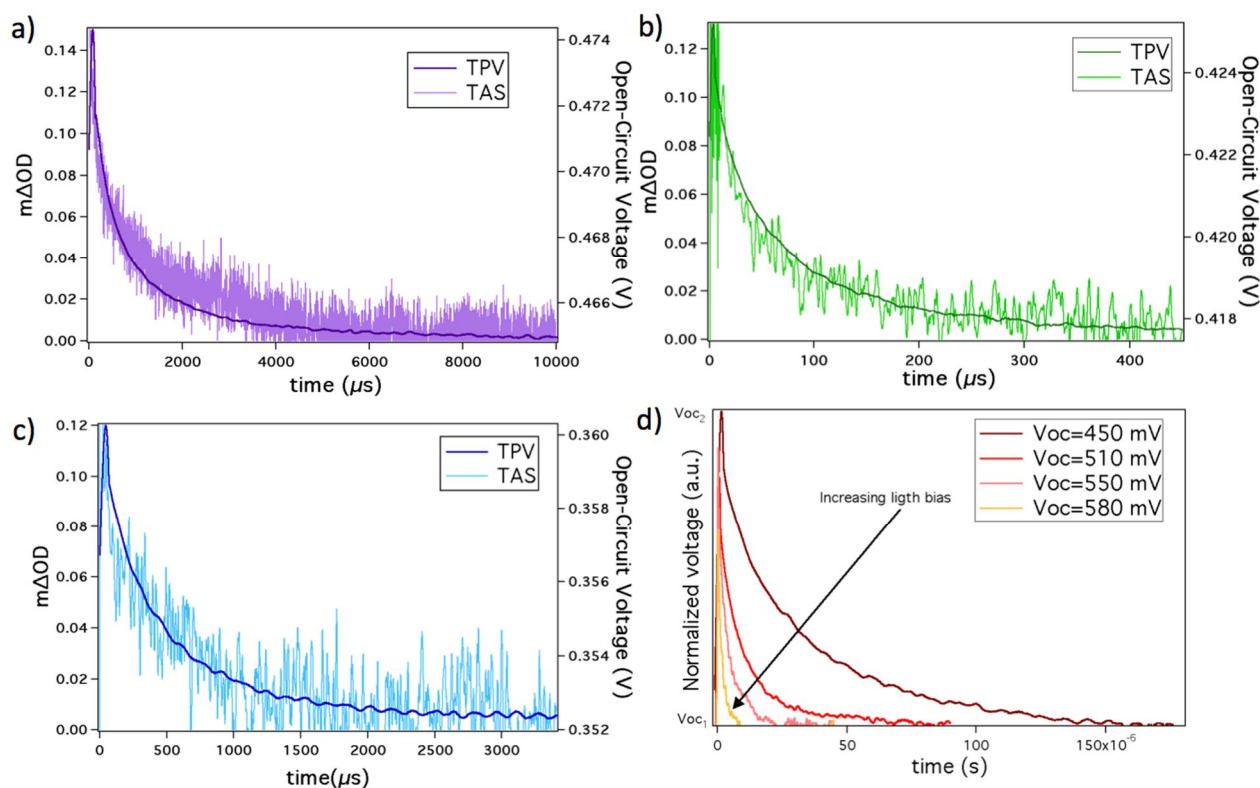

Figure 4. PIT-PV and L-TAS decays measured for the different devices. Notice the different Voc (right Y axis) for the different devices. **a)** Spiro-OMeTAD, **b)** PTB7, **c)** PTB1 and **d)** different PIT-PV decays at different light bias (solar cell photovoltage at different light intensities) for the PTB1 device.

PIT-PV is a technique that allows the measurement of the photo-induced recombination kinetics in complete devices under device working conditions[14,15]. Upon light illumination the solar cells generate a photovoltage (V_{oc_1}) that can be perturbed using a fast-pulsed laser. Upon excitation it generates a small increment of charges injected from the organolead halide to the TiO_2 raising the photovoltage to V_{oc_2}. This increase in Voc, ΔV_0, is proportional to the raise in the Fermi level of the TiO_2. After the laser pulse, the original V_{oc_1} is restored with a lifetime (τ) that is the time that it takes the excess photoinjected charges (resulting from the laser pulse) to recombine and return the solar cell to the initial photovoltage V_{oc_1}. It is important to note that the laser pulse must be small in energy ($\Delta V < 15mV$). **Figure 4** shows the PIT-PV decays for the devices studied in this work.

UNIVERSITAT ROVIRA I VIRGILI
SOLUTION PROCESSED INORGANIC SEMICONDUCTOR SOLAR CELLS
José Manuel Marín Beloqui
Dipòsit Legal: T 68-2016

Chapter 6   **PhD Thesis**

As can be seen, the PIT-PV and L-TAS decays fit in good agreement implying that, indeed, in both cases the charge transfer reaction measured corresponds unequivocally to the recombination reaction between the photo-injected electrons, from the $MAPbI_{3-x}Cl_x$ to the oxidised HTM^+. Moreover, as shown in **Figure 3d**, the increase of the light intensity (higher Voc) leads to faster PIT-PV decays (faster charge recombination), which implies a direct relationship between increasing the charge density, increasing the solar cell Voc and faster recombination kinetics between the photo-injected electrons at the TiO_2 and the oxidised materials used as HTM.

Conclusions

We have fabricated efficient solar cells using $MAPbI_{3-x}Cl_x$ as the light harvesting material and low band gap semiconductor polymers such as PTB1 and PTB7 as HTM. The interfacial charge transfer dynamics were probed using micro-second to millisecond L-TAS. The L-TAS signals suggest better regeneration kinetics for the spiro-OMeTAD and the PTB1 polymer in complete $MAPbI_{3-x}Cl_x$ solar cells. Moreover, the L-TAS kinetics appear slower for the spiro-OMeTAD films. To confirm our hypothesis we measured PIT-PV in complete devices, at different light bias, and we found that for low light intensities, close to the ones used in our L-TAS experiments, the PIT-PV and L-TAS decays fit in perfect agreement. The increase of the light intensity leads to higher device Voc with faster PIT-PV decays in all cases, suggesting that there is a direct correlation between photo-induced charge density, solar cell open circuit voltage (Voc) and faster recombination kinetics. Thus, in order to compare recombination kinetics in organolead halide based solar cells, it will be necessary to know beforehand the charge density in the devices under illumination as different device charge lifetime may well be due to the different charge density at the solar cell.

UNIVERSITAT ROVIRA I VIRGILI
SOLUTION PROCESSED INORGANIC SEMICONDUCTOR SOLAR CELLS
José Manuel Marín Beloqui
Dipòsit Legal: T 68-2016

PhD Thesis   **Chapter 6 - References**

References

1   B. Li, L. Wang, B. Kang, P. Wang and Y. Qiu, *Sol. Energy Mater. Sol. Cells*, 2006, **90**, 549–573.

2   H. J. Snaith and L. Schmidt-Mende, *Adv. Mater.*, 2007, **19**, 3187–3200.

3   L. Yang, U. B. Cappel, E. L. Unger, M. Karlsson, K. M. Karlsson, E. Gabrielsson, L. Sun, G. Boschloo, A. Hagfeldt and E. M. J. Johansson, *Phys. Chem. Chem. Phys.*, 2012, **14**, 779–89.

4   F. S. Freitas, J. N. Clifford, E. Palomares and A. F. Nogueira, *Phys. Chem. Chem. Phys.*, 2012, **14**, 11990–3.

5   M. M. Lee, J. Teuscher, T. Miyasaka, T. N. Murakami and H. J. Snaith, *Science (80-.).*, 2012, **338**, 643–647.

6   G. Xing, N. Mathews, S. Sun, S. S. Lim, Y. M. Lam, M. Grätzel, S. Mhaisalkar and T. C. Sum, *Science*, 2013, **342**, 344–7.

7   J. Burschka, N. Pellet, S.-J. Moon, R. Humphry-Baker, P. Gao, M. K. Nazeeruddin and M. Grätzel, *Nature*, 2013, **499**, 316–9.

8   S. Ryu, J. H. Noh, N. J. Jeon, Y. Chan Kim, W. S. Yang, J. Seo and S. Il Seok, *Energy Environ. Sci.*, 2014, **7**, 2614.

9   J. You, Z. Hong, Y. M. Yang, Q. Chen, M. Cai, T.-B. Song, C.-C. Chen, S. Lu, Y. Liu, H. Zhou and Y. Yang, *ACS Nano*, 2014, **8**, 1674–80.

10 S. Lv, L. Han, J. Xiao, L. Zhu, J. Shi, H. Wei, Y. Xu, J. Dong, X. Xu, D. Li, S. Wang, Y. Luo, Q. Meng and X. Li, *Chem. Commun. (Camb).*, 2014, **50**, 6931–4.

11 N. J. Jeon, J. Lee, J. H. Noh, M. K. Nazeeruddin, M. Grätzel and S. Il Seok, *J. Am. Chem. Soc.*, 2013, **135**, 19087–90.

12 V. Gonzalez-Pedro, E. J. Juarez-Perez, W.-S. Arsyad, E. M. Barea, F. Fabregat-Santiago, I. Mora-Sero and J. Bisquert, *Nano Lett.*, 2014, **14**, 888–93.

13 J. H. Heo, S. H. Im, J. H. Noh, T. N. Mandal, C.-S. Lim, J. A. Chang, Y. H. Lee, H. Kim, A. Sarkar, M. K. Nazeeruddin, M. Grätzel and S. Il Seok, *Nat. Photonics*, 2013, **7**, 486–491.

14 D. Joly, L. Pellejà, S. Narbey, F. Oswald, J. Chiron, J. N. Clifford, E. Palomares and R. Demadrille, *Sci. Rep.*, 2014, **4**, 4033.

UNIVERSITAT ROVIRA I VIRGILI
SOLUTION PROCESSED INORGANIC SEMICONDUCTOR SOLAR CELLS
José Manuel Marín Beloqui
Dipòsit Legal: T 68-2016

Chapter 6 - References   **PhD Thesis**

15   A. Reynal, A. Forneli, E. Martinez-Ferrero, A. Sánchez-Díaz, A. Vidal-Ferran, B. C. O'Regan and E. Palomares, *J. Am. Chem. Soc.*, 2008, **130**, 13558–67.

Chapter 7

Decreasing Charge Losses in Perovskite Solar Cells Through the mp-TiO$_2$/MAPI Interface Engineering

The use of methyl ammonium lead iodide (MAPI) perovskite-type semiconductor material has been the focus of increase interest for the development of efficient solar cells[1–3]. In less than 5 years solar-to-electrical conversion efficiency have been increased from η=3.8%[4] efficiencies to near 20%[5], exceeding the top best efficiencies measured for other so-called third-generation solar cells such as DSSC[6] (Dye Sensitized Solar Cells), OSC[7] (Organic Solar Cells) and QDSC[8] (Quantum Dot Solar Cells). The easy-to-fabricate procedures, materials low cost and past experience on the above mentioned solar cell technologies have paved the way for MAPI solar cells to become a hot spot in materials science for energy conversion devices such as solar cells and light-emitting diodes[9]. Moreover, the recent discovery of the use of MAPI as semiconductor for solar cells, has also presented novel scientific challenges as for example, the explanation of the unusual large amount of measured charge on MAPI solar cells[10], the presence of hysteresis effects[11–14], the bi-exponential nature of the registered small-perturbation based Voc decays[15,16] and/or the presence of

interfacial dipoles[17,18]. Whilst, the increase in solar cell efficiency has been spectacular, with a learning-curve never seen for other solar cell technologies alike CdTe and CIS, among others[19], the knowledge, however, on the detailed mechanisms that allows the efficient conversion of sun-light into electrical current have been less explored with remarkable exceptions[16,20–23] and, moreover, there is still the scientific challenge to approach MAPI solar cells to their maximum theoretical efficiency through the reduction of non-radiate charge recombination losses[24], better spectral response[25] and , moreover, increasing operational stability[26].

One particular issue of MAPI perovskite solar cells is that the semiconductor thin film can be used in different device configurations as for example: (a) the use of mesoporous metal oxide scaffolds alike Al_2O_3, TiO_2 or ZnO_2[27] as contacts, (b) without the mesoporous scaffold and (c) using organic materials as selective contacts[28]. Nonetheless, it is worthy to mention that the best certified devices have been described, to the best of our knowledge, with the archetypal device configuration[5] of FTO/d-TiO_2/mp-$TiO_2/MAPI/HTM/Au$ where FTO is the fluorine doped tin oxide semiconductor layer deposited on glass, d-TiO_2 is a thinner (~50nm) dense layer of TiO_2, mp-TiO_2 is a thin mesoporous layer (~450nm) and the HTM is the organic hole transport material. The choice of metal contact is usually gold (Au) on this class of device architecture too.

For the reasons given below the above described device configuration is the standard used in this work unless otherwise stated: On the one hand, our experience on the deposition of the TiO_2 metal oxide[29], its characterization and previous encouraging results in relation with this work using this device structure[15] and, on the other hand, to clarify further the role on the mp-TiO_2 layer in the MAPI perovskite solar cell.

It is well known that reducing the charge losses due to inconvenient interfacial charge recombination reactions under operation is paramount to increase the solar cell efficiency[30]. Learning from past studies in DSSC, we have observed that direct back-electron transfer from the photo-injected electrons at the mp-TiO_2 to the oxidized electrolyte was a major issue to overcome to increase the solar cell efficiency. Indeed, reducing this particular charge recombination reaction through better dye design and rational interface engineering lead to better and more reproducible DSSC[31].

In our first communication using the MAPI perovskite semiconductor in solar cells[15], we hypothesized that several interfacial and band to band recombination pathways can be found in MAPI/mp-TiO$_2$/HTM sample as illustrated in **Scheme 1**. For one, after electron injection from the MAPI to the TiO$_2$ conduction band (reaction 1, **Scheme 1**) subsequent interfacial back electron transfer may takes place (reaction 2, **Scheme 1**). For another, the photo-injected electrons at the TiO$_2$ can also recombine with holes at the oxidized HTM (analogously to the reaction occurring in solid-state DSSC but it his case cannot be a direct recombination as there is a thin layer of MAPI perovskite between the TiO$_2$ and the HTM) and as measured by Moser and co-workers using laser transient absorption spectroscopy[20], (reaction 3, **Scheme 1**). Moreover, electrons at the MAPI perovskite can also recombine with the holes at the oxidized HTM (reaction 4, **Scheme 1**). Last but not least, band to band non-radiate and radiate charge recombination reactions at the MAPI perovskite (reaction 1, **Scheme 1**) have to be also considered.

Hence, the modification of the mp-TiO$_2$/MAPI perovskite interface may affect at least one of the recombination pathways that limit the solar cell performance.

The use of conformally deposited insulating overlayers onto the TiO$_2$ nanocrystals surface have been previously explored by our group and others in DSSC[32–34]. Indeed, it has been demonstrated that the interfacial engineering onto the semiconductor nanocrystals, either TiO$_2$ or ZnO, leads to a substantial decrease of the charge losses due to interfacial recombination processes. In fact, a recent publication[35] by Jung and co-workers describes the use of MgO onto mp-TiO$_2$ in MAPI solar cells, however, the device electronic characterization to understand the changes in solar cell Voc remained unclear.

In the present work we have fabricated MAPI perovskite solar cells with the archetypal structure mentioned above as well as MAPI perovskite solar cells with an Al$_2$O$_3$ insulating thin layer onto the nanocrystalline TiO$_2$ particles that conform the mp-TiO$_2$ layer. The former will be described along this work as MAPI perovskite solar cells, while the latter will be designed as Al$_2$O$_3$-coated perovskite solar cells. Moreover, we have used advanced photo-induced characterisation techniques, namely photo-induced transient photo-voltage (PIT-PV), photo-induced differential charging (PIDC) and photo-induced transient photo-current (PIT-PC) to thoroughly analyse the

UNIVERSITAT ROVIRA I VIRGILI
SOLUTION PROCESSED INORGANIC SEMICONDUCTOR SOLAR CELLS
José Manuel Marín Beloqui
Dipòsit Legal: T 68-2016

Chapter 7   **PhD Thesis**

differences in charge density (defined as the total accumulated charge in the device at a given bias), the charge recombination lifetime and the relationship between both mentioned parameters. The findings described below are key to (a) understand further the device charge recombination processes that hamper the solar-to-electrical powerconversion efficiency and (b) to increase the device fabrication reproducibility through interface engineering.
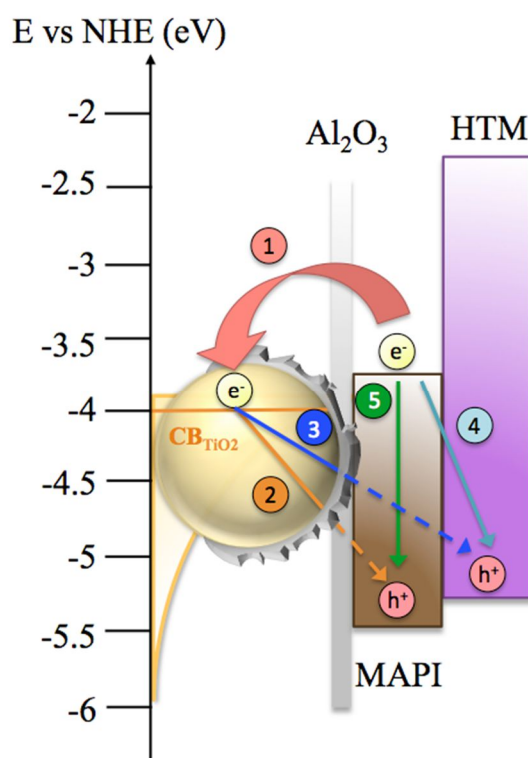
Scheme 1. The photo-induced interfacial charge transfer recombination reactions in MAPI perovskite solar cells; **(1)** interfacial electron transfer from MAPI conduction band (CB) to TiO_2, **(2)** interfacial electron transfer from the TiO_2 CB to the MAPI, **(3)** interfacial electron transfer from TiO_2 CB to the HTM, **(4)** interfacial electron transfer from the MAPI CB to the HTM and **(5)** band to band radiate and non-radiate recombination.

Figure 1 illustrates the current density vs voltage measurements (IV curves) for archetypal MAPI perovskite solar cells and the Al_2O_3 coated ones under standard sun-simulated irradiation condition (100mW/cm^2 @1.5 AM G).
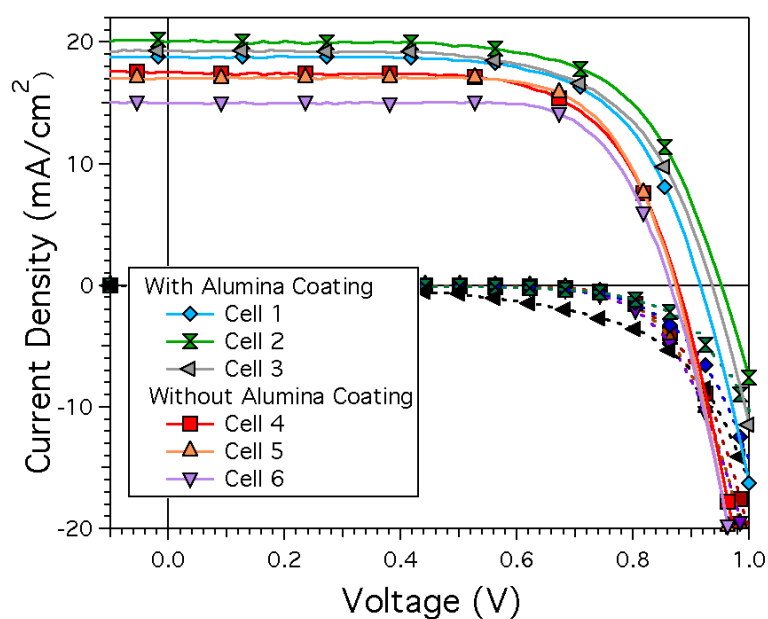
Figure 1. Several MAPI perovskite solar cells with and without the Al_2O_3 modified mp-TiO_2/MAPI interface under 1 sun illumination and the corresponding dark curves (dashed lines)

As can be seen in **Figure 1**, solar cells using Al_2O_3 mp-TiO_2 coated show an increase in Voc and photocurrent leading to an average efficiency of η_{Al2O3}=12% in contrast to standard MAPI perovskite solar cell that show a standard average efficiency of η=10.2%. **Table 1** lists all the relevant parameters for the measured cells in this work.

Table 1. Most relevant parameters obtained from the IV curves illustrated in **Figure 1**.

Device	Jsc (mA/cm^2)	Voc (mV)	FF (%)[1]	PCE, η (%)	Al_2O_3 Coating
Cell 1	920	18.6	67.8	11.6	yes
Cell 2	960	20.1	66.1	12.7	yes
Cell 3	939	19.3	65.1	11.8	yes
Cell 4	870	17.6	67.9	10.4	no
Cell 5	870	17.0	72.3	10.7	no
Cell 6	860	15.0	73.6	9.5	no

[1]device fill factor. Solar cell area of 0.25 cm^2. All solar cells were fabricated and measured under the same conditions.

UNIVERSITAT ROVIRA I VIRGILI
SOLUTION PROCESSED INORGANIC SEMICONDUCTOR SOLAR CELLS
José Manuel Marín Beloqui
Dipòsit Legal: T 68-2016

Chapter 7   **PhD Thesis**

Further measurements of solar cells (**Figure 2**) fabricated in different days and conditions, from the devices depicted and listed in **Figure 1** and **Table 1** respectively, but always keeping identical measurement and fabrication conditions within each set of samples of Al_2O_3 coated mp-TiO_2 and the corresponding MAPI perovskite solar cells are presented. As seen, control show identical trend with the Al_2O_3 modified mp-TiO_2/MAPI interface having higher Voc and, in average, higher solar-to-energy conversion efficiency.
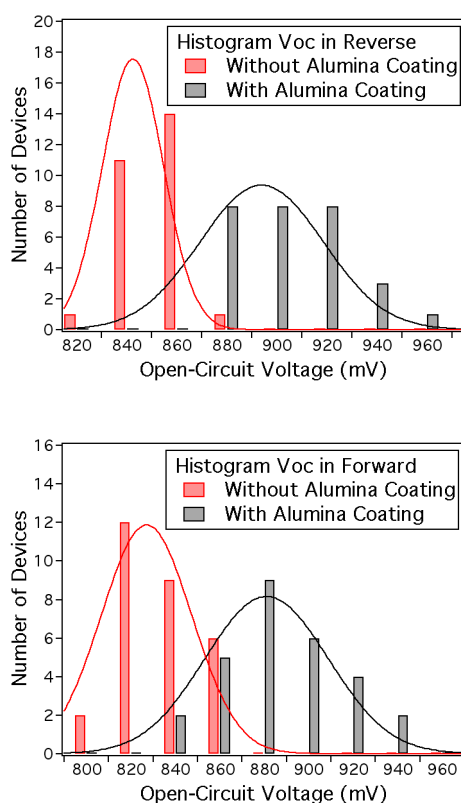

Figure 2. Solar cell open-circuit voltage (Voc) distribution for 28 Al_2O_3 coated mp-TiO_2 devices (grey) and 27 MAPI perovskite solar cells (red). Top, devices measured under reverse bias. Bottom, devices measured under forward bias.

In order to understand the effect of the Al_2O_3 onto the mp-TiO_2 and the overall solar cell performance and compare to what has been observed in DSSC we have carried out different experiments detailed below. The use of photo-induced differential charging (PIDC) has been very useful to analyse the accumulated[36] charge at the solar cell under different light-bias (solar cell voltage induced by different illumination intensities) in DSSC[37], QDSC[38], OSC[39] and more recently in MAPI solar cells[16]. Moreover, it allows comparing the photo-generated charge density, at the

112

same Voc, for different solar cells and, furthermore, is a key measurement in order to fairly compare charge recombination lifetime between different types of solar cells.

Photo-Induced Differential Charging (PIDC).

The details for the PIDC technique can be found at the Supplementary information of this manuscript. In brief, the charge is measured using PIT-PV and PIT-PC (photo-induced transient photo-current) as our group and others have previously demonstrated[40]. The use of PIDC is particularly necessary when the PICE decay has a longer lifetime than the measured PIT-PV decay at 1 sun (as for MAPI perovskite solar cells in **Figure 3**).
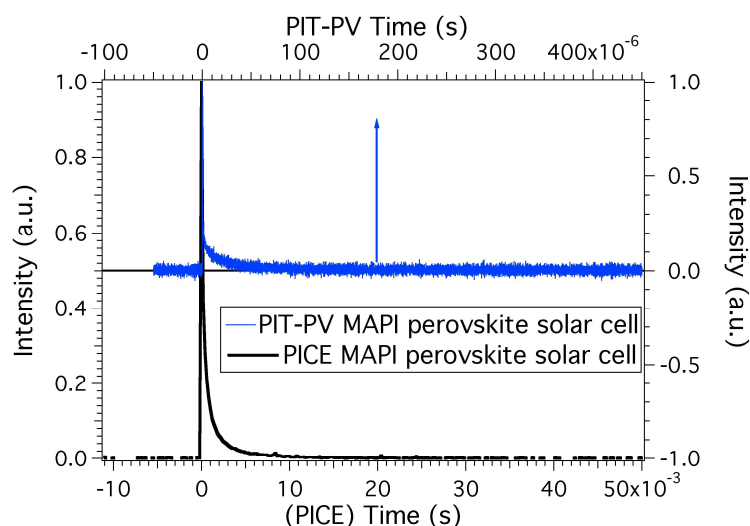

Figure 3. PICE decay (black line) for a MAPI perovskite solar cell and the PIT-PV transient (blue line) upon sun-simulated illumination equivalent to 1 sun. Notice the different time scales for the PICE (bottom axis) and the PIT-PV (top axis).

To estimate the photo-generated charge stored at the MAPI perovskite solar cell we must assume that (a) the solar cell has not charge losses at short circuit and (b) the PIT-PC under 1 sun and in the dark are similar. In other words, the charge generation efficiency is similar at short-circuit and at open circuit solar cell conditions. **Figure 4** shows the PIT-PC measurements for both types of MAPI perovskite solar cells.
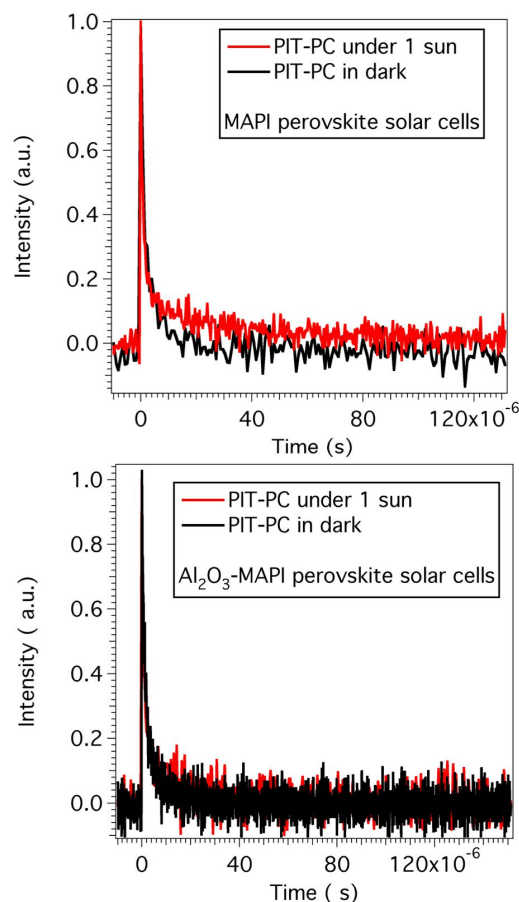
Figure 4. PIT-PC decays measured for (top) $mpTiO_2$/MAPI perovskite and (bottom) Al_2O_3/$mpTiO_2$/ MAPI perovskite solar cells.

As can be seen in **Figure 4**, either the PIT-PC under 1 sun or under dark for both type of solar cells are quite close. Hence, we carried out the PIDC for both type of solar cell devices. **Figure 5** illustrates the charge measured from the PIDC vs solar cell voltage.

In contrast to previous measurements on DSSC with the Al_2O_3 coating, there is no sensible and reproducible shift between the measured exponential curves[41]. In DSSC with the mp-TiO_2 conformally coated with Al_2O_3 a shift of the measured charge vs voltage exponential curve is observed and assigned to a shift of the TiO_2 conduction band edge with concomitant shift of the quasi-Fermi level for the electrons at the mp-TiO_2. The mp-TiO_2 conduction band shift plus the measured slower interfacial recombination kinetics between the electrons at the mp-TiO_2 and the oxidized electrolyte, in DSSC, lead to a measured increase in the open circuit

voltage of the DSSC. Thus, next is to measure the PIT-PV in the MAPI perovskite solar cells and see if there is correlation with the measured higher open circuit voltage.
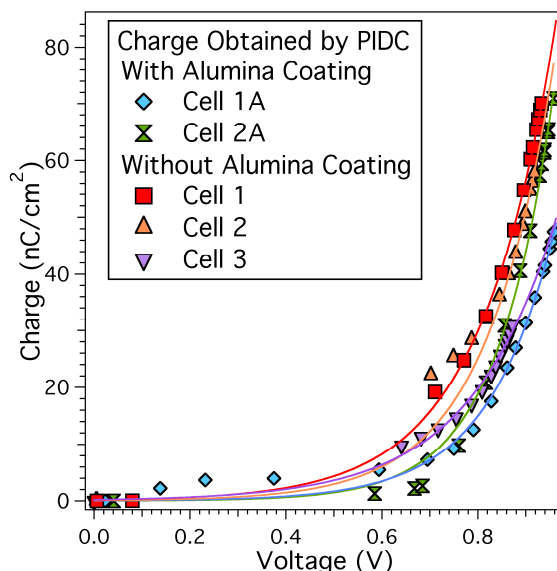

Figure 5. Measured charge using PIDC at different solar cell voltage from MAPI perovskite solar cells and Al$_2$O$_3$–coated perovskite solar cells. The Cell 3A has been removed for clarity read-out of the data in the figure.

Photo-Induced Transient Photovoltage (PIT-PV).

The PIT-PV technique has been widely used to correlate the measured charge, at a given voltage, with the charge recombination lifetime. In a seminal paper[42], Bisquert and Zaban defined the Voc decay technique for DSSC and later our group and others used a modified version of the technique, which is based in small perturbation of the open-circuit cell voltage using a fast light pulse. The fast pulse disrupts the equilibrium raising the quasi-Fermi level for the electrons at the mp-TiO$_2$, which is restored after the pulse finishes to the original energy level and, thus, restoring the initial open-circuit voltage. In DSSC, the voltage decay promoted by the fast light pulse results in a mono-exponential decay with an amplitude always smaller than 10mV to ensure a minor perturbation of the cell open-circuit voltage.
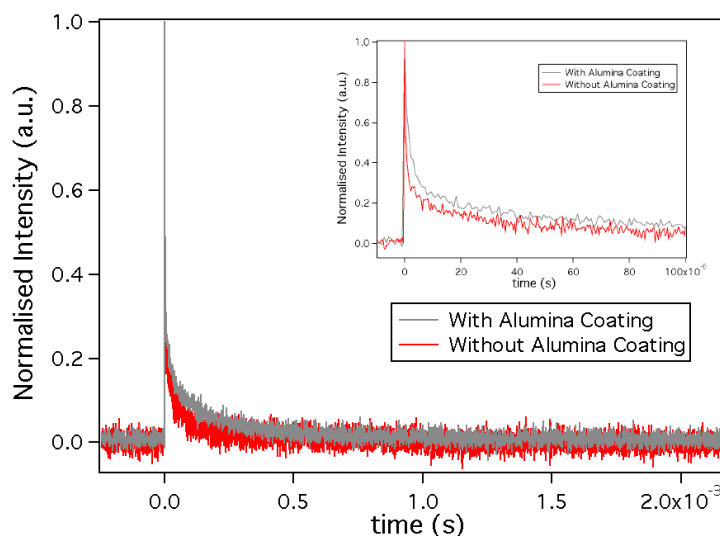
Figure 6. Measured PIT-PV for a MAPI perovskite solar cell (black) and an Al_2O_3-coated MAPI perovskite solar cell (red) at 100mW/cm^2 light irradiation. The inset shows the fastest component of the PIT-PV..

Figure 6 illustrates the PIT-PV decays for our MAPI perovskite solar cells.

The first difference observed in comparison to the PIT-PV decays in DSSC is the bi-exponential nature of the decays measured either with the Al_2O_3 coating or the MAPI perovskite as control. As shown in **Figure 6** both samples show bi-exponential decays with $\tau_1 = 175$ μs (20%) and $\tau_2 = 3$ μs (80%) for Al_2O_3 coated solar cells and $\tau_1 = 73$ μs (20%) and $\tau_2 = 0.8$ μs (80%) for MAPI perovskite solar cells under similar charge density ~35nC/cm2. This result is in good agreement with previous data[16,23].

In MAPI perovskite solar cells, there is still far from clear the origin of the large photo-voltage measured that in some cases is overpassing 1 V. Moreover, the large differences in charge density measured using PICE and PIDC and the different chemical nature that both types of charges may have, taking into account the differences in the kinetics from the bi-exponential PIT-PV decay, makes even more challenging to assign the processes that gives rise to the accumulated charges measured. Thus, it may well be that the measured transient photo-voltage does not correspond to a charge recombination process (charge losses) but to, for example, a reorganization of dipoles at the MAPI that leads to a change in voltage or to a combination of both processes. Nevertheless, we have studied in detail the PIT-PV and we have proposed that the fast component of the PIT-PV decay is the product of

the electron-hole recombination process and hence the photo-induced charge recombination lifetime[16]. Hence, based in our past experience we have also used for comparison purposes between MAPI solar cells the charge measured by PIDC and the fastest component of the PIT-PV decay.

Charge recombination lifetime vs charge density.

It is important to notice that for the comparison we use the measured charge from PIDC, instead of the measured cell Voc at different light intensities (so called light bias) because it is well established for other solar cells such as DSSC, OPV and QDSC that it may well be that at the same Voc different solar cells have very different amount of stored charge and thus, the compared charge recombination lifetime will not be meaningful and appropriate. **Figure 7** illustrates the carrier recombination lifetime vs electrical charge for both types of solar cells.
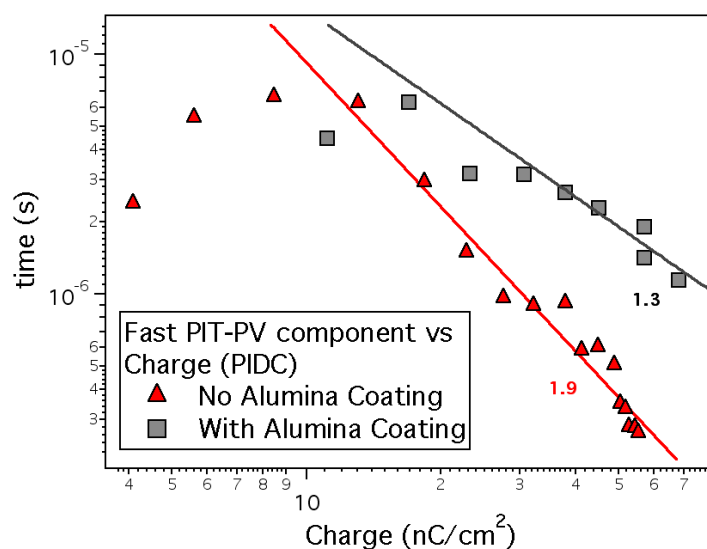

Figure 7. Non-radiate carrier recombination lifetime (fast component PIT-PV decay) vs solar cell electrical charge measured by PIDC. The numbers correspond to the recombination order factor (OF).

UNIVERSITAT ROVIRA I VIRGILI
SOLUTION PROCESSED INORGANIC SEMICONDUCTOR SOLAR CELLS
José Manuel Marín Beloqui
Dipòsit Legal: T 68-2016

Chapter 7   **PhD Thesis**

As illustrated in **Figure 7**, the use of Al_2O_3 conformal coating leads to slower interfacial charge recombination lifetimes when compared to the standard $mpTiO_2$ film.

We also would like to emphasize that although the slowest component of the PIT-PV decay, either with the charge measured using PICE or the charge measured using PIDC, cannot reproduce fairly the Jrec and, thus, seems that is not related to the "electrical charge" (understanding as electrical charge electrons and holes) at the MAPI perovskite still accounts for at least 20% of the PIT-PV decay and, interestingly the PIT-PV slow component of the decay is slower for Al_2O_3. A comparison of both types of solar cells, the Al_2O_3 coated and the MAPI perovskite device is illustrated in **Figure 8**.
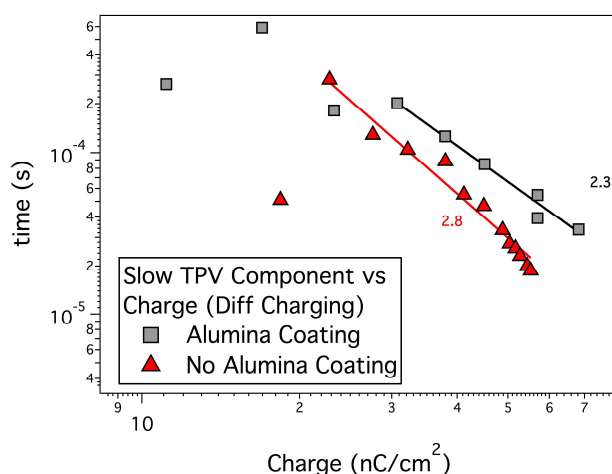

Figure 8. The slow component for the PIT-PV decays vs solar cell measured charge by PIDC at different light bias. The numbers correspond to the recombination order factor (OF)

Conclusions

We have used Al_2O_3 conformal coating from solution-processed methods onto mesoporous TiO_2 electrodes ($mpTiO_2$) used in the preparation of efficient MAPI perovskite solar cells. The use of Al_2O_3 coating leads to an improvement in the solar cell efficiency mainly due to a higher open circuit voltage (Voc). The increase in Voc is systematic and reproducible. Moreover, we have studied the interfacial charge

recombination processes using photo-induced time resolved methods in complete devices under sun-simulated irradiation conditions. Using PIDC we have not observed a clear shift on the exponential charge distribution as it was demonstrated for Al_2O_3/mpTiO$_2$ coated DSSC.

The analysis of the PIT-PV decays shows two different time components, in good agreement with previous measurements with other MAPI perovskite solar cells. In fact, for Al_2O_3 coated solar cells both time components present at the PIT-PV decay are slower in comparison with the standard MAPI perovskite solar cell. A careful comparison of both charge recombination lifetime components at the same charge density further confirms that the recombination lifetime for Al_2O_3 treated solar cells is significantly slower.

Hence, it seems clear that the slower charge recombination kinetics in the Al_2O_3 coated MAPI perovskite solar cells can be directly correlated with the solar cell Voc improvement. However, unlike the case of DSSC, it was unclear why both PIT-PV time components are affected by the presence of the Al_2O_3 coating onto the mesoporous TiO_2. A feasible hypothesis in the light of the results obtained in this work is that both PIT-PV components can be assigned to two different charge recombination processes; one process related to the charge transfer of electrons from the TiO_2, upon electron transfer from the MAPI perovskite under illumination, with the holes at the HTM and a second, and faster charge recombination process, between electrons at the TiO_2 and holes at the MAPI perovskite. In both cases the Al_2O_3 will act as a physical barrier (alike in the case of DSSC) decreasing the rate of the back electron transfer reaction upon photo-induced electron injection from the MAPI perovskite to the TiO_2 CB.

References

1   B. Li, L. Wang, B. Kang, P. Wang and Y. Qiu, *Sol. Energy Mater. Sol. Cells*, 2006, **90**, 549–573.

2   H. J. Snaith and L. Schmidt-Mende, *Adv. Mater.*, 2007, **19**, 3187–3200.

3   L. Yang, U. B. Cappel, E. L. Unger, M. Karlsson, K. M. Karlsson, E. Gabrielsson, L. Sun, G. Boschloo, A. Hagfeldt and E. M. J. Johansson, *Phys. Chem. Chem. Phys.*, 2012, **14**, 779–89.

4   F. S. Freitas, J. N. Clifford, E. Palomares and A. F. Nogueira, *Phys. Chem. Chem. Phys.*, 2012, **14**, 11990–3.

5   M. M. Lee, J. Teuscher, T. Miyasaka, T. N. Murakami and H. J. Snaith, *Science (80-.).*, 2012, **338**, 643–647.

6   G. Xing, N. Mathews, S. Sun, S. S. Lim, Y. M. Lam, M. Grätzel, S. Mhaisalkar and T. C. Sum, *Science*, 2013, **342**, 344–7.

7   J. Burschka, N. Pellet, S.-J. Moon, R. Humphry-Baker, P. Gao, M. K. Nazeeruddin and M. Grätzel, *Nature*, 2013, **499**, 316–9.

8   S. Ryu, J. H. Noh, N. J. Jeon, Y. Chan Kim, W. S. Yang, J. Seo and S. Il Seok, *Energy Environ. Sci.*, 2014, **7**, 2614.

9   J. You, Z. Hong, Y. M. Yang, Q. Chen, M. Cai, T.-B. Song, C.-C. Chen, S. Lu, Y. Liu, H. Zhou and Y. Yang, *ACS Nano*, 2014, **8**, 1674–80.

10   S. Lv, L. Han, J. Xiao, L. Zhu, J. Shi, H. Wei, Y. Xu, J. Dong, X. Xu, D. Li, S. Wang, Y. Luo, Q. Meng and X. Li, *Chem. Commun. (Camb).*, 2014, **50**, 6931–4.

11   N. J. Jeon, J. Lee, J. H. Noh, M. K. Nazeeruddin, M. Grätzel and S. Il Seok, *J. Am. Chem. Soc.*, 2013, **135**, 19087–90.

12   V. Gonzalez-Pedro, E. J. Juarez-Perez, W.-S. Arsyad, E. M. Barea, F. Fabregat-Santiago, I. Mora-Sero and J. Bisquert, *Nano Lett.*, 2014, **14**, 888–93.

13   J. H. Heo, S. H. Im, J. H. Noh, T. N. Mandal, C.-S. Lim, J. A. Chang, Y. H. Lee, H. Kim, A. Sarkar, M. K. Nazeeruddin, M. Grätzel and S. Il Seok, *Nat. Photonics*, 2013, **7**, 486–491.

14   D. Joly, L. Pellejà, S. Narbey, F. Oswald, J. Chiron, J. N. Clifford, E. Palomares and R. Demadrille, *Sci. Rep.*, 2014, **4**, 4033.

15   A. Reynal, A. Forneli, E. Martinez-Ferrero, A. Sánchez-Díaz, A. Vidal-Ferran, B. C. O'Regan and E. Palomares, *J. Am. Chem. Soc.*, 2008, **130**, 13558–67.

Chapter 8

Experimental Device Preparation

In this chapter an exhaustive description of device fabrication related along the thesis, PbS/evaporated C60 and perovskite, will be explained. The substrate cleaning, deposition by spin-coating and evaporation steps will be reported.

5.1 Substrate Preparation

During the PhD, solar devices were prepared over glass substrates coated with a Fluor (FTO) or Indium (ITO) doped tin oxide layer. During these years, ITO substrates were already cut and patterned, indicating where the electrodes must to be placed. However, due to the FTO nature, FTO substrates were needed to be cut and etched in the lab.

UNIVERSITAT ROVIRA I VIRGILI
SOLUTION PROCESSED INORGANIC SEMICONDUCTOR SOLAR CELLS
José Manuel Marín Beloqui
Dipòsit Legal: T 68-2016

Chapter 8   **PhD Thesis**

First step is to remove the conductive layer over the substrate to denote the position of the electrodes in the device. The process of removing the conductive layer of the substrate is called "etching". To do etching, a tape is used to cover substrate except from the part where the FTO should be removed. After the tape coverage, some Zn powder is placed over the uncovered part of the substrate, dropping then some diluted HCl. Then, a vigorous reaction between HCl and Zn takes place, reaching temperatures high enough to remove the conductive layer.

Once the FTO was removed, the next step was to clean the substrates. To clean substrates they were placed in a rack where they were maintained in vertical position allowing the solvent to remove all the dirt. The rack with the substrate was sunken in a vessel filled with solvent and substrates were sonicated for 15 minutes three times, changing the solvent and rising both, substrates and the vessel to remove any remaining dirt. The solvents used were Hellmanex soap in water, water and ethanol for FTO substrates and acetone and twice 2-propanol for ITO substrates. Then, the substrates were dried with nitrogen and a Ozone/UV treatment was performed for 20-30 minutes.

After Ozone/UV treatment substrates were ready for the active layer deposition.

5.2 Spin-coating

Spin-coating is a technique to deposit uniform thin films using the centrifugal force. This technique is widely used due to their low-price, the homogeneity of the final film and its versatility. The deposition with this technique is very industrially focused, as it is cheaper than other deposition methods such as high vacuum process, atomic layer deposition, etc, being this one of the most promising characteristics of most of the third generation solar cells.

In this technique, the material solution to create the film is deposited in the centre of the substrate, that it is stuck in the spin-coater by vacuum, totally covering it. Then, the substrate starts to spin until the solvent is evaporated and the homogeneous layer is created. The thickness of the film will depend of several

factors, such as the concentration of the material solution, the spinning angular speed of and solution viscosity.
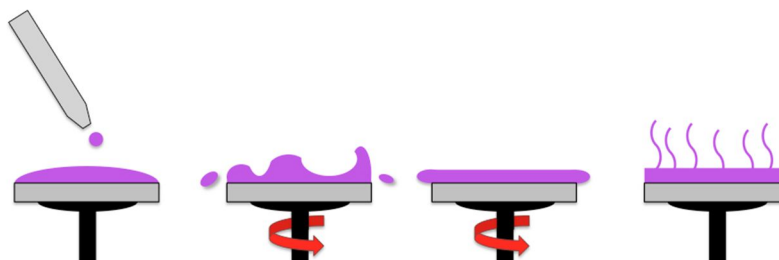

Figure 1. Scheme representing the spin-coating process.

Along this thesis several materials have been deposited by spin-coating, being depicted their particular spin-coating conditions in its corresponding experimental section.

Inside the spin-coating processes carried out through this thesis, QD deposition by layer-by-layer need to be explained more in detail. This process involves the deposition of very thin layers of QDs, PbS in the case depicted in the thesis, performing the ligand exchange of the QD in situ. Then the process was repeated in order to obtain thicker film thickness but ensuring a proper ligand exchange along the whole QD layer.

In this case, deposition of QD was performed surrounded of Oleic Acid, that is a long acid chain that protects and solubilized the QDs. After the deposition of the thin layer of PbS QD (around 5 nm), a solution of MPA or Ethanodithiol (EDT) was spin-coated over the PbS layer in order to exchange the oleic acid by this new ligand. This new ligand is always shorter and bidentate to improve the connectivity of the QDs and, in this way, to improve their electrical performance. After this step, some solvent, methanol in the case of MPA and acetonitrile with the EDT, was spin-coated to remove any remaining ligand unattached to the QD. Then, another spin-coated was performed with the solvent of the QD to remove any unstuck QD. With this, the first cycle was completed, then the whole process was repeated to get the desired QD film thickness.
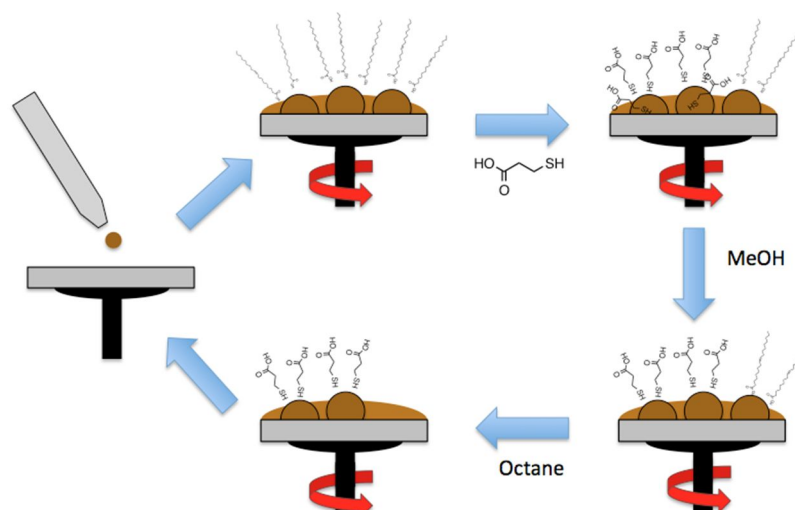
UNIVERSITAT ROVIRA I VIRGILI
SOLUTION PROCESSED INORGANIC SEMICONDUCTOR SOLAR CELLS
José Manuel Marín Beloqui
Dipòsit Legal: T 68-2016

Chapter 8   **PhD Thesis**

Figure 2. Scheme of the layer by layer process where every step is depicted.

5.3 High Vacuum Thermal Evaporation

High Vacuum Thermal Evaporation is a technique carried out in an evaporator (**Figure 3**) where very high vacuum levels are reached, lower than 10^{-6} mbar. At this pressure level, the boiling point of the materials get highly decreased, allowing to evaporate materials with high boiling point such as metals and other inorganic materials.

The material is placed in solid state in a boat or a crucible, that will be connected to the power supply of the evaporator, that will be controlling the current that goes through the boat or crucible heating the material until it evaporates. Once the material is evaporated the rate of evaporation has to be maintained constant to guarantee a right deposition. The evaporation system used along this thesis has a controller that automatically varies the amount of applied power to decrease or increase the evaporation rate.

With this technique, organic molecules have also been deposited along the PhD. However, the organic molecules evaporation is not suitable with the controller and the evaporation has been performed manually, controlling the power applied to the crucible, while the rate is controlled.

There were two vessels depending of the origin of the material nature to evaporate. Boron Nitride crucibles were used for organic substances, meanwhile the inorganic materials such as MoO_3, Au, Ag, were evaporated using Tungsten boats.
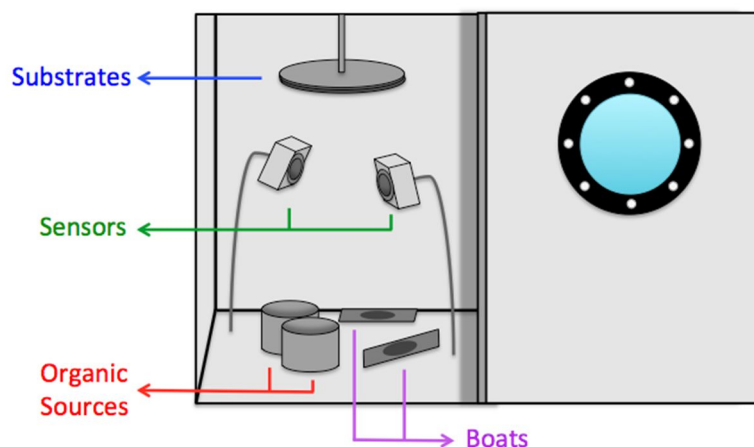

Figure 3. Scheme of the evaporator used in the work along this thesis.

The substrates have to be placed in masks with hollow parts in the top of the evaporator, and when the material is evaporated goes through the shadow mask depositing over the substrate.

Chapter 9

Synthesis and Characterization

UNIVERSITAT ROVIRA I VIRGILI
SOLUTION PROCESSED INORGANIC SEMICONDUCTOR SOLAR CELLS
José Manuel Marín Beloqui
Dipòsit Legal: T 68-2016

PhD Thesis **Chapter 9**

PbS QDs Synthesis

PbS QDs were prepared along this thesis following a slightly modified procedure described by Sargent *et al.*[1]. This method was based in the hot-injection method, in which the precursor was heated up, and the QD was formed with the injection of the sulfur precursor (TMS) to the metal precursor hot solution (lead surrounded by the oleic acid).

Although the procedure was changed to obtain different QDs sizes, the "standard" used synthesis was described next. The reaction was performed in a three-necked flask, where the three necks were used with a septum to perform the injection, the refrigerant and the thermometer, as depicted in **Figure 1.**
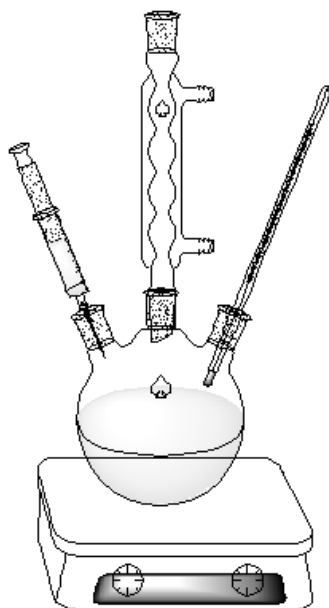
UNIVERSITAT ROVIRA I VIRGILI
SOLUTION PROCESSED INORGANIC SEMICONDUCTOR SOLAR CELLS
José Manuel Marín Beloqui
Dipòsit Legal: T 68-2016

Chapter 9   **PhD Thesis**

Figure 1. Scheme of the set-up used in the synthesis of QDs.

35 ml of 1-octadecene (ODE) were heated at 80 °C under vacuum for 9 hours. Following this, 0.45 g of PbO, 1.3 ml of oleic acid and 3 ml of distilled ODE was placed under vacuum for 16 hours at 95 °C. The colour of the solution changed from yellow to transparent, then 15 ml of degassed ODE were added and subsequently the temperature was raised to 120 °C. When temperature became constant a degassed solution of 210 µl of bis(trimethylsilyl)sulphide (TMS) in 10 ml of ODE was steadily injected, changing the solution colour from transparent to dark brown. The solution was then allowed to cool to room temperature. The solution was precipitated three times with acetone and re-dispersed in toluene to remove the reaction side-products. The dried product was then dispersed in 3 ml of toluene and 1 ml of distilled oleyamine was added. This solution was stored in a glove-bod under a N_2 atmosphere for two days without disturbing. The CQD solution was then precipitated with methanol and re-dispersed in toluene three times. Finally, the CQDs were dispersed in anhydrous octane at a concentration of 10 mg/ml.
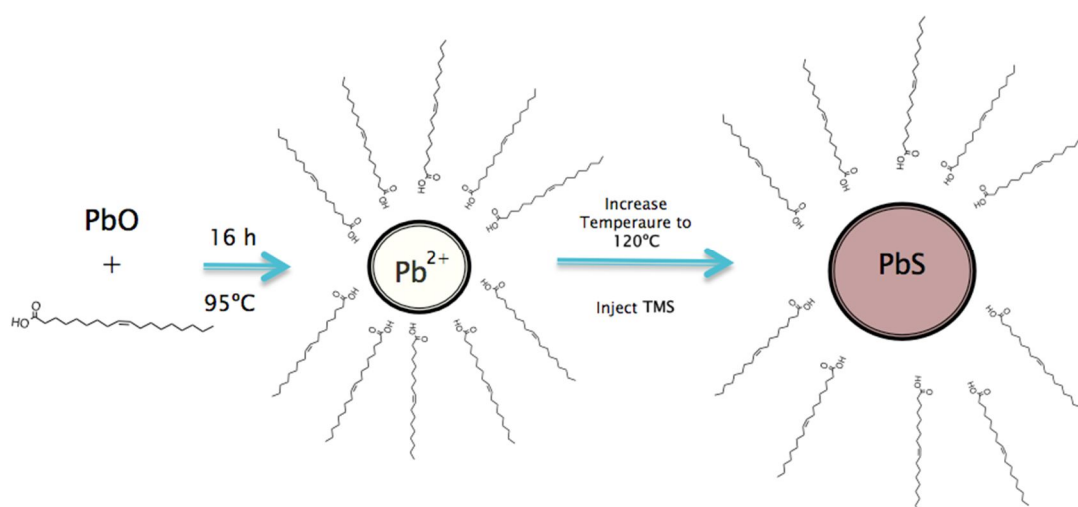
Figure 2. Scheme of the reaction for PbS QD formation.

In PbS QDs synthesis 1-Octadecene is used as a solvent because lower temperature (120ºC-150ºC) than other different QDs is required. In the case of, for example, CdSe QDs synthesis, phosphine derivatives are needed because the injection is made at nearly 300ºC.

The amount of oleic acid added to the synthesis was very important to obtain the desired size, as more oleic acid was added higher the QD size. Also, injection temperature was changed to obtain different sizes. Conditions to obtain different QD sizes synthesized in this work and optical properties are summarized in **Table 1**.

Inj. Temp. (ºC)	Oleic Acid (ml)	QD Size (nm)	Absorption λ_{max}
120	14	5.1	1395
150	1.5	3.7	1095
150	1.3	3.5	1030
120	1.5	3.3	1000
120	1.3	3.2	980

Table 1. Conditions and properties of some QDs synthesized in this thesis. QD size was calculated as reported elsewhere[2].

Perovskite Synthesis

Perovskite synthesis is performed in situ over the substrate, after an annealing process that occurs consecutive to the spin-coating process. After the spin-coating process the substrate is yellow indicating the presence of PbI_2. Then, the substrate is annealed to evaporate the solvent and to form the crystalline perovskite, as indicated by its dark brown colour.

To confirm the presence of perovskite, XRD experiments were performed (**Figure 3**), and then compared with other XRD diffractogram reported in bibliography[3].
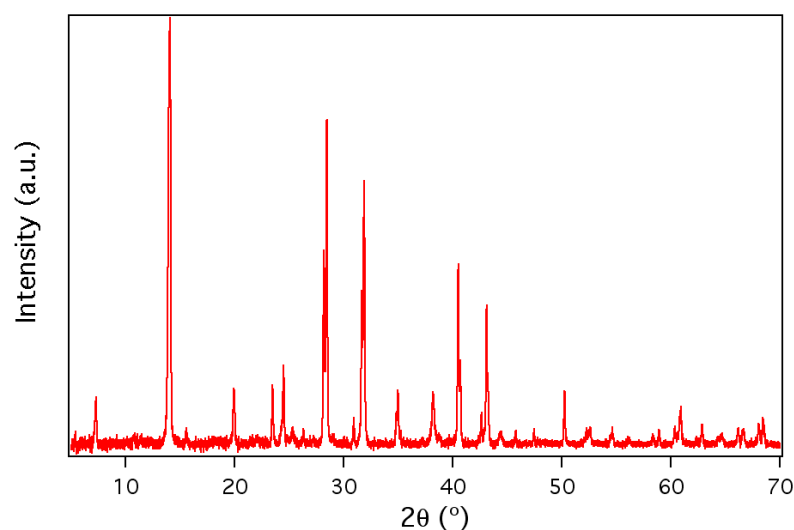

Figure 3. Diffractogram of a perovskite/TiO_2 substrate annealed at 110ºC for 40 minutes.

References

1   J. Tang, L. Brzozowski, D. A. R. Barkhouse, X. Wang, R. Debnath, R. Wolowiec, E. Palmiano, L. Levina, A. G. Pattantyus-Abraham, D. Jamakosmanovic and E. H. Sargent, *ACS Nano*, 2010, **4**, 869–78.

2   I. Moreels, K. Lambert, D. Smeets, D. De Muynck, T. Nollet, J. C. Martins, F. Vanhaecke, A. Vantomme, C. Delerue, G. Allan and Z. Hens, *ACS Nano*, 2009, **3**, 3023–30.

3   J. Burschka, N. Pellet, S.-J. Moon, R. Humphry-Baker, P. Gao, M. K. Nazeeruddin and M. Grätzel, *Nature*, 2013, **499**, 316–9.

Chapter 10

Output and Perspectives

The main purpose of this thesis was to understand the different losses mechanism in inorganic solution processed solar cells such as perovskite and PbS quantum dot solar cells. In the case of the QDSC, purpose has been accomplished. However, in the case of the perovskite the case was quite more complicated,despite this thesis has brought some knowledge for a better understanding to how the cells works, more research is still needed.

In the **third chapter** the PbS/C60 solar cell fabrication by the layer-by-layer deposition method is described. This method involves the ligand exchange in situ over the substrate in order to obtain high quality films where the MPA has replaced the oleic acid along the whole material thickness. Afterwards, an intensive optoelectronic study was performed on the as-fabricated devices. From the J-V curves obtained at different light intensities, we could confirm that non-genimate recombination was negligible at short-circuit and that Voc was originated with the split of the Fermi

UNIVERSITAT ROVIRA I VIRGILI
SOLUTION PROCESSED INORGANIC SEMICONDUCTOR SOLAR CELLS
José Manuel Marín Beloqui
Dipòsit Legal: T 68-2016

Chapter 10   **PhD Thesis**

levels of the QDs and the C60. In addition, J-V curve was reconstructed by using only the data obtained by PICE and PIT-PV indicating the voltage of the device is field-independent and can be highly increased decreasing the non-geminate recombination.

Chapter 5 focused in the optoelectronic study of perovskite solar cells. In this chapter it was confirmed that charge obtained by PICE, method widely used for OSC and DSSC, was not right, as the calculated charge was unrealistically high. Despite this, PIDC was shown as a suitable method to obtain charge in perovskite devices. Also biexponential behaviour of the PIT-PV indicating two possible different processes was depicted. However, both processes were not identified.

In **Chapter 6** different PTB7, PTB1 and OMeTAD were used as HTM in efficient perovskite solar cells. Measuring fluorescence Time-Correlated Single Photon Counting (TCSPC) the hole regeneration of perovskite by the HTM was found to be over 90% in all the cases. Besides L-TAS and PIT-PV measured in dark conditions were compared and they completely matched, indicating that in dark conditions the voltage decay corresponds to the recombination of holes in the HTM with the electrons in the mp-TiO$_2$.

Finally, in **Chapter 7** an insulating atomic Al$_2$O$_3$ layer was deposited by chemical bath deposition over the mesoporous TiO$_2$ to improve the Voc of perovskite devices. The differences of both devices were studied by PIDC and PIT-PV, and it was found that the enhancement of the Voc was not due to a mp-TiO$_2$ conduction band displacement, as it happened when this layer was used in DSSC. In fact, as the PIT-PV demonstrated, the improvement of cells voltage was due to a slow down in the recombination inside the solar cell.

Third generation solar cells efficiency keeps growing until making them to be very close to the market. However, it will be very difficult to overcome the silicon solar cells for outdoor applications, as it getting cheaper and cheaper. However, there are still plenty of room for these solar cells as for example solar windows and indoor applications, as silicon cells can't be transparent or collect indoor light.

Between all the third generation solar cells, perovskite devices seem to be the most promising to be commercialised as its efficiencies have reached 20% and its suitability to be part of tandem solar cells (where the expected efficiency is quite higher). However, stability is still a great issue, and is very far of silicon solar cells even with the encapsulation.

In the other hand, QDSC have been totally overcome by the perovskites, as they present the same advantages, such as inorganic earth-abundant materials, quick efficiency enhancement, but the perovskite ones does not involve a synthesis step and has much higher efficiency and much higher reproducibility.

Despite the high efficiencies obtained by the perovskite devices, there is still several things that need much more research. Although hysteresis has brought much attention in these years, there is still so much controversy due to the different possible mechanism involver in this effect. Despite all the efforts destined to this issue, last top efficiencies reported show no hysteresis.

Besides hysteresis, the different electrical inner mechanism that occurs when the cell is under working conditions are still unclear, as well as the V_{oc} origin. The understanding of these phenomena not only will help to improve the efficiency, it will also help to improve the stability as it will identify the different processes that decrease the efficiency the cell degrades.